Final Report

FDOT Contract Nos. BD545, RPWO #87
UF Project 00069605

ANALYSES OF EMBEDDED DATA COLLECTOR (EDC)

Principal Investigator: Michael McVay, PhD
Co-Principal Investigator: David Bloomquist, PhD, PE
Graduate Students: Yipeng Xie, Jengsoo Ko, and Scott Wasman
Engineer & Assistant: Jimmy Joiner, and Zachary Faraone

Department of Civil and Coastal Engineering
University of Florida
Gainesville, Florida 32611-6580

Developed for the

Peter Lai, P.E., David Horhota, P.E., Project Managers

June 2009

DISCLAIMER

"The opinions, findings, and conclusions expressed in this publication are those of the authors and not necessarily those of the State of Florida Department of Transportation or the U.S. Department of Transportation.

Prepared in cooperation with the State of Florida Department of Transportation and the U.S. Department of Transportation."

SI (MODERN METRIC) CONVERSION FACTORS (from FHWA)

APPROXIMATE CONVERSIONS TO SI UNITS

SYMBOL	WHEN YOU KNOW	MULTIPLY BY	TO FIND	SYMBOL
LENGTH				
in	inches	25.4	millimeters	mm
ft	feet	0.305	meters	m
yd	yards	0.914	meters	m
mi	miles	1.61	kilometers	km

SYMBOL	WHEN YOU KNOW	MULTIPLY BY	TO FIND	SYMBOL
AREA				
in^2	squareinches	645.2	square millimeters	mm^2
ft^2	squarefeet	0.093	square meters	m^2
yd^2	square yard	0.836	square meters	m^2
ac	acres	0.405	hectares	ha
mi^2	square miles	2.59	square kilometers	km^2

SYMBOL	WHEN YOU KNOW	MULTIPLY BY	TO FIND	SYMBOL
VOLUME				
fl oz	fluid ounces	29.57	milliliters	mL
gal	gallons	3.785	liters	L
ft^3	cubic feet	0.028	cubic meters	m^3
yd^3	cubic yards	0.765	cubic meters	m^3
NOTE: volumes greater than 1000 L shall be shown in m^3				

SYMBOL	WHEN YOU KNOW	MULTIPLY BY	TO FIND	SYMBOL
MASS				
oz	ounces	28.35	grams	g
lb	pounds	0.454	kilograms	kg
T	short tons (2000 lb)	0.907	megagrams (or "metric ton")	Mg (or "t")

SYMBOL	WHEN YOU KNOW	MULTIPLY BY	TO FIND	SYMBOL
TEMPERATURE (exact degrees)				
^oF	Fahrenheit	5 (F-32)/9 or (F-32)/1.8	Celsius	^oC

SYMBOL	WHEN YOU KNOW	MULTIPLY BY	TO FIND	SYMBOL
ILLUMINATION				
fc	foot-candles	10.76	lux	lx
fl	foot-Lamberts	3.426	candela/m^2	cd/m^2

SYMBOL	WHEN YOU KNOW	MULTIPLY BY	TO FIND	SYMBOL
FORCE and PRESSURE or STRESS				
lbf	poundforce	4.45	newtons	N
lbf/in^2	poundforce per square inch	6.89	kilopascals	kPa

APPROXIMATE CONVERSIONS TO SI UNITS

SYMBOL	WHEN YOU KNOW	MULTIPLY BY	TO FIND	SYMBOL
		LENGTH		
mm	millimeters	0.039	inches	in
m	meters	3.28	feet	ft
m	meters	1.09	yards	yd
km	kilometers	0.621	miles	mi

SYMBOL	WHEN YOU KNOW	MULTIPLY BY	TO FIND	SYMBOL
		AREA		
mm^2	square millimeters	0.0016	square inches	in^2
m^2	square meters	10.764	square feet	ft^2
m^2	square meters	1.195	square yards	yd^2
ha	hectares	2.47	acres	ac
km^2	square kilometers	0.386	square miles	mi^2

SYMBOL	WHEN YOU KNOW	MULTIPLY BY	TO FIND	SYMBOL
		VOLUME		
mL	milliliters	0.034	fluid ounces	fl oz
L	liters	0.264	gallons	gal
m^3	cubic meters	35.314	cubic feet	ft^3
m^3	cubic meters	1.307	cubic yards	yd^3

SYMBOL	WHEN YOU KNOW	MULTIPLY BY	TO FIND	SYMBOL
		MASS		
g	grams	0.035	ounces	oz
kg	kilograms	2.202	pounds	lb
Mg (or "t")	megagrams (or "metric ton")	1.103	short tons (2000 lb)	T

SYMBOL	WHEN YOU KNOW	MULTIPLY BY	TO FIND	SYMBOL
		TEMPERATURE (exact degrees)		
^oC	Celsius	1.8C+32	Fahrenheit	^oF

SYMBOL	WHEN YOU KNOW	MULTIPLY BY	TO FIND	SYMBOL
		ILLUMINATION		
lx	lux	0.0929	foot-candles	fc
cd/m^2	candela/m^2	0.2919	foot-Lamberts	fl

SYMBOL	WHEN YOU KNOW	MULTIPLY BY	TO FIND	SYMBOL
		FORCE and PRESSURE or STRESS		
N	newtons	0.225	poundforce	lbf
kPa	kilopascals	0.145	poundforce per square inch	lbf/in^2

*SI is the symbol for International System of Units. Appropriate rounding should be made to comply with Section 4 of ASTM E380. (Revised March 2003)

TECHNICAL REPORT DOCUMENTATION PAGE

1. Report No.	2. Government Accession No.	3. Recipient's Catalog No.

4. Title and Subtitle	5. Report Date
Analysis of Embedded Data Collectors (EDC)	June 2009
	6. Performing Organization Code

7. Author(s)	8. Performing Organization Report No.
Michael McVay, David Bloomquist, Yipeng Xie, James Johnson, Jengsoo Ko, Scott Wasman, and Zachary Faraone	

9. Performing Organization Name and Address	10. Work Unit No. (TRAIS)
Department of Civil and Coastal Engineering 365 Weil Hall – P.O. Box 116580 University of Florida Gainesville, FL 32611-6580	11. Contract or Grant No. BD-545 #87

12. Sponsoring Agency Name and Address	13. Type of Report and Period Covered
Florida Department of Transportation 605 Suwannee Street, MS 30 Tallahassee, FL 32399	Final Report 09/22/07 - 06/01/09
	14. Sponsoring Agency Code

15. Supplementary Notes

16. Abstract

This work validates measured particle motions, and stresses measured internally (Embedded Data Collector, EDC) and externally at the top and bottom of prestressed concrete piles subject to dynamic hammer impacts. The first series of tests involved a horizontally supported pile in air subject to a 1000-lb hammer impact. Experimental results showed good correlation between internal vs. external gages, as well as good agreement with wave mechanics principles (e.g., reflection of compression wave with tension wave, etc.). The second series of tests involved an instrumented (internally and externally) 18-in × 18-in × 30-ft pile embedded 20 ft horizontally into a 15-ft × 20-ft × 45-ft sand embankment. The pile was struck at variable drop heights (1ft to 6 ft) with a 1000-lb hammer and monitored. Again, the internal and external measured particle displacements, strains, and forces compared quite favorably between the external (e.g., PDA) and internal (EDC) gages at both the top and bottom of the pile. Subsequently, a one-dimensional wave equation was developed (inclusion of skin friction and damping) to model the experiments. The analytical solution of the equation revealed the potential of dispersion. Wavelet and spectral analysis of the top and bottom measured response revealed no dispersion, but a special case of theory, i.e., damping (c) and stiffness of T-Z curve being correlated (i.e., Smith damping). The work shows great promise in uniquely determining the side response (damping and static skin friction) separate from tip response (static tip and damping) using the top and bottom EDC gages.

17. Key Words	18. Distribution Statement
Deep Foundations, EDC, Wave Propagation, Damping Soil-Pile Skin Friction, Wavelet Analysis	No restrictions.

19. Security Classif. (of this report)	20. Security Classif. (of this page)	21. No. of Pages	22. Price
Unclassified	Unclassified	109	

Form DOT F 1700.7 (8-72) Reproduction of completed page authorized

ACKNOWLEDGMENTS

The researchers would first like to thank the Florida Department of Transportation (FDOT) for the financial support to carry out this research as well as the guidance of the project managers for its successful outcome. In addition, this research could not have been completed without the aide of the State Materials Office in locating and trucking all the soil to the facility, as well as conducting all of the soil monitoring, and testing (e.g., nuclear density, compaction, strength, and insitu DMT and PMT tests), as well as providing the PDA equipment for pile monitoring. Finally, the researchers would like to recognize Applied Foundation Testing for making available the 18-in × 18-in × 15-ft Embedded Data Collector (EDC) instrumented pile for testing in the laboratory without any soil.

EXECUTIVE SUMMARY

Monitoring the installation of driven pile foundations is of critical importance for ensuring adequate safety of pile supported bridges. Dynamic load testing of driven test piles is currently the preferred alternative used by industry on the grounds that it is a cost effective and reliable method. Current practice for estimating static pile capacity during driving is to externally attach strain and accelerometer gages to the top of the pile and to monitor the top dynamic forces for each blow of the hammer. During the drive, the wave down and wave up forces at the top of the pile are computed using the top gages from which the driving stresses and total static pile capacity are estimated for each blow (i.e., PDA). In the office, the End of Drive (EOD) or Beginning of Restrike (BOR) blows are subsequently analyzed using the finite difference code CAPWAP. The software, using a match quality index, adjusts the static resistance and damping along both the side and the pile tip until the wave up forces at the top of the pile matches the recorded measured values.

To reduce cost, improve safety, and provide a real-time assessment of stresses and capacities during driving, the FDOT developed the Embedded Data Collector (EDC) system. The EDC system employs two (2) sets of instrumentation which are installed in the pile during casting and are monitored wirelessly in the field during driving. From both sets of gages, the EDC software assesses stresses (top and bottom), total pile capacity, and "real-time" bearing and skin friction for every blow of the hammer without any user input.

Of concern, and the focus of this research, was the accuracy of external versus internal mounted gages and EDC's indirect assessment of static side friction. Specifically, EDC assesses the latter by subtracting the static tip resistance (unloading point approach)

from the total static pile capacity (Case Static Resistance Equation using lumped damping, J_{cL}), but a real-time direct assessment of static side resistance would be useful.

For validation of internal and externally mounted gages, two laboratory dynamically impacted piles were studied. In the first series of tests an 18-in × 18-in × 15-ft horizontally supported pile in the air was subject to a 1000-lb hammer impact. Experimental results showed good correlation between internal vs. external gages, as well as good agreement with wave mechanics principles (e.g., reflection of compression wave with tension wave, etc.). The second series of tests involved an instrumented (internally and externally) 18-in ×18-in ×30-ft pile embedded 20 ft horizontally into a 15-ft ×20-ft ×45-ft sand embankment. The pile was struck at variable drop heights (1 ft to 6 ft) with a 1000-lb hammer and monitored. Again, the internal and external measured particle displacements, strains, and forces compared quite favorably between the external (e.g., PDA) and internal (EDC) gages at both the top and bottom of the pile.

To improve the EDC side friction assessment, a one-dimensional wave equation was developed (inclusion of skin friction and damping) to model the experiments. The analytical solution of the equation revealed the potential of dispersion. However, wavelet and spectral analysis of the top and bottom measured response revealed that there was no dispersion. In such a case of the theory, the damping (c) is directly related to the slope of the T-Z curve, i.e., Smith damping. Moreover, the analytical solution provides a direct assessment of side damping (e.g., Case – J_{cs} or Smith – J_{ss}) as well as static side resistance and quake.

For the laboratory embedded pile-soil experiment, the analytical side damping (i.e., Smith, Case, etc.) was found to be similar to the existing software (CAPWAP) solution. Also, the total static pile capacity (R_{Static}^{Total}) of 45 to 56 kips estimated from the Case equation with the lumped Case damping parameter (J_{cL}) using the peak force ratio (Zang et

al. 2001) agreed with CAPWAP. However, the distribution of forces within the pile (i.e., R_T^{Side}, $R_{Damping}^{Side}$, R_{Static}^{Side}, R_T^{Toe}, and R_{Static}^{Toe}) between CAPWAP and analytical or EDC are not in agreement. The latter suggests that the CAPWAP is having a difficult time in separating the R_T^{Side} from R_T^{Toe}. It should be noted that the EDC system measures R_T^{Side} from R_T^{Toe} directly, i.e., they are **not estimated**. The latter findings are in agreement with FDOT EDC Phase I study which revealed a tip stress ratio (EDC/PDA) of 0.8 and a COV of 0.4.

In conclusion, the research showed that the embedded EDC instrumentation gives quite comparable results with externally mounted gages. Moreover, the use of top and bottom sets of instruments allows **direct** assessment of damping and static skin friction for both the side and the tip of the pile. In addition, the assessment may be real time and it will require no interpretation or multiple assessments to check match quality. It is also strongly recommended that the work be continued under full-scale field testing, in order to add to our understanding of wave propagation (i.e., dispersion) layering, etc.

TABLE OF CONTENTS

LIST OF TABLES

LIST OF FIGURES

CHAPTER 1
INTRODUCTION

1.1 Background

The Florida Department of Transportation (FDOT) is in the process of implementing Embedded Data Collector (EDC) systems in driven prestressed concrete piles throughout Florida. The system involves internal pile sensors at both the top and bottom of the pile, as well as a wireless radio (Bluetooth), receiver and laptop software to analyze the data. The EDC system is an improvement over existing technology (PDI) since it requires no external wires (i.e., climbing leads, etc.), records information at both the top and the bottom of the pile, and provides real time stresses and capacity assessments.

The EDC system is being verified with existing equipment (PDI) on a number of sites throughout Florida. Unfortunately, the latter comparison can only occur with the top set of gages on the pile where external PDI gages are mounted. The latter only allows validation of: 1) capacity assessment from the Case Method; or 2) maximum compression and tension stresses from top gage assessment only. The use of the bottom gages to assess tip stresses or separation of skin from tip resistance as proposed by research (FDOT 99700-3600-119, BB-349) may not be validated.

1.2 Objectives and Supporting Tasks

To corroborate the bottom set of gage results, the FDOT decided to compare in laboratory conditions the internally cast gages with externally attached accelerometers and strain gages. The gages were to be attached along the length of test pile sections (e.g., top and bottom) and tested with the EDC system under free, fixed, and intermediate end

restraint conditions. In the case of no soil (i.e., laboratory), the gages should show zero velocities and doubling of compression stress at the bottom of the pile under fixed condition, and a doubling of the velocity and zero stress in the case of a free condition. Of great interest is the case of soil along the length of the pile (i.e., field conditions). The gages should show a reduction in peak stress and velocity as the compression stress wave travels down the pile from soil resistance (static and dynamic); and at the end of the pile the compression wave should reflect with conditions in between the fixed and free condition in the laboratory. Validation of the latter is critical in separating skin and tip resistance (dynamic and static) from the applied dynamic force. Also, the full instrumentation will shed more light on velocity profile (i.e., side and tip), and damping along the side and tip of the pile. The latter will be used to validate and improve the current capacity assessments suggested in FDOT 99700-3600-119, BB-349. To accomplish the latter, the following scope of services or tasks are proposed.

1.2.1 Task I – Pile Wave Propagation without Soil

Task I involves the assessment of wave propagation of typical FDOT full-scale piles in the laboratory under free conditions. Specifically, the strain and acceleration data recorded along the length of the pile will be used to validate one-dimensional wave transmission within elastic bodies. Specifically, the wave down and wave up stresses and velocities within the pile will be predicted from the top set of gages and measured/validated with the lower gages. In addition, differences in the measured and predicted values will be researched and explained. For instance, a potential increase in magnitude of the propagated stress wave could be the results of lower modulus under high stresses.

1.2.2 Task II – Pile Wave Propagation with Soil

Once the laboratory monitoring and analysis of wave propagation in a pile without soil is complete, the work will focus on dynamic pile soil interaction. This work will involve monitoring an impacted instrumented (top and bottom) pile in uniform soil conditions. The uniform pile-soil interaction, i.e., constant skin friction, will be developed by placing the pile horizontally within an embankment. Subsequently, the pile will be struck by the hammer with variable height strokes to develop variable skin and tip resistance. The pile will be instrumented both internally (EDC) and externally (PDA) at both the top and the bottom to assess wave down and wave up forces as well as separating skin and tip resistance.

1.2.3 Task III – Estimating Pile-Soil Damping and Static Skin Friction

Using the experimental results, the effort will focus on evaluating existing methods of determining pile capacity in the field (i.e., Case), the method proposed in FDOT 99700-3600-119, BB-349, as well as the methods used by "SmartPile" in their field/laptop software. Of interest are improved ways of separating static skin and tip resistance, as well as assessing pile-soil damping. The work considers analytical solutions incorporating damping, along with wavelet and spectral analysis of surface waves (SASW) approaches.

CHAPTER 2
EXPERIMENTAL PILE WAVE PROPAGATION WITHOUT SOIL

2.1 Experimental Setup and Instrumentation

For the pile wave propagation in air (i.e., no soil), a donated 18-in × 18-in × 15-ft pile with precast EDC in top and bottom was used, Figure 2-1. The pile was supported in the air through 6-ft long cargo straps suspended through two steel A-frames. The dynamic impulse was provided by a 1000-lb hammer, constructed from 2-ft inside diameter by 3-ft long by 1/2-in thick steel pipe filled with concrete. The hammer was attached to a 1-in × 1-in × 20-ft tubular steel suspended from a 28-ft tall forklift frame with a rolling bearing, Figure 2-2. To prevent damage to the pile during impact, a 3-in plywood cushion was placed between the hammer and the pile, Figure 2-2. For each blow, the hammer was pulled back to a specified vertical elevation (e.g., 3 ft or 4 ft), the hammer was released and the instrumentation was triggered.

Shown in Figure 2-1 is the layout of the instrumentation which includes: 1) EDC strain and accelerometers cast within the top and bottom of the pile, 2) PDA strain and accelerometers attached to the outside of the pile at the top and bottom; and 3) UF strain and accelerometers attached next to the PDA instruments. The PDA used piezo-resistance gages at the top of the pile and piezo-electric gages at the bottom of the pile. The UF strain gages were obtained from micro measurements and were attached to the pile through epoxy. The UF accelerometers were 500-g piezo-resistive gages obtained from the PCB Corporation. The eight gages (four strain and four accelerometer at top and bottom) were read by a USB 1608 HS-2AO 8-channel, 16-bit, simultaneous 250,000 samples/channel/sec data acquisition system (DAQ).

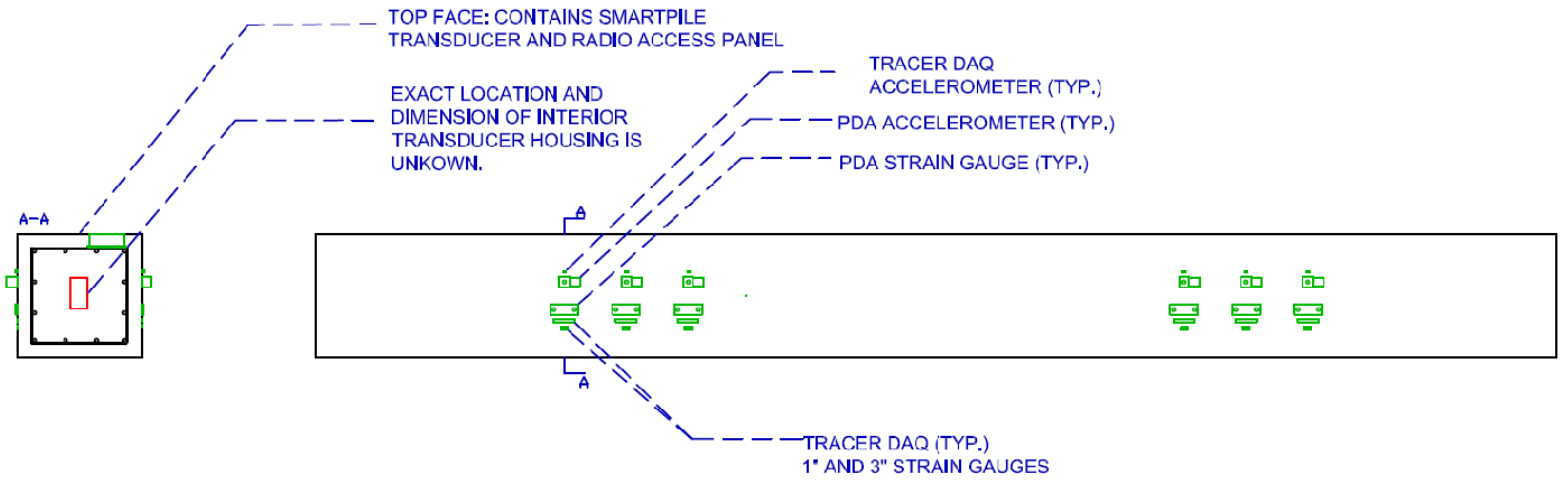

NOTES:

THIS MOUNTING PATTERN REPRESENTS THE EXTERNAL INSTRUMENTATION LAYOUT THAT WILL BE ADDED ON BOTH SIDE FACES OF THE PILE. THE TOP FACE, AS NOTED ON THE CROSS SECTION A-A, CONTAINS THE ACCESS PANELS FOR THE INTERNAL SMARTPILE TRANSDUCER AND RADIO EQUIPMENT.

EACH TRANSDUCER GROUPING SHOWN ABOVE IS POSITIONED ON THE EXPECTED CENTER LINE OF THE INTERIOR SMARTPILE TRANSDUCERS. THE POSITION OF THE FIRST SET OF INTERNAL TRANSDUCERS IS EXPECTED TO BE 36" ON CENTER FROM THE PILE TOP, WITH THE SECOND AND THIRD SET EACH SPACED 9" ON CENTER FOLLOWING THE FIRST SET. THIS SPACING SCHEME IS ALSO EXPECTED FOR THE PILE TIP WHERE THE LOWEST TRANSDUCER PAIR IS 36" ON CENTER FROM THE PILE TIP.

BOTH EXTERNAL DATA AQUISITION SYSTEMS ARE CAPABLE OF COLLECTING DATA FROM 8 CHANNELS AT ONCE. SINCE IT WILL REQUIRE 4 EXTERNAL CHANNELS TO MONITOR ONE INTERNAL TRANSDUCER LOCATION THE EXTERNAL TRANSDUCERS WILL BE ADJACENTLY MOUNTED TO ONLY TWO OF THE SIX INTERNAL LOCATIONS AT ANY ONE TIME. THE DATA COLLECTION PROTOCOL WILL THEN CALL FOR THE INTERMITTENT RELOCATION OF THE EXTERNAL TRANSDUCERS IN ORDER TO COLLECT DATA AT ALL SIX SMARTPILE TRANSDUCER LOCATIONS.

Figure 2-1. A side view and cross section of the instrumented concrete pile showing the layout of the independent, external transducers and their relative position to the interior EDC transducers.

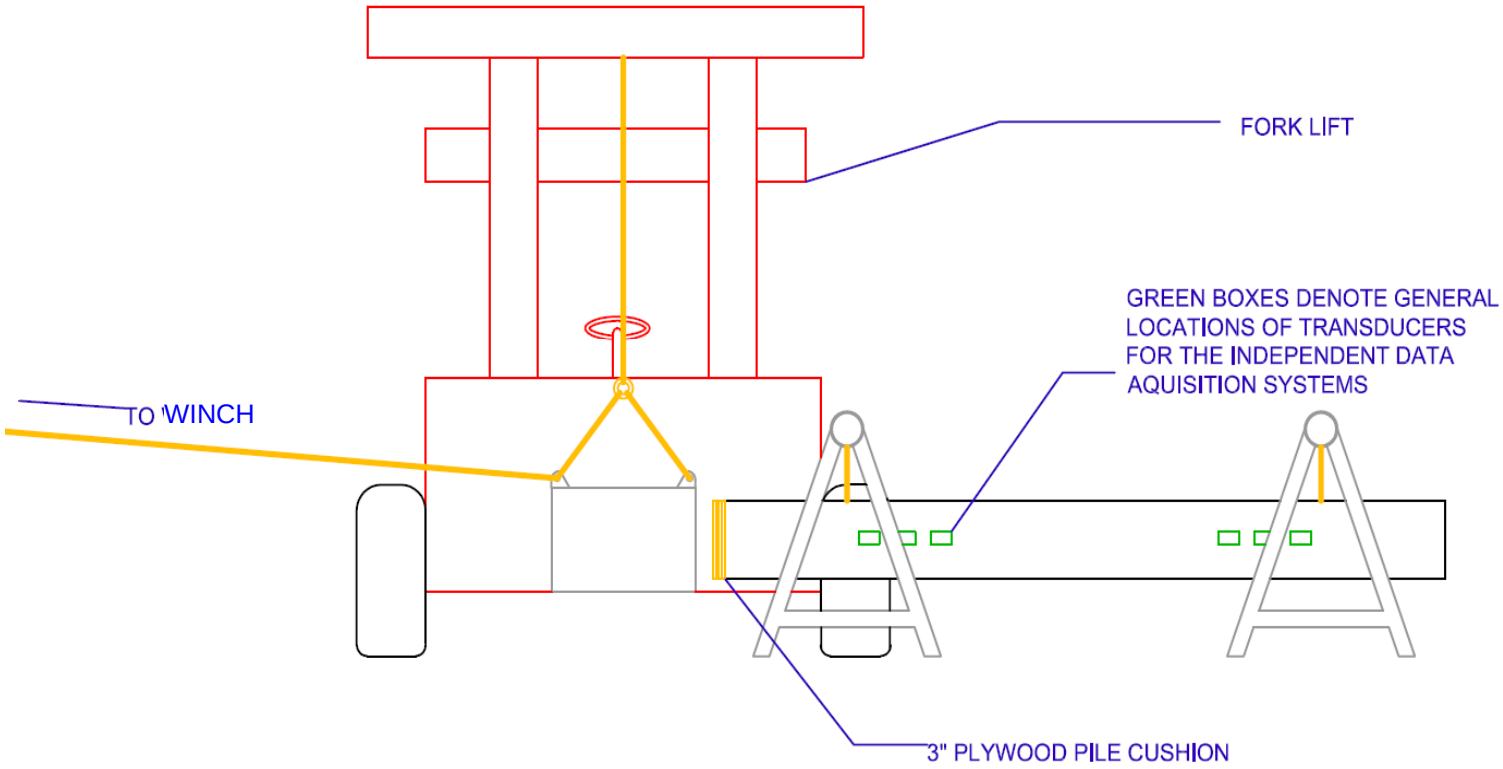

Figure 2-2. A 1000-lb hammer striking the 15-ft instrumented pile (3-ft to 5-ft drop heights).

2.2 Experimental Results

Shown in Figures 2-3 and 2-4 are the raw data from the accelerometers (top of pile) and the strain gages (bottom of pile) from a 4-ft hammer blow. In the case of the acceleration data, the period or frequency of signals is approximately 0.0017 sec [2 × (15 ft – 3 ft)/14000 ft/sec] corresponding to the time for transmission of compression wave from top to the bottom of the pile and back. Also evident from the acceleration traces is the good comparison of particle motions between both sides of the pile; however, not expected was the high frequency particle motion observed in the DAQ data. The DAQ system recorded particle motion 50 times faster than the other two systems. The latter high frequency motion may be attributed to surface waves (i.e., Rayleigh waves) which have elliptic particle motion which dampen out quickly (see trace). Also, it should be noted that the PDA trace has been integrated (velocity) within the PDA hardware (analog filter) and subsequently differentiated to obtain accelerations.

Shown in Figure 2-4 are measured strains at the tip of the pile for the accelerations shown in Figure 2-3. Evident from the figure, the strains on both sides of the pile are not equal (e.g., PDA red vs. orange values) as observed with accelerations. However, the strains on both sides of the pile do exhibit the same periods and when averaged will compare favorably to the centerline values recorded by EDC . Also of interest is the reduction in high frequency surface waves observed in acceleration data. Evidently, the elliptic particle motions (i.e., accelerations) do not necessarily generate strains.

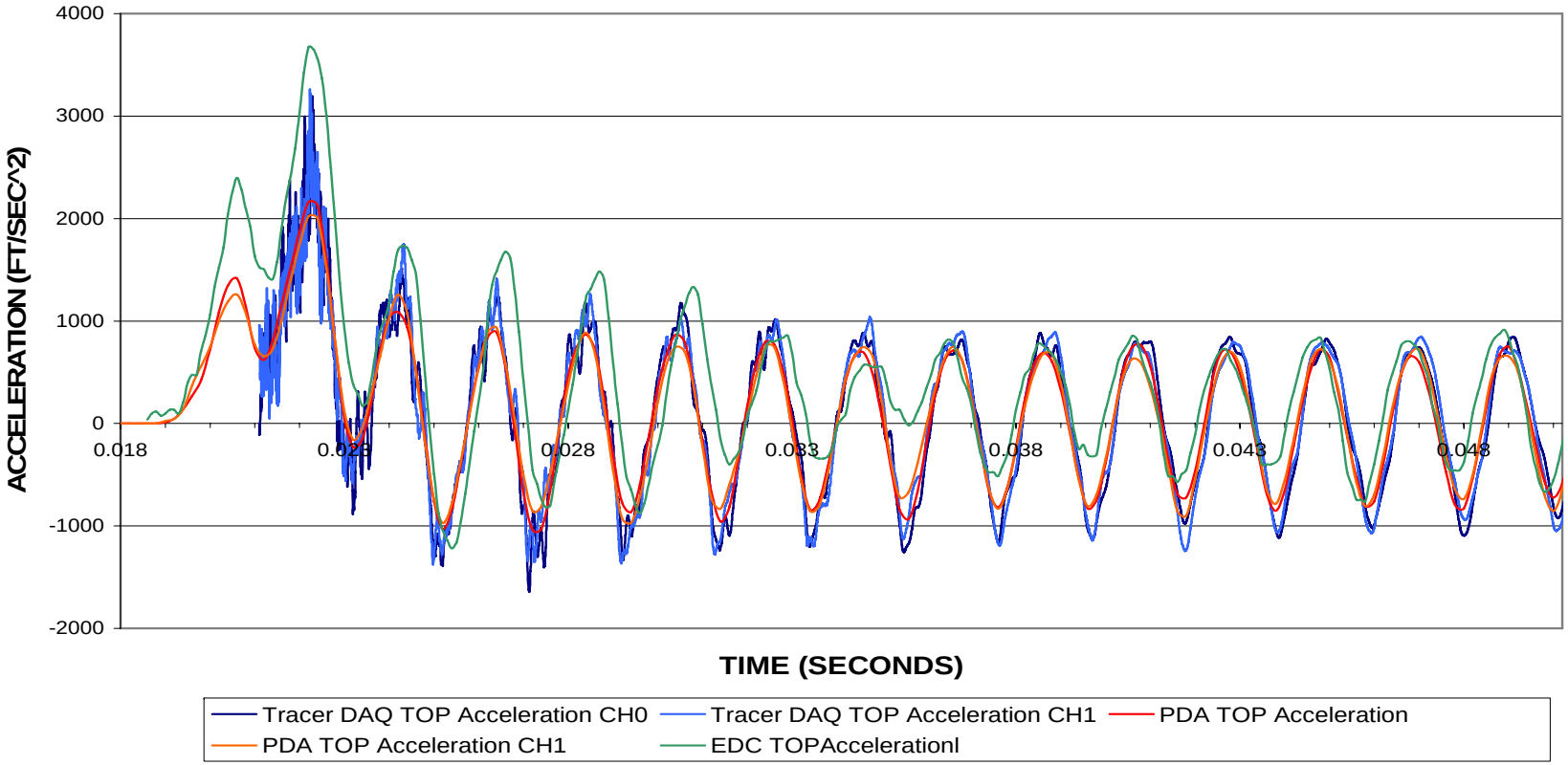

Figure 2-3. Raw acceleration from PDA, EDC, and UF DAQ at top of pile.

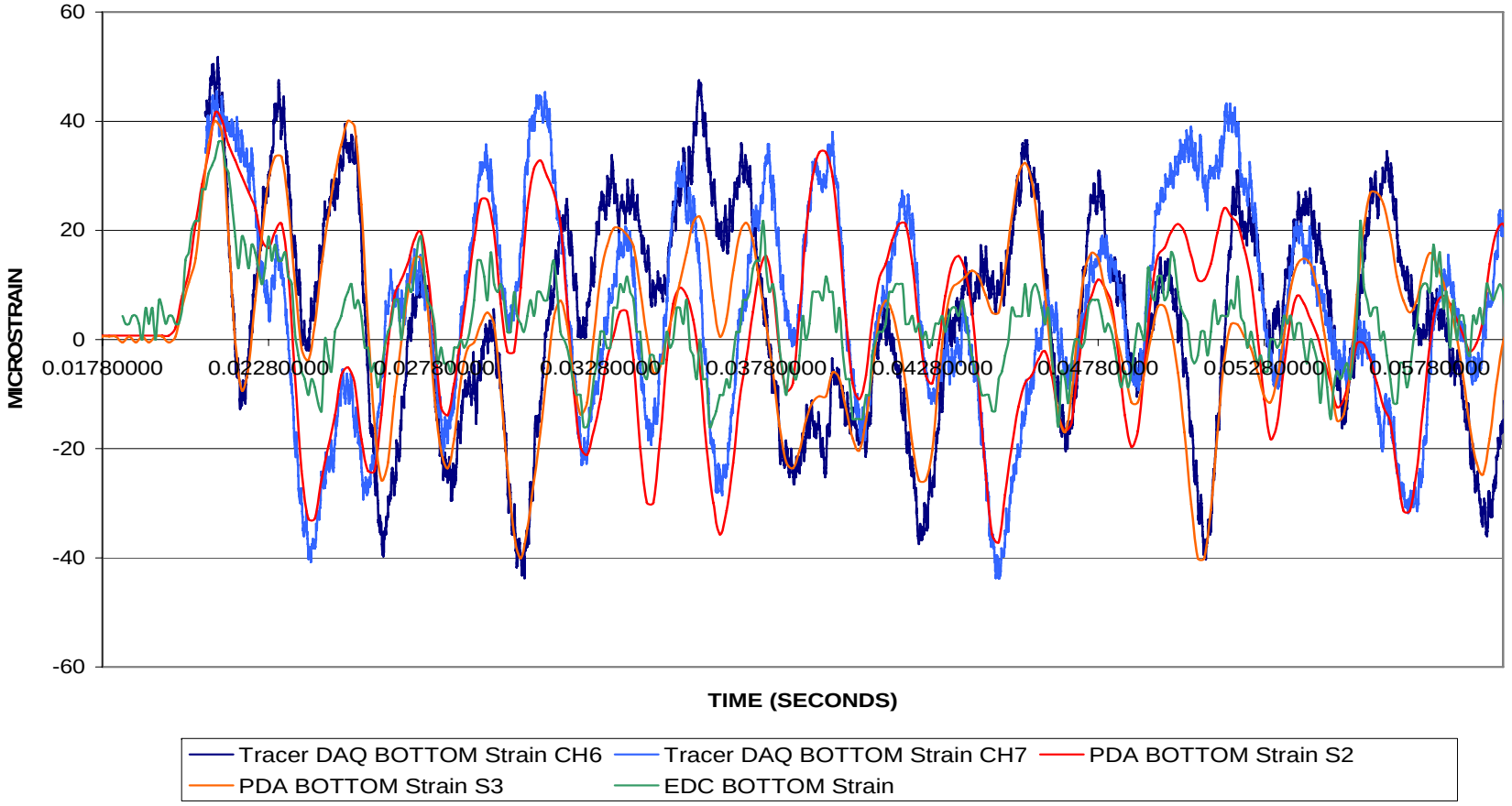

Figure 2-4. Raw strain data from PDA, EDC, and UF DAQ at bottom of pile.

2.2.1 Filtering the Raw Data

Since the focus of the research is the assessment of stresses at a point (i.e., tip), as well as the propagation of stresses along the pile, the estimation of particle velocities from accelerations are critical. The PDA data is already filtered (i.e., analog filter), SmartPile software offers both filtered and unfiltered data, whereas the Tracer DAQ was only available unfiltered. Consequently, the Tracer DAQ and EDC data was filtered using Fast Fourier Transform as discussed subsequently.

2.2.1.1 Fourier Analysis Background - In general, a *Fourier Transform* provides the means of transforming a signal defined in the time domain into one defined in the frequency domain. In the case where both the time and the frequency variables are discrete (i.e., data acquisition, e.g., samples/sec), the process is referred to as discrete Fourier transform, DFT. Let $x(n\mathrm{T})$ represent the discrete time signal, and let $\mathrm{X}(m\mathrm{F})$ represent the discrete frequency transform function. The forward transform to frequency domain given by

$$X(mF) = \sum_{n} x(nT)\, e^{-inm2\pi FT} \qquad \text{(Eq. 2-1)}$$

and the inverse transform to the time domain is given

$$x(nT) = \frac{1}{N} \sum_{m} X(mF)\, e^{inm2\pi FT} \qquad \text{(Eq. 2-2)}$$

where T = time increment

F = frequency

There are several ways to calculate the Discrete Fourier Transform (DFT), a typical approach is the Fast Fourier Transform (FFT) available in Microsoft Excel spreadsheets. Shown in Figure 2-5 is the DFT (Eq. 2-1) for one of the Trace DAQ acceleration signals.

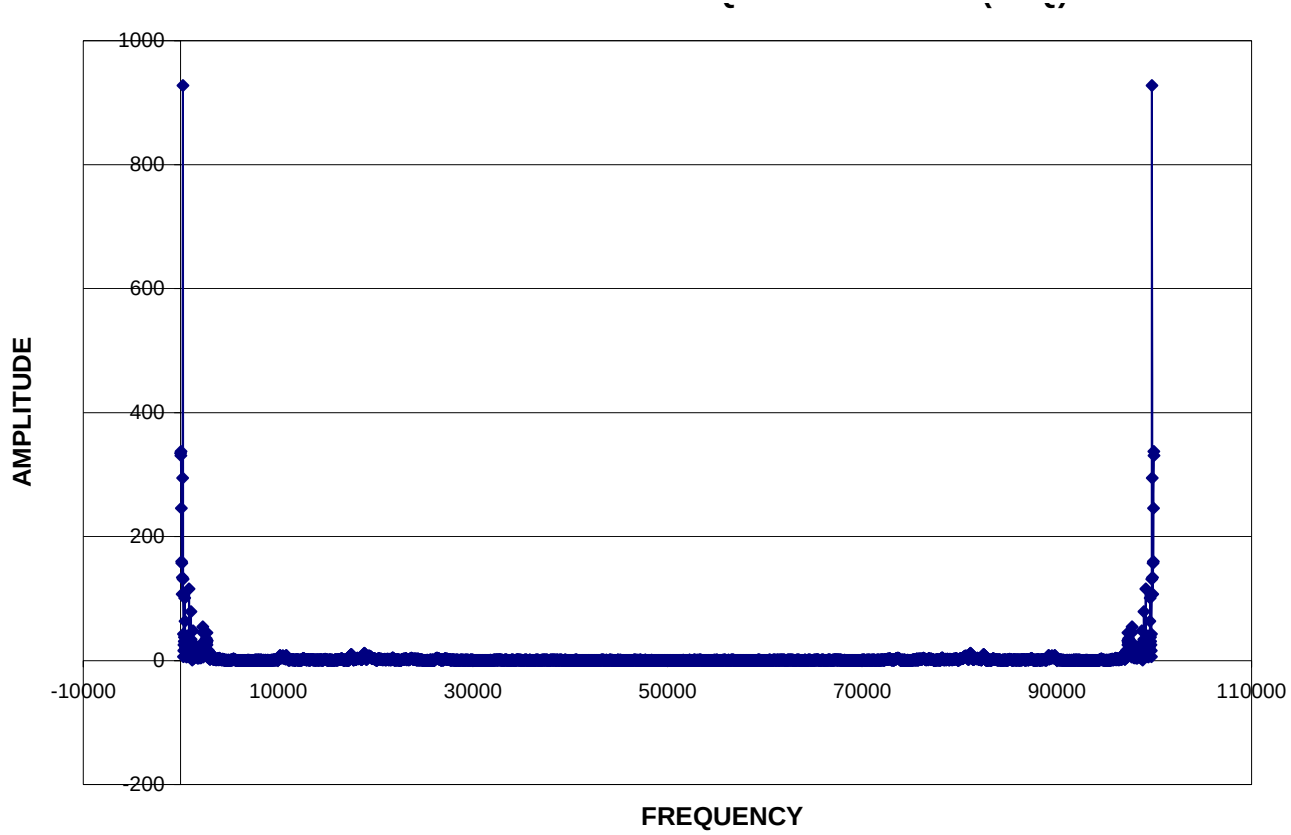

Figure 2-5. Frequency and amplitude content of Tracer DAQ acceleration record.

The X axis identifies the frequency within the data signal and the y axis gives the amplitude of the specific frequency. If one wishes to remove specific frequencies, e.g., noise, surface waves, etc., they can be simply left out when transforming back to the time domain using Eq. 2-2.

2.2.1.2 Fourier Analysis of Experimental Data – Using the Excel sheet filtering, all the DAQ and EDC acceleration traces were filtered to eliminate frequencies greater than 1000 Hz. For instance, shown in Figures 2-6 and 2-7 are top acceleration signals from the top left and right side gages. Evident from the plots, the surface waves identified in the raw DAQ systems were definitely filtered (<1000 Hz) out. Also shown in each plot is EDC, signal filtered with the SmartPile software, as well as the FFT method.

Similar to the top of the pile, the acceleration data at the bottom of the pile was filtered for the DAQ and EDC systems as shown in Figures 2-8 and 2-9. As expected, the bottom raw DAQ data showed lower surface wave acceleration at the pile tip. Also, the filtered EDC signals from the SmartPile software had different initial amplitudes than the FFT filtered results. All of the measured gages gave very similar frequency of primary signal.

Shown in Figures 2-10 and 2-11 are the average top and bottom acceleration signals from the PDA, and Tracer DAQ compared to the EDC signal located at the center of the pile cross-section. Again all had similar frequency content, with slightly different signal amplitudes. The latter signals will be used in generating the up and down waves traveling within the pile.

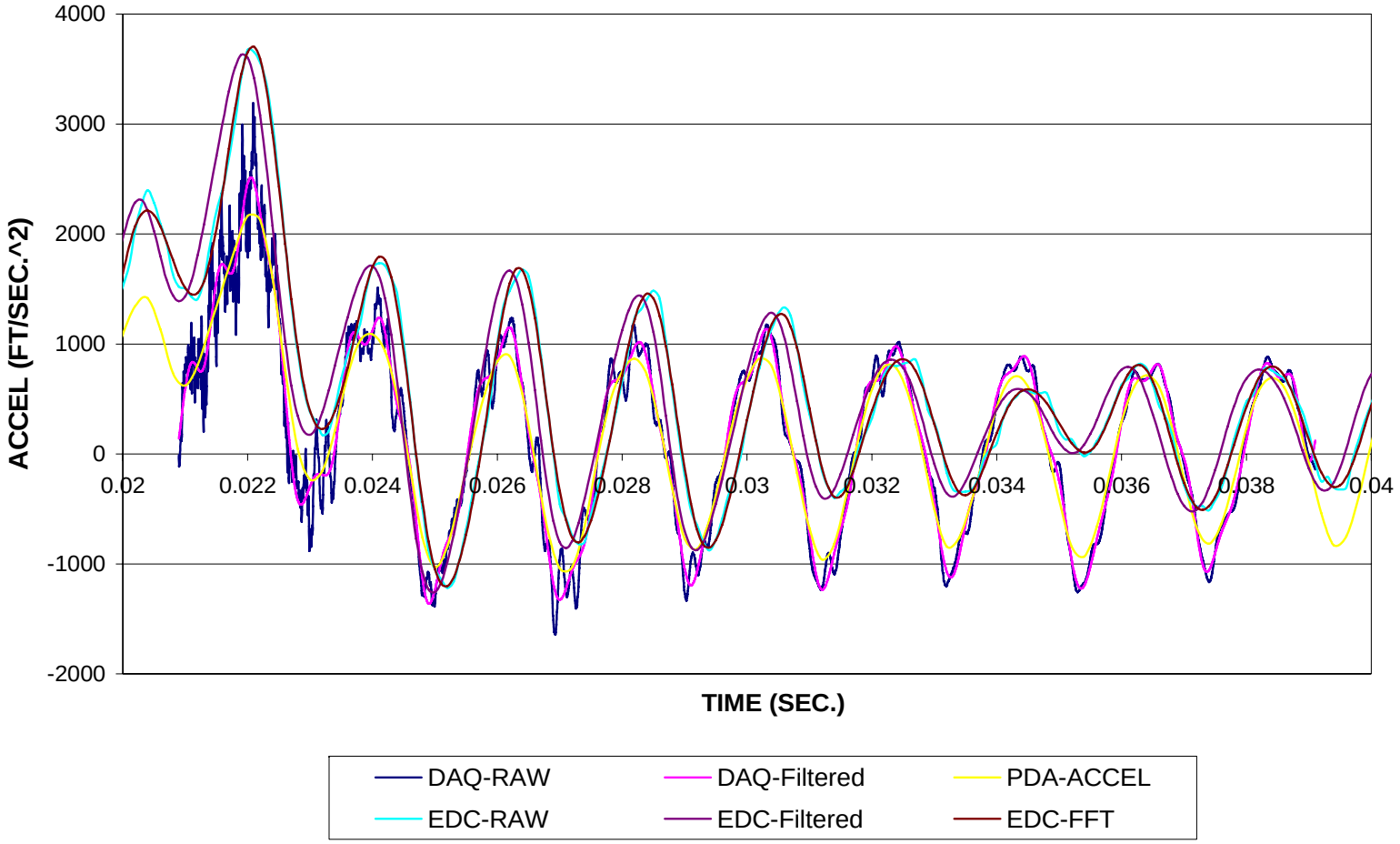

Figure 2-6. Filtered and unfiltered data from top accelerometer (left side of pile).

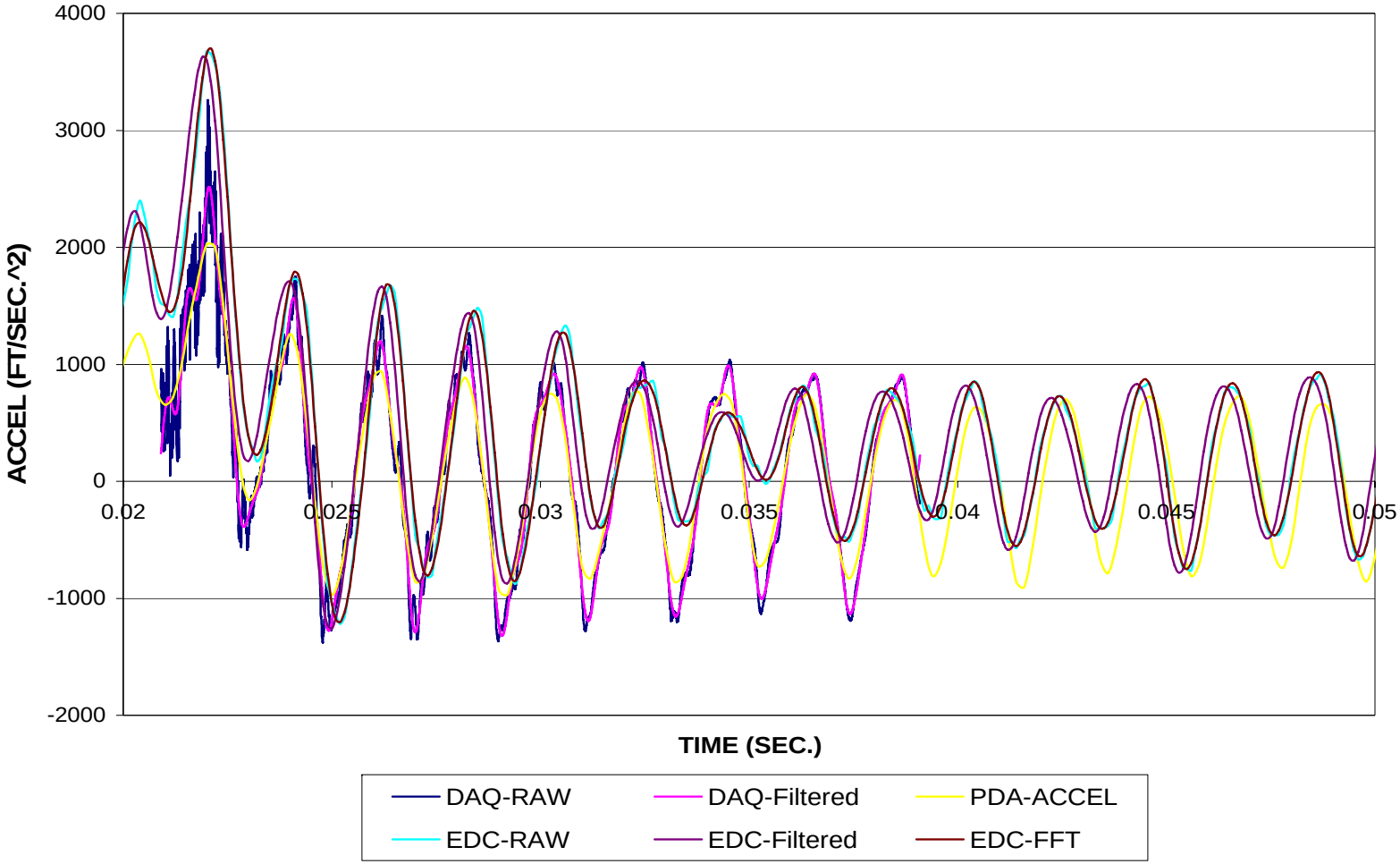

Figure 2-7. Filtered and unfiltered data from top accelerometer (right side of pile).

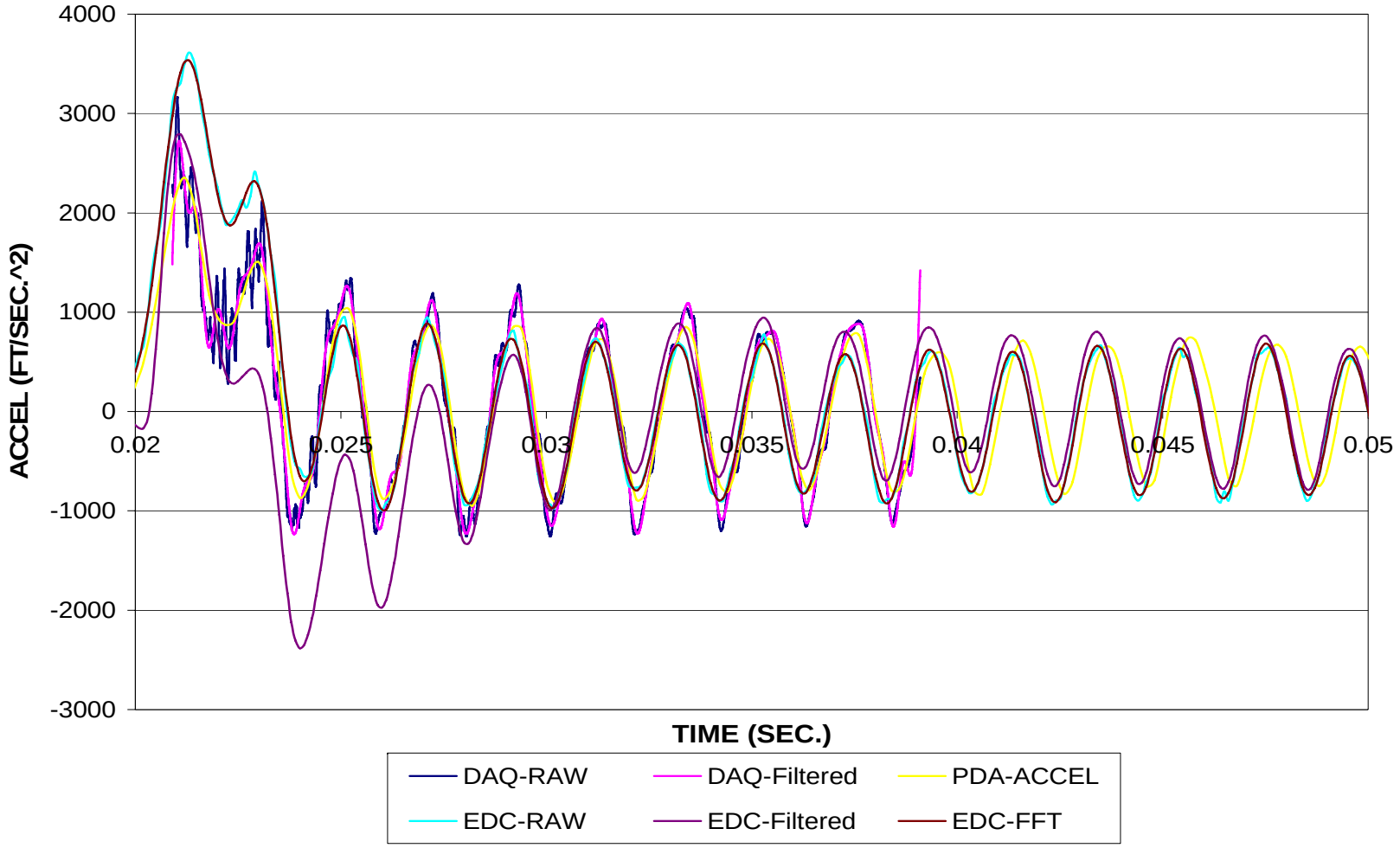

Figure 2-8. Filtered and unfiltered data from tip accelerometer (left side of pile).

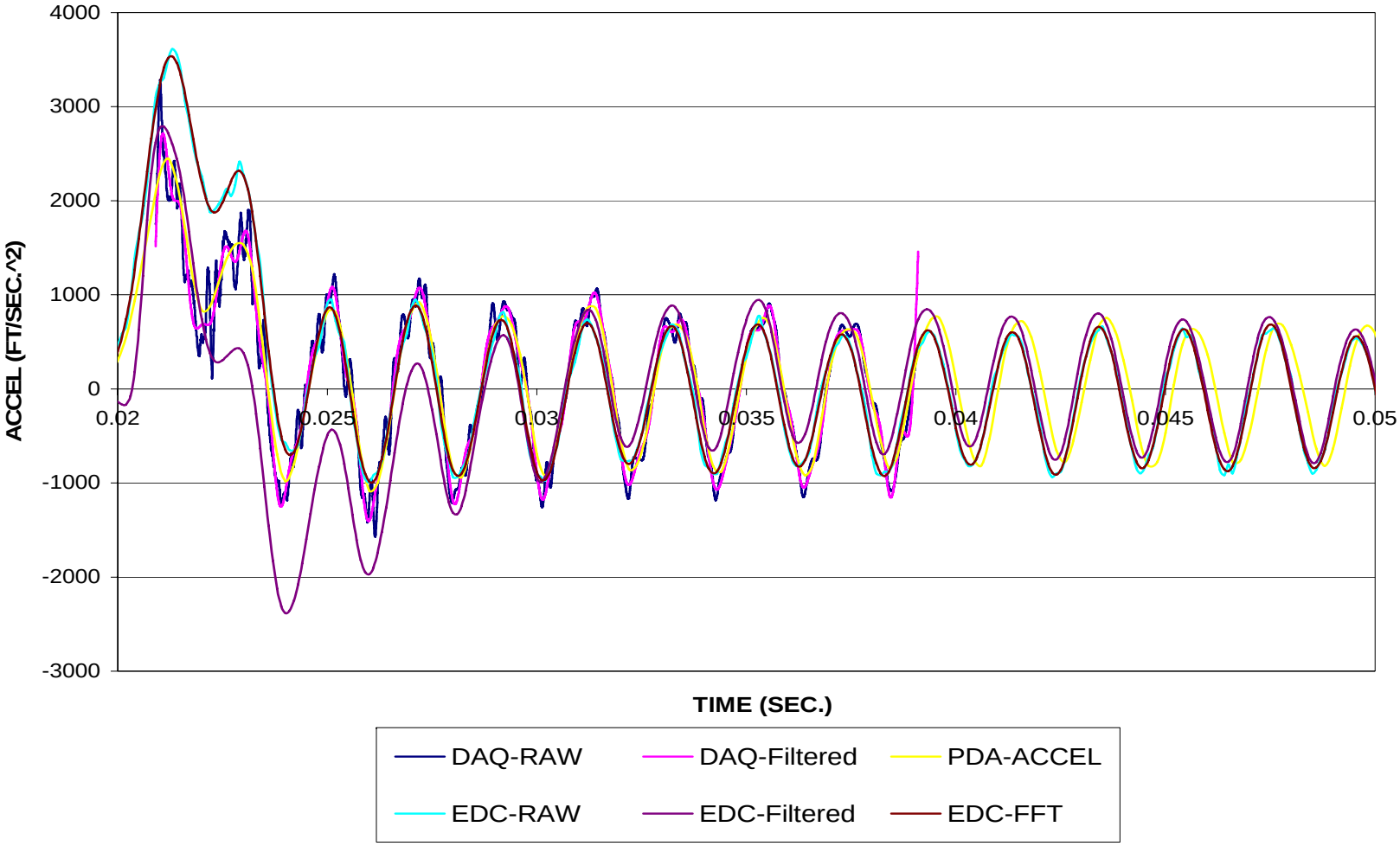

Figure 2-9. Filtered and unfiltered data from tip accelerometer (right side of pile).

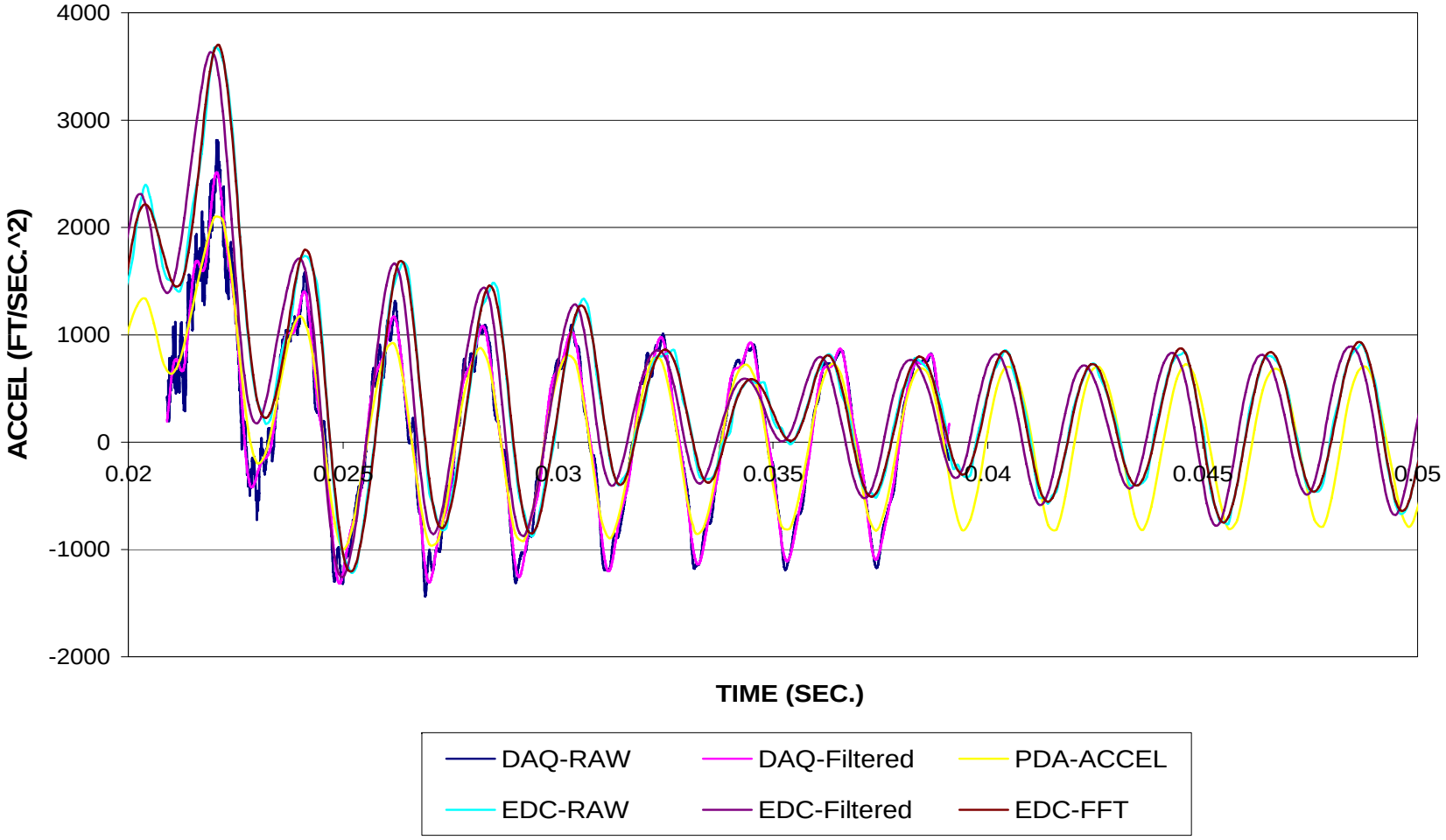

Figure 2-10. Average filtered and unfiltered acceleration data from top of pile.

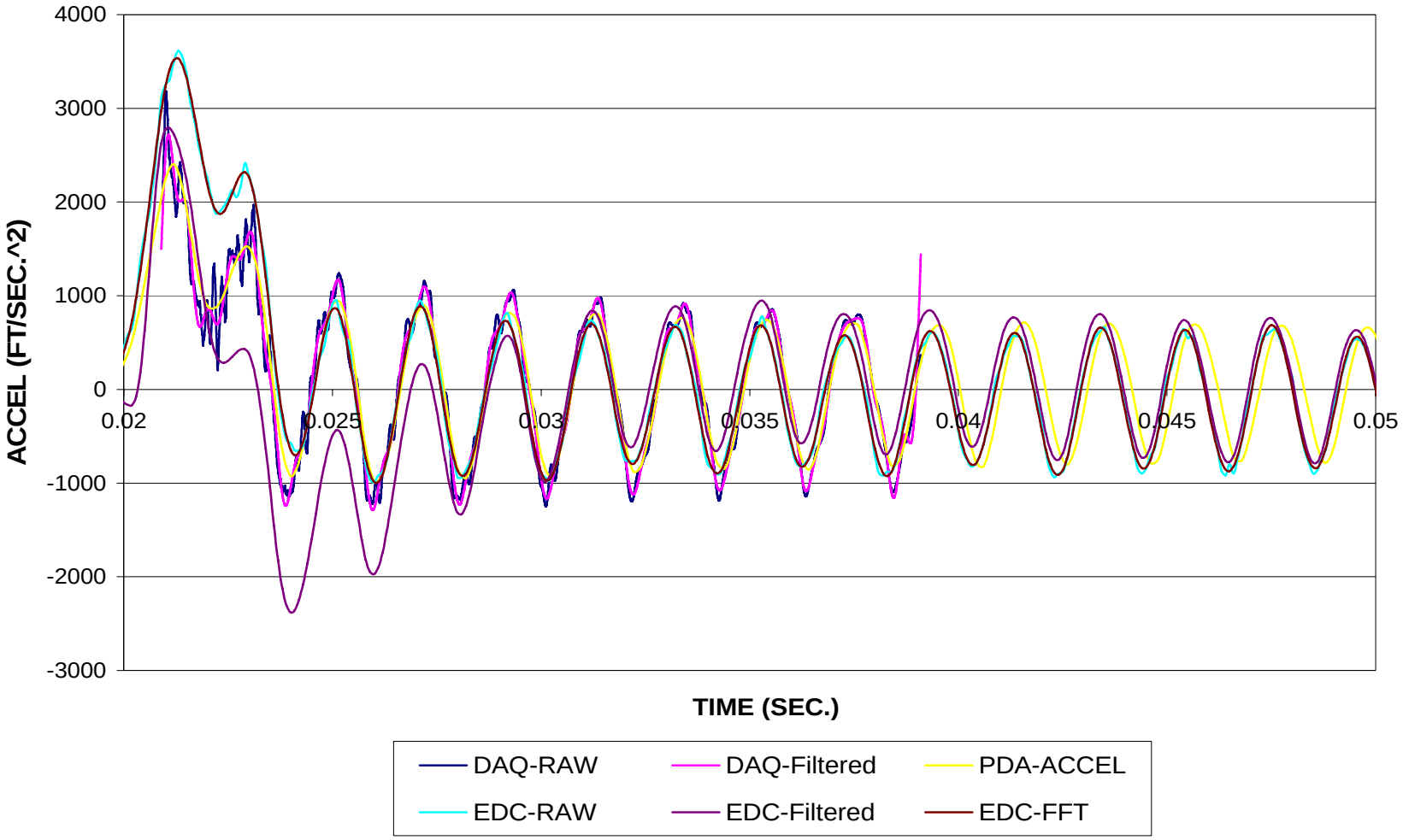

Figure 2-11. Average filtered and unfiltered acceleration data from bottom of the pile.

2.3 Wave Propagation Analysis

2.3.1 Background Theory

In the case of one-dimensional wave propagation, there are at most two possible waves, Figure 2-12, passing any given point in time: 1) downward traveling wave with force, $F_{dw,}$ and 2) the upward traveling wave with force, F_{up}.

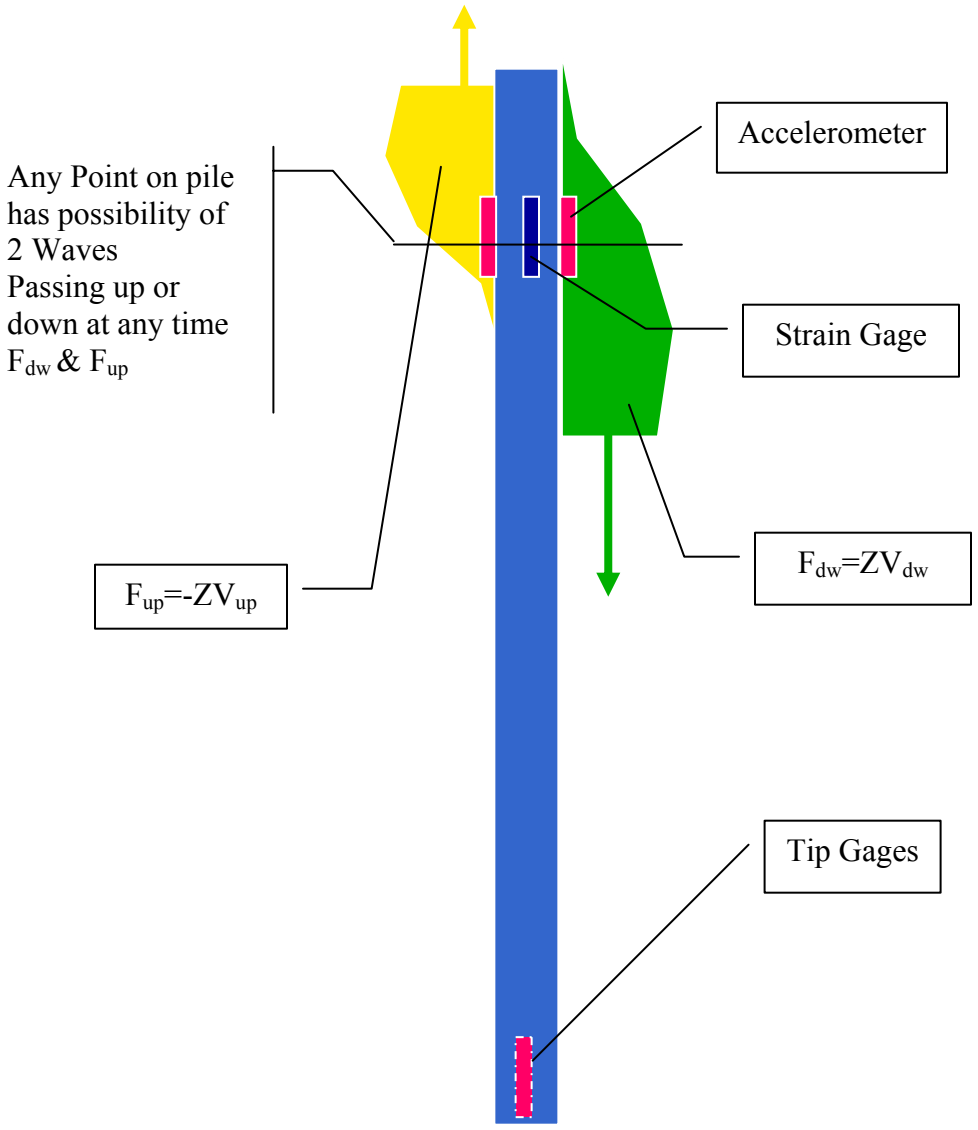

Figure 2-12. One-dimensional wave propagation.

Based on kinematics (i.e., deformations), and strength of materials (i.e., Hookean material), the force in each traveling wave may be equated to particle velocity through the medium's impedance, Z as

$$F = Z\,V \qquad \text{(Eq. 2-3)}$$

where $$Z=EA/C \qquad \text{(Eq. 2-4)}$$

$$C = \text{Wave Speed} = \sqrt{E/\rho} \qquad \text{(Eq. 2-5)}$$

$$\rho = \text{density of the pile} \qquad \text{(Eq. 2-6)}$$

$$E = \text{Young's Modulus of Pile Material} \qquad \text{(Eq. 2-7)}$$

Using compression as positive forces and defining positive particle velocity as pointed downward, the upward and downward traveling wave forces may be readily assessed as,

$$F_{up}= - ZV_{up}\,, \qquad F_{dw} = ZV_{dw} \qquad \text{(Eq. 2-8)}$$

Next, multiplying the longitudinal or axial strain from the gages by the pile's dynamic Young's Modulus, E, and cross-sectional area, the resultant axial force, P, in the pile at a point may be determined; however, from equilibrium on a cross-section, the resultant force must be also equal to the sum of the upward and downward wave forces passing the gage point, or

$$P=\varepsilon\, E\, A_{cross} = F_{dw} + F_{up} \qquad \text{(Eq. 2-9)}$$

Next, the particle velocity may be obtained by integrating the acceleration data; but from kinematics the measured particle velocity, V_T, must be the sum of any downward traveling wave velocity, V_{dw} and upward traveling wave velocity, V_{up}.

$$V_T = \int a\,dt\,,\ V_T=V_{up}+V_{dw} \qquad \text{(Eq. 2-10)}$$

Consequently, from Eqs. 2-8, 2-9, and 2-10, the wave up and down forces may be assessed from the experimental data (P and V_T) as

$$F_{up} = (P - Z V_T) / 2, \; F_{dw} = (P + Z V_T) / 2 \qquad \text{(Eq. 2-11)}$$

In the case of a free end, i.e., no tip resistance, R=0, then the value of F_{up} should equal the negative of F_{dw}, from statics, while for fixed tip support condition, where V_T is 0, then F_{up} will equal F_{dw} from kinematics. Of great interest is the value of F_{up} and F_{dw} from our experimental data.

2.3.2 Wave Down and Up Forces

Using the EDC strain gage data and the average for DAQ and PDA (Figure 2-4), the total force (P) was found from Eq. 2-9 using a Young's Modulus (E) of 6800 ksi, and cross-sectional area (A) of 324 in^2. Next, the acceleration was integrated (Eq. 2-10) and multiplied by pile impedance (Z) of 151.9 kip-sec/ft, for ZV_T. Both P and ZV_T are shown in Figures 2-13 and 2-14 for the top and bottom of the pile.

Evident from Figure 2-13 (top of pile), the forces computed from strain (P) and acceleration (ZV) are very close at start of trace (0.0195 sec) until 0.0212 sec, whereupon they diverge due to returning upward traveling waves in combination with downward traveling waves. Note that the strain gage force (P) built to a peak of 150 kips to 250 kips and then decayed to zero at 0.0245 sec. The latter occurred when the hammer separated from the pile top after contact. The signal after 0.0245 sec varied from ± 50 kips or within the accuracy of the instrumentation (5%) of zero.

The tip set of gages (Figure 2-14) show a maximum tip force (P) from the strain gages of 100 kips (DAQ) for the first peak, but for all subsequent peaks it is less than ± 50 kips. It is expected that P should be closed to zero because of the free end condition.

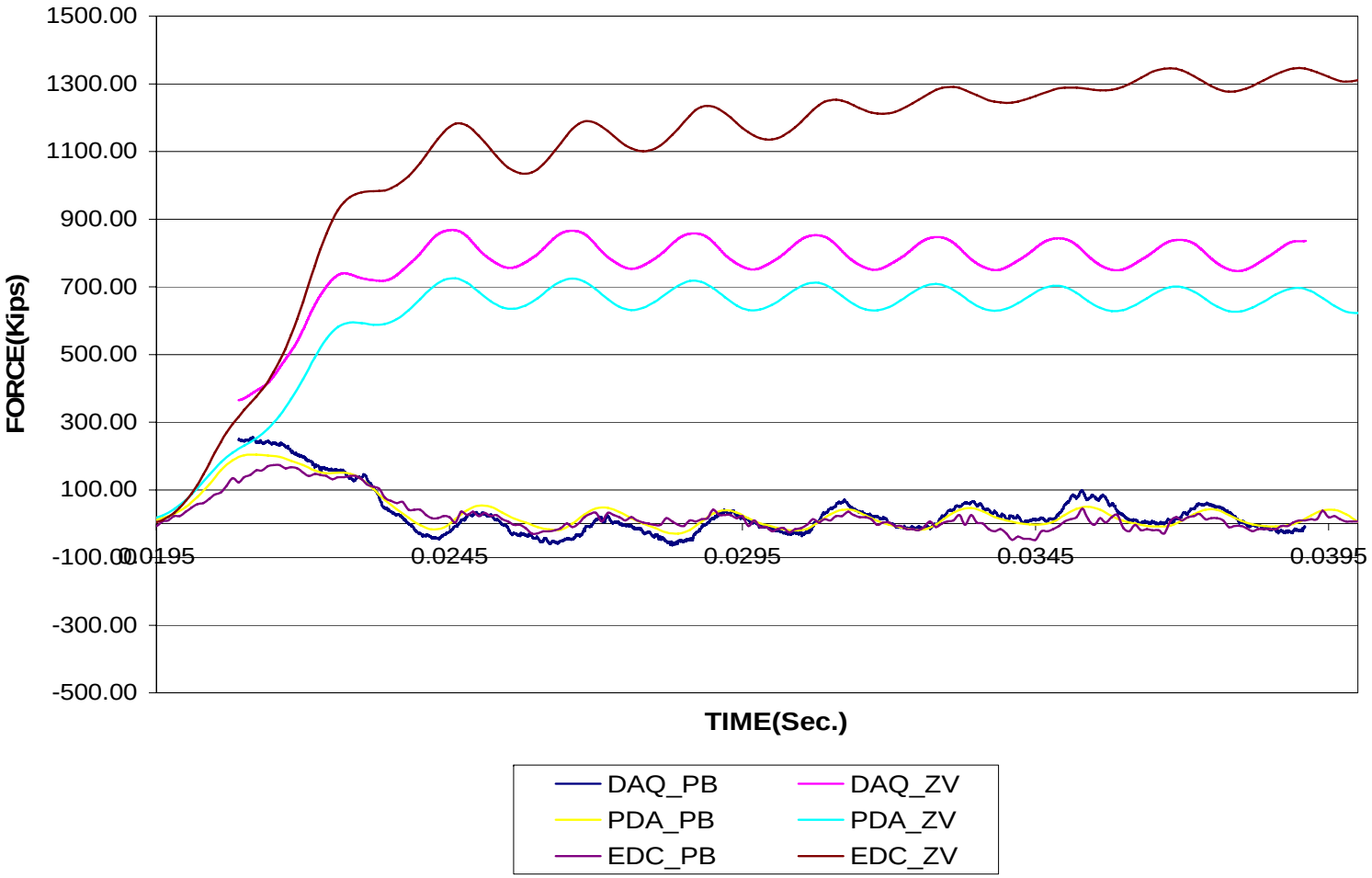

Figure 2-13. Computed forces vs. time at pile top (near hammer).

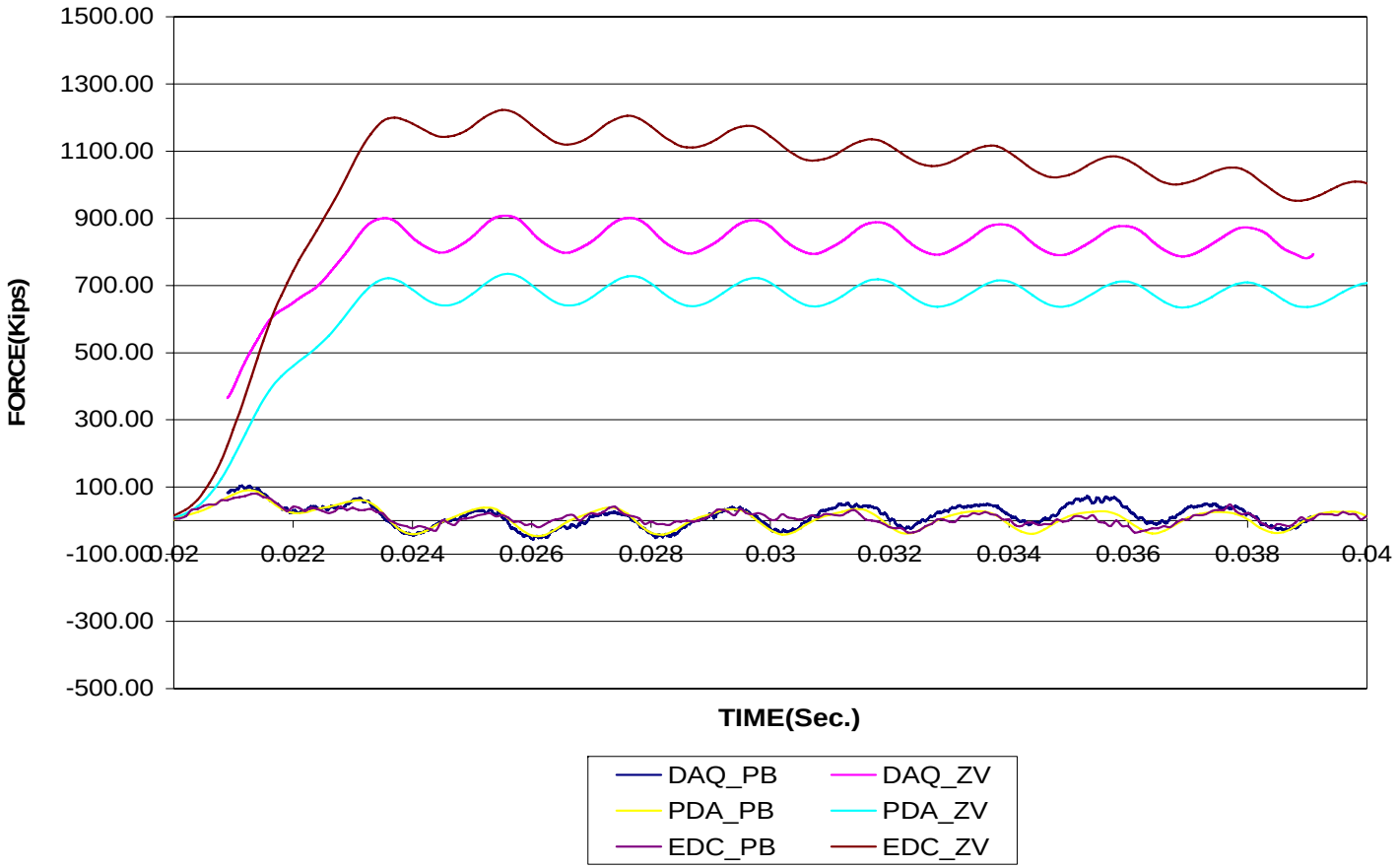

Figure 2-14. Computed forces vs. time at pile bottom.

The error was due to the location of the gages (36 in from tip) which generated a cyclical inertial force (m a) equal to approximately 35 kips (see Figure 2-11 accel.) from the mass below the gages.

After assessing P and ZV_T, the wave up (F_{up}) and down (F_{dw}) forces were computed from Eq. 2-11. Shown in Table 2-1 and 2-2 are calculations for the Tracer DAQ signal. Plotted in Figures 2-15 and 2-16 are the wave up (F_{up}) and down (F_{dw}) forces as a function of time for the top and bottom of the pile.

In the case of the top gages, F_{dw} built quickly from the start at 0.019 sec to the peak (341 kips for PDA, 401 kips for Tracer DAQ, and 595 kips for EDC) at 0.023 sec; whereupon it remained with cyclicity of ±40 kips and periodicity of 0.0017 sec which corresponded to 2L/c. The upward traveling wave (F_{up}) built slower, which did not reach a peak until 0.025 sec (2L/c behind F_{dw}) with slightly lower maximum values (tension) as shown in Table 2-3. The tip gages showed a F_{dw} of 425 kips for DAQ, 565 kips for EDC, and 340 kips for PDA and upward traveling F_{up} values of -419 kips from DAQ, -559 kips from EDC, and -340 kips from PDA.

Evident from Table 2-3 and Figures 2-15 and 2-16, the hammer blows developed a downward traveling compression wave into the pile which was reflected from the tip as a tension wave (Figure 2-16) traveled to the pile top (Figure 2-15) as tension and reflected back at the top as compression. Because the material is linear elastic, the wave travels up and down the object with only a slight loss in amplitude to pile damping.

Also, theoretically speaking, top F_{dw} should be bigger than tip F_{dw} for downward wave due to energy losing during wave propagation, and vice versa for upward wave. Shown in Figures 2-16 and 2-17 are the results for each system (i.e., DAQ, EDC, and PDA).

Table 2-1. Excel Calculation Sheet for F_{up} and F_{dw} (TracerDAQ Partial)

C(ft/sec)	14500.00	E(ksi)	6800.00	A(in^2)	324.00	Z(kip*s/ft)	151.94					
FORCE_UP IN kips							FORCE_DOWN IN kips					
Top		Bottom		Top	Bottom		Top		Bottom		Top	Bottom
CH 1	CH2	CH3	CH4	AVERAGE	AVERAGE		CH 1	CH2	CH3	CH4	AVERAGE	AVERAGE
…	…	…	…	…	….		…	…	…	…	…	…
-376.70	-393.31	-455.98	-440.38	-385.01	-448.18		361.28	377.89	458.73	446.44	369.59	452.59
-377.64	-393.11	-456.18	-441.20	-385.38	-448.69		360.57	378.24	458.39	445.61	369.40	452.00
-378.31	-393.19	-458.59	-442.29	-385.75	-450.44		360.13	378.31	455.84	444.49	369.22	450.17
-378.43	-392.72	-457.69	-442.00	-385.57	-449.85		360.26	378.95	456.59	444.75	369.60	450.67
-378.01	-391.70	-458.16	-441.98	-384.86	-450.07		360.94	380.13	455.96	444.73	370.53	450.35
-380.35	-389.59	-458.36	-443.61	-384.97	-450.98		358.87	382.43	455.60	443.06	370.65	449.33
-380.49	-390.51	-458.27	-440.55	-385.50	-449.41		359.00	381.69	455.52	446.06	370.35	450.79
-382.83	-390.61	-459.00	-441.34	-386.72	-450.17		356.94	381.79	454.60	445.20	369.37	449.90
-382.43	-390.16	-458.91	-441.85	-386.29	-450.38		357.64	382.45	454.50	444.60	370.05	449.55
-382.58	-390.27	-459.64	-442.08	-386.42	-450.86		357.80	382.56	453.58	444.28	370.18	448.93
-383.56	-390.38	-459.53	-442.03	-386.97	-450.78		357.13	382.67	453.47	444.23	369.90	448.85
-383.45	-389.39	-459.42	-441.98	-386.42	-450.70		357.56	383.89	453.37	444.18	370.72	448.77
-380.59	-389.51	-459.86	-443.29	-385.05	-451.58		360.76	384.01	452.70	442.74	372.38	447.72
-380.20	-389.64	-460.02	-443.23	-384.92	-451.62		361.48	384.13	452.31	442.68	372.80	447.49
-382.03	-390.04	-457.97	-443.43	-386.03	-450.70		360.00	383.98	454.12	442.33	371.99	448.22
-382.20	-390.72	-458.12	-443.91	-386.46	-451.01		360.17	383.56	453.72	441.70	371.87	447.71
…	…	…	…	…	…		…	…	…	…	…	…

Table 2-2. Excel Calculation Sheet for P_B and ZV (TracerDAQ Partial)

P_B IN kips					
Top		Bottom		Top	Bottom
CH 1	CH2	CH3	CH4	AVERAGE	AVERAGE
…	…	…	…	…	…
85.37	-18.18	39.66	-21.48	33.60	9.09
84.27	-18.18	39.11	-21.48	33.05	8.81
82.62	-22.03	34.15	-23.13	30.29	5.51
82.07	-19.83	35.80	-23.13	31.12	6.33
80.42	-21.48	35.80	-23.68	29.47	6.06
85.92	-21.48	34.70	-25.89	32.22	4.41
85.37	-20.38	34.15	-26.44	32.50	3.86
82.62	-20.38	36.35	-27.54	31.12	4.41
80.42	-22.03	33.05	-28.09	29.19	2.48
82.07	-20.38	34.15	-32.50	30.84	0.83
83.72	-23.68	34.70	-31.40	30.02	1.65
82.07	-27.54	34.15	-35.80	27.26	-0.83
80.42	-26.44	39.66	-35.80	26.99	1.93
80.42	-24.79	39.11	-38.01	27.82	0.55
76.01	-28.09	38.01	-40.76	23.96	-1.38
77.11	-24.79	36.35	-40.76	26.16	-2.20
77.11	-24.79	37.45	-41.86	26.16	-2.20
74.36	-24.79	41.86	-41.86	24.79	0.00
73.81	-18.18	39.66	-43.51	27.82	-1.93
71.60	-16.52	39.66	-43.51	27.54	-1.93
71.60	-16.52	39.11	-43.51	27.54	-2.20
…	…	…	…	…	…

ZV IN kips					
Top		Bottom		Top	Bottom
CH 1	CH2	CH3	CH4	AVERAGE	AVERAGE
…	…	…	…	…	…
728.74	722.05	894.82	905.58	725.39	900.20
729.14	722.50	894.83	905.67	725.82	900.25
729.56	722.95	894.83	905.75	726.25	900.29
729.99	723.41	894.83	905.83	726.70	900.33
730.44	723.88	894.81	905.90	727.16	900.35
730.90	724.35	894.78	905.95	727.63	900.37
731.38	724.84	894.75	906.00	728.11	900.37
731.86	725.33	894.70	906.04	728.60	900.37
732.37	725.83	894.64	906.07	729.10	900.35
732.88	726.33	894.57	906.09	729.61	900.33
733.41	726.84	894.49	906.10	730.13	900.29
733.95	727.36	894.40	906.09	730.65	900.25
734.50	727.88	894.29	906.08	731.19	900.19
735.07	728.41	894.18	906.06	731.74	900.12
735.64	728.95	894.05	906.02	732.30	900.04
736.23	729.49	893.91	905.98	732.86	899.94
736.83	730.04	893.76	905.92	733.43	899.84
737.44	730.59	893.59	905.85	734.01	899.72
738.06	731.14	893.41	905.77	734.60	899.59
738.69	731.70	893.22	905.67	735.20	899.45
739.33	732.27	893.02	905.56	735.80	899.29
…	…	…	…	…	…

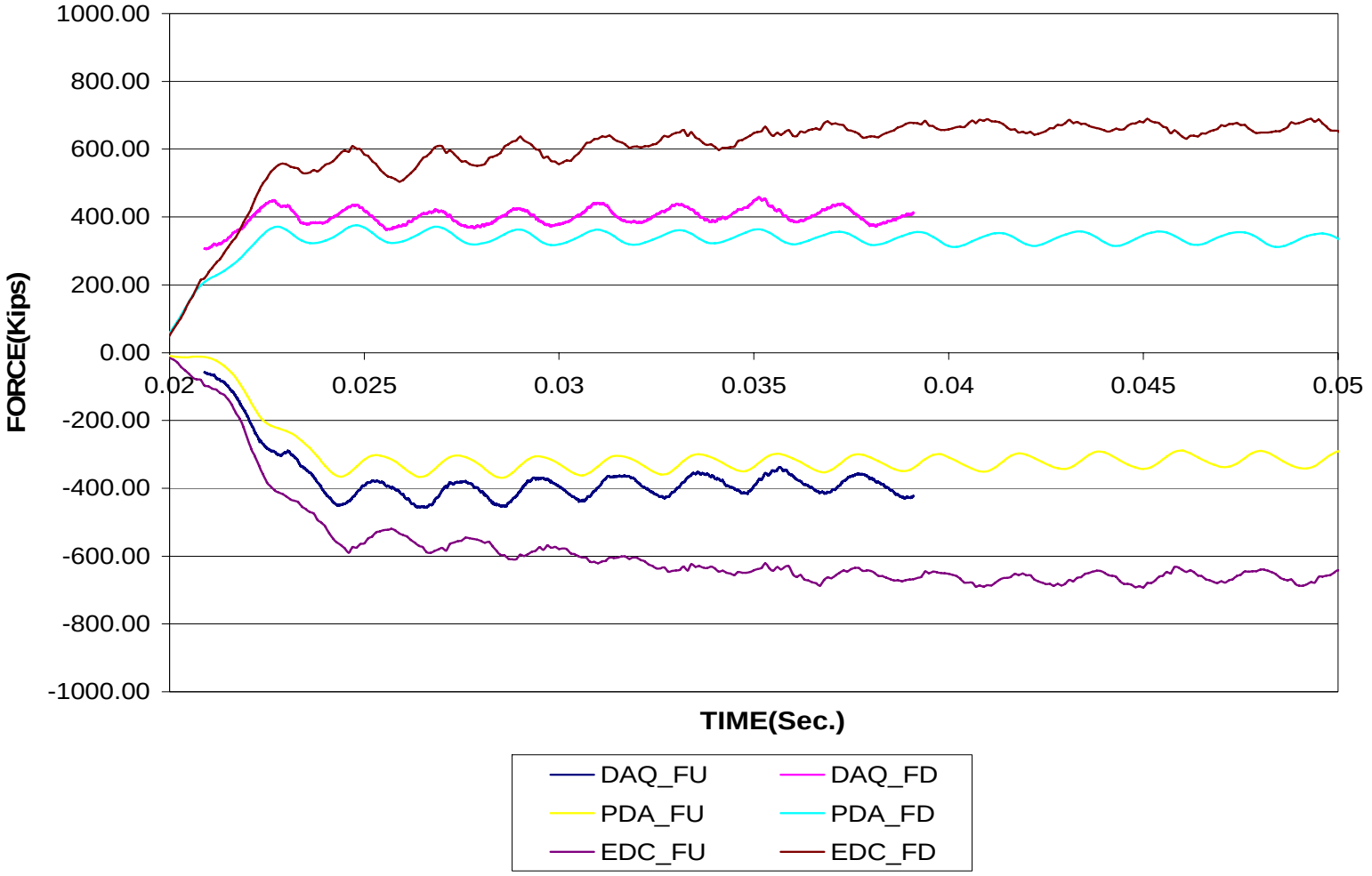

Figure 2-15. F_{up} and F_{dw} at the top of the pile (near hammer).

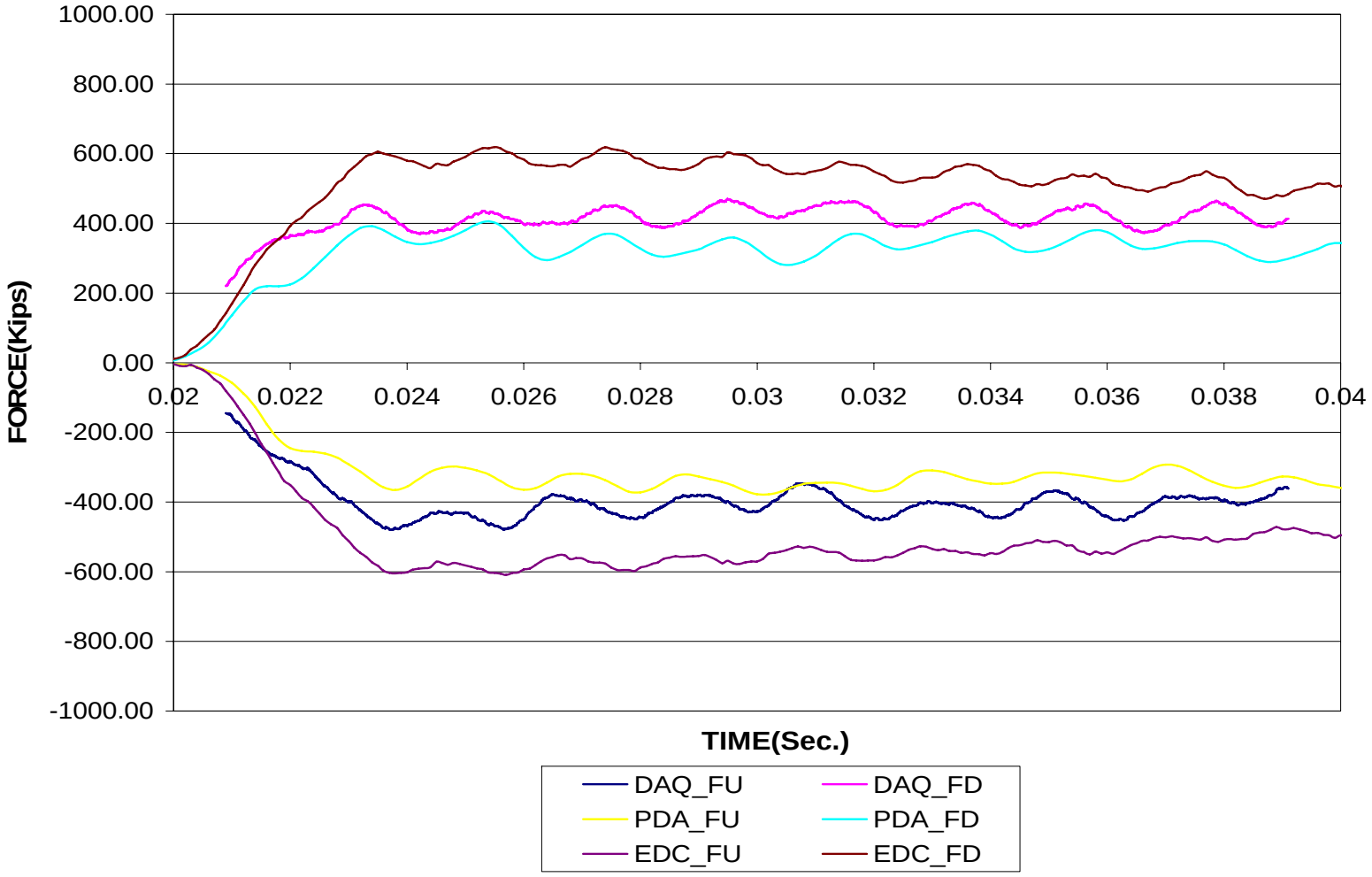

Figure 2-16. F_{up} and F_{dw} at the bottom of the pile.

Generally, there is a loss with a few exceptions; however, the difference is well within the accuracy of the instrumentation. The latter would not be the case if the pile had been embedded in soil.

Table 2-3. Statistic Analysis for F_{up} and F_{dw}

		DAQ (kips)		EDC (kips)		PDA(kips)	
		Average	Stdev	Average	Stdev	Average	Stdev
F_{up}	Top	-400	27	-595	37	-330	21
	Tip	-419	22	-559	24	-340	19
F_{dw}	Top	401	21	595	36	341	16
	Tip	425	25	565	29	340	22

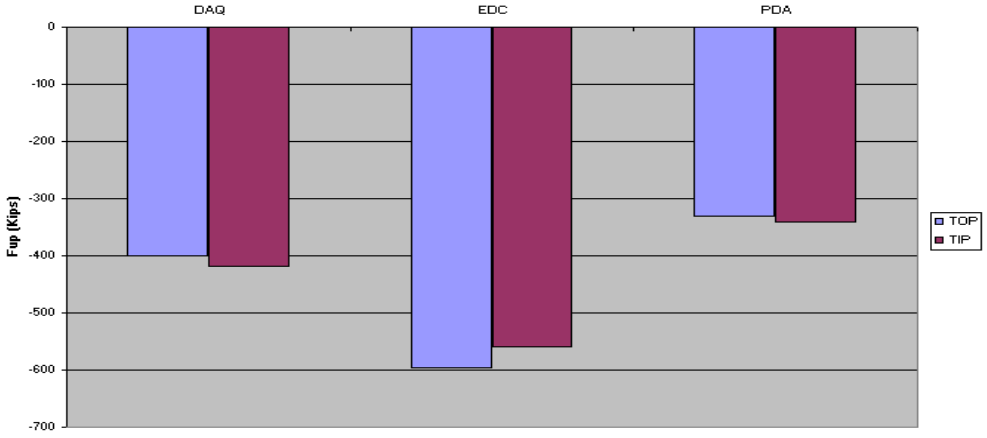

Figure 2-17. Comparison of peak F_{up} between tip and top of pile.

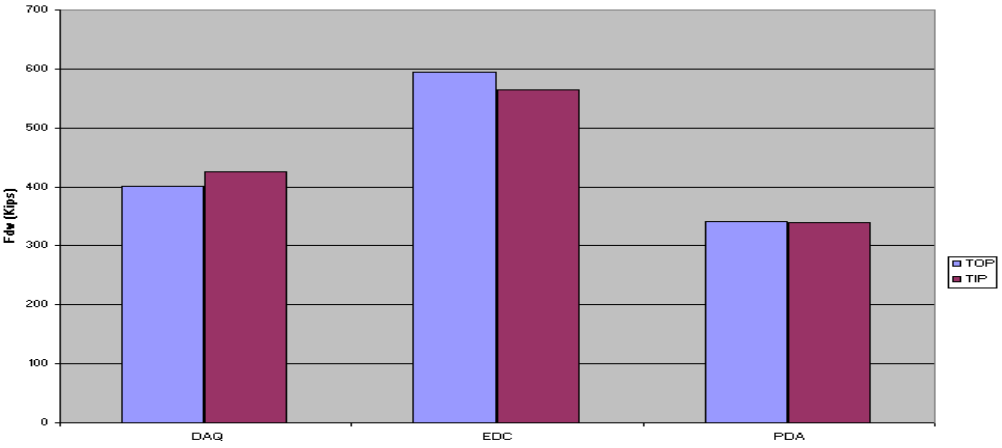

Figure 2-18. Comparison of peak F_{dw} between tip and top of pile.

2.4 Conclusions of Pile Wave Analyses without Soil

The following conclusions were drawn from this effort:

- Raw strain and acceleration data collected from the three different data acquisition systems were very similar, with the Tracer DAQ showing the most noise which was attributed to surface waves.
- Using Excel Fourier Analysis filtering tools can successfully mitigate noise, as does SmartPile Review software.
- Top acceleration data from EDC seems offset more on positive than negative at the beginning, which will affect integrated velocity and thus force.
- Wave propagation analysis shows that average P wave matches among three data acquisition systems within ±50 Kips along "0" horizontal axle. The variance might be attributed to laboratory error which is about 5-10% pile capacity.
- The trend for ZV wave is almost the same among three systems; PDA was the smallest, following by DAQ and EDC, so do F_{up} and F_{dw} waves.
- Theoretically speaking, top F_{dw} should be bigger than tip F_{dw} for downward wave due to energy lost during wave propagation, vice versa for upward wave. However, this trend is not obvious at least from Figures 2-17 to 2-18. A couple of systems (DAQ, EDC) were almost equivalent, and slightly less, such as F_{up} for EDC and F_{dw} for DAQ. However, due to the standard deviation of the data and accuracy of the systems, they were within acceptable values.

CHAPTER 3
EXPERIMENTAL PILE WAVE PROPAGATION WITH SOIL

3.1 Pile-Soil Placement

For second and third phases, involving verification of pile particle motions and stresses due to soil-pile interaction, it was decided to place a standard 18-in × 18-in × 30-ft pile in a Florida silty-sand soil horizontally, as shown in Figure 3-1. The placement of the pile horizontally results in uniform soil stress state along the pile length which would ensure a uniform skin friction and damping per unit length of the pile. The 150 cubic yards of silty-sand (Figure 3-2) was obtained from a FDOT borrow pit and trucked to the UF coastal facility by SMO. Prior to placement, SMO performed ASTM T180 Proctor testing and established optimum moisture (11%) and dry densities (110 pcf) for the soil. Approximately 3.5 ft of silty sand was placed in 8-in lifts at T180 optimum conditions (Figure 3-3) before the pile was placed. All compaction was performed with two walk behind compactors (Figure 3-3). For every lift or second lift, SMO personnel ran nuclear densities to assess dry densities and moistures. Figure 3-4 shows the completed compacted embankment with the 18-in × 18-in × 30-ft prestressed concrete pile embedded 20 ft into the compacted silty-sand.

3.2 Pile Instrumentation

3.2.1 Internal Pile Instrumentation

A new 18-in × 18-in × 30-ft instrumented pile was cast at Durastress for the second phase of soil-pile interaction. The new pile had two independent sets of EDC sensors. Each set had three separate sensor packs (strain and acceleration) which were placed on

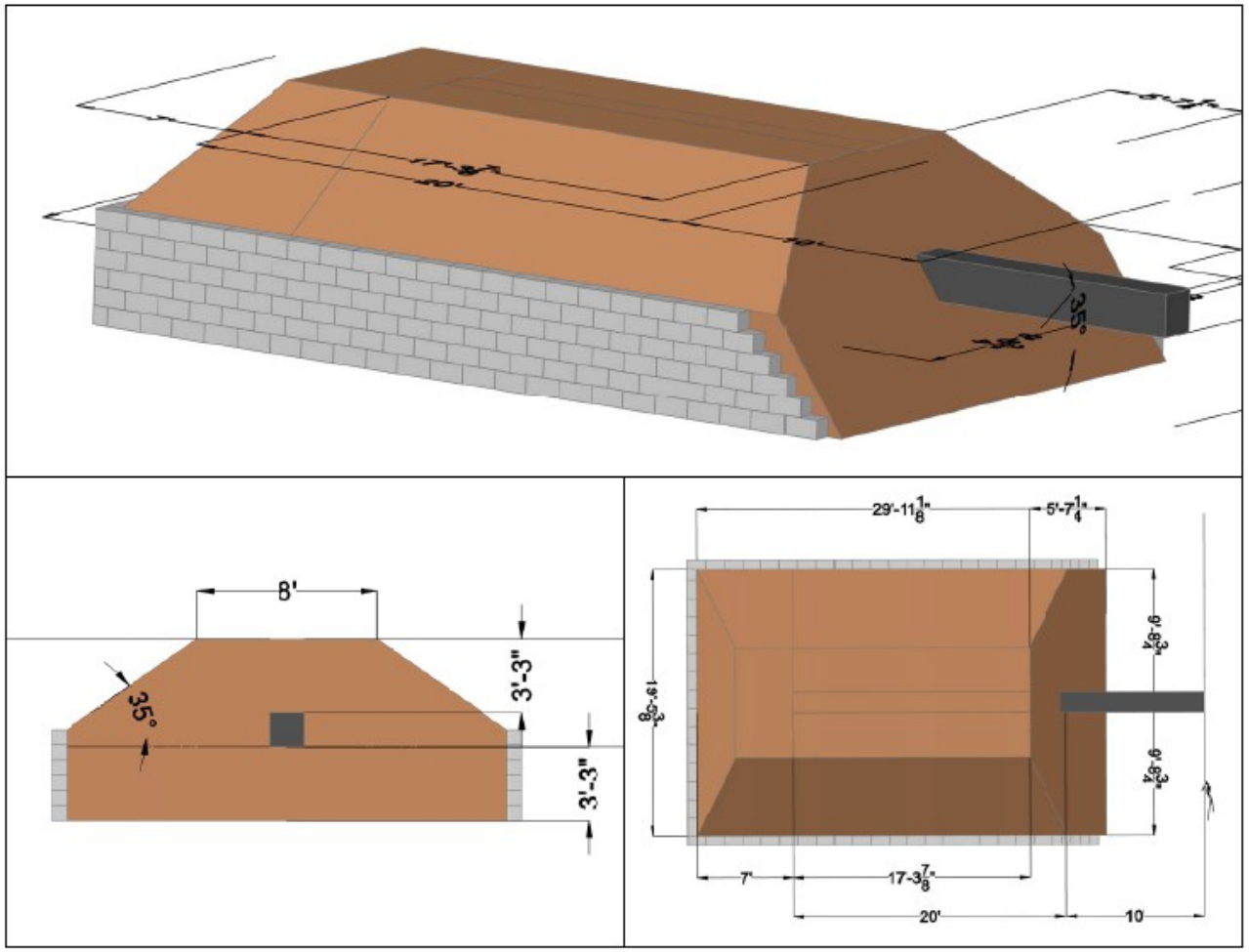

Figure 3-1. Layout of soil embankment and test pile for pile-soil dynamic testing.

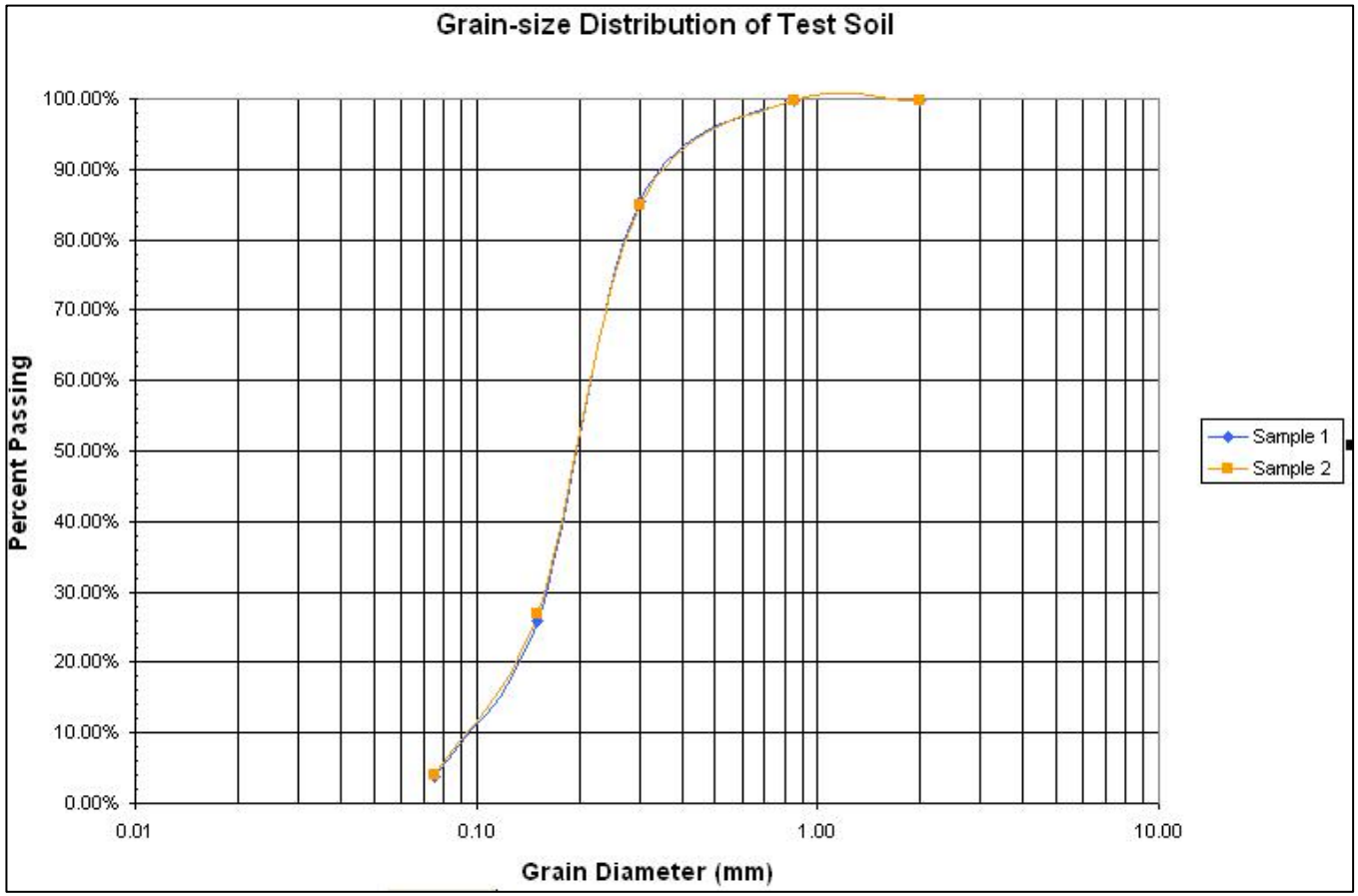

Figure 3-2. Test soil, silty-sand from Lake City, Florida.

Figure 3-3. Placement of compacted silty-sand adjacent to instrumented pile.

Figure 3-4. Compacted 7-ft high embankment with 18-in×18-in×30-ft precast pile embedded 20 ft.

the centerline of the pile near the top, bottom and middle of the pile as shown in Figure 3-5. For instance, set D1, was placed at 3 ft from top, 10 ft from the tip and 18 in from the tip, whereas, set D2, was placed 3 ft 9 in from top, 15 ft from top, and 5 ft from the tip. Also cast within the pile are two sets of sister bar strain gages (Figure 3-5) located 3 ft 9 in from the top and 5 ft from the tip. Each set of sister bars had 3 in of cover to differentiate bending from axial strains within the pile. The EDC instrumentation was donated by Smart-Structures Inc, and the sister bar instruments were donated by AFT.

3.2.2 External Pile Instrumentation

As undertaken in Chapter 2, a comparison of particle pile motion and stresses from internal and external gages was to be performed on the pile embedded in soil. Again, the particle accelerations would be integrated to give velocities at top and bottom of pile which would be used with pile strains to obtain wave down and wave up forces at both locations.

Figure 3-5 shows the layout, and Figures 3-6 and 3-7 show the final placed instruments on the pile. Again, each set (e.g., strain and acceleration) was placed on each side of the pile to separate the bending from the axial behavior. In the case of the PDI equipment, the piezo-resistant accelerometers were placed at the bottom and the piezo-electric accelerometers were placed at the top. Two separate sets of instruments (PDI and Tracer DAQ) were employed to study the influence of sampling rate.

To protect each instrument's wires, each were run in a 1/2-in × 1/2-in channel cut into the pile and covered with high strength tape (Figure 3-6). To ensure that the external instruments were not sheared off due to driving, the instruments were covered with Styrofoam and a metal box. The final pile instrumentation and wiring prior to placement in the soil is shown in Figure 3-3.

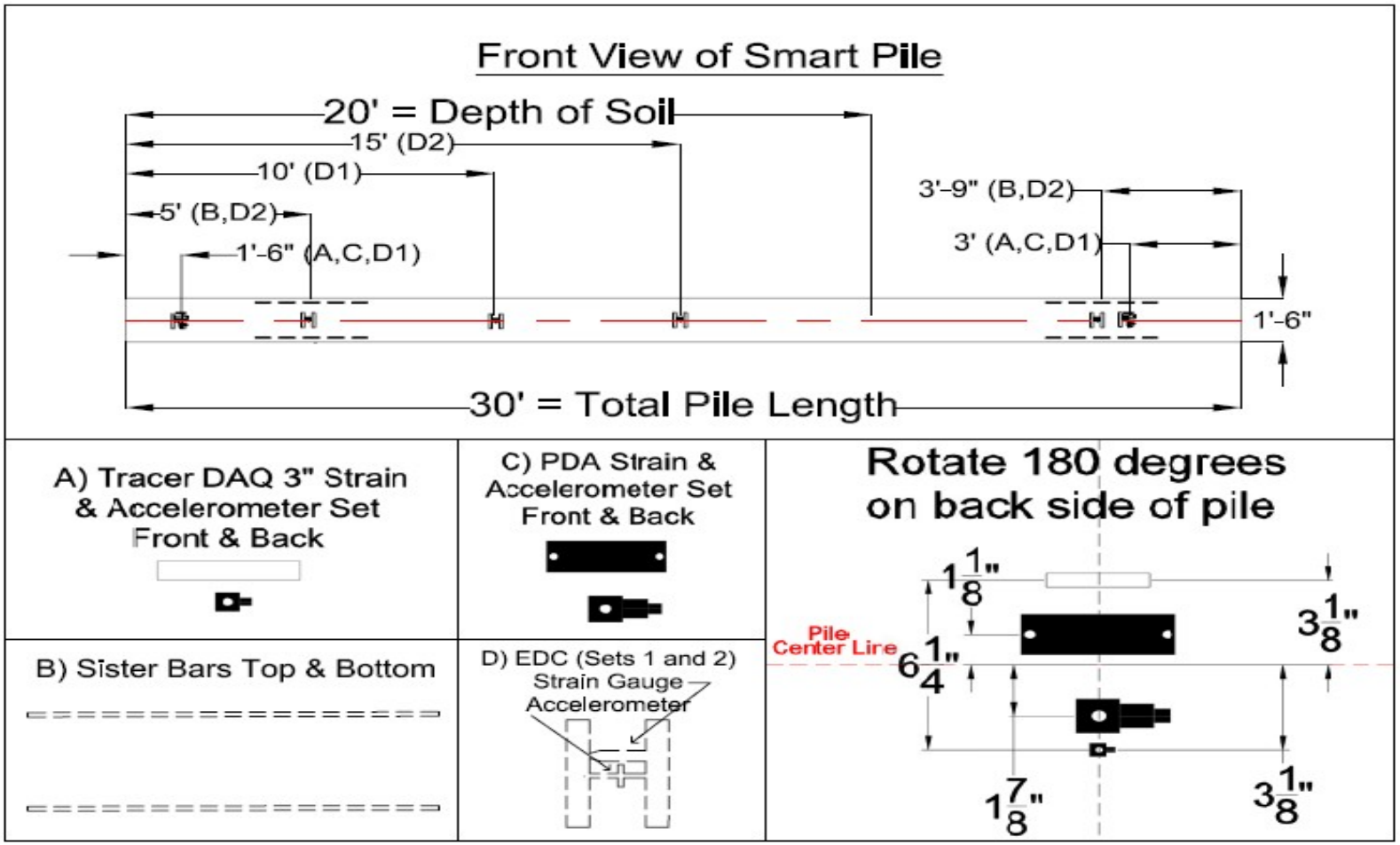

Figure 3-5. Layout of the internally and externally instrumented 18-in ×18-in ×30-ft test pile.

Figure 3-6. Prestressed 18-in × 18-in × 30-ft pile with external sensors being attached.

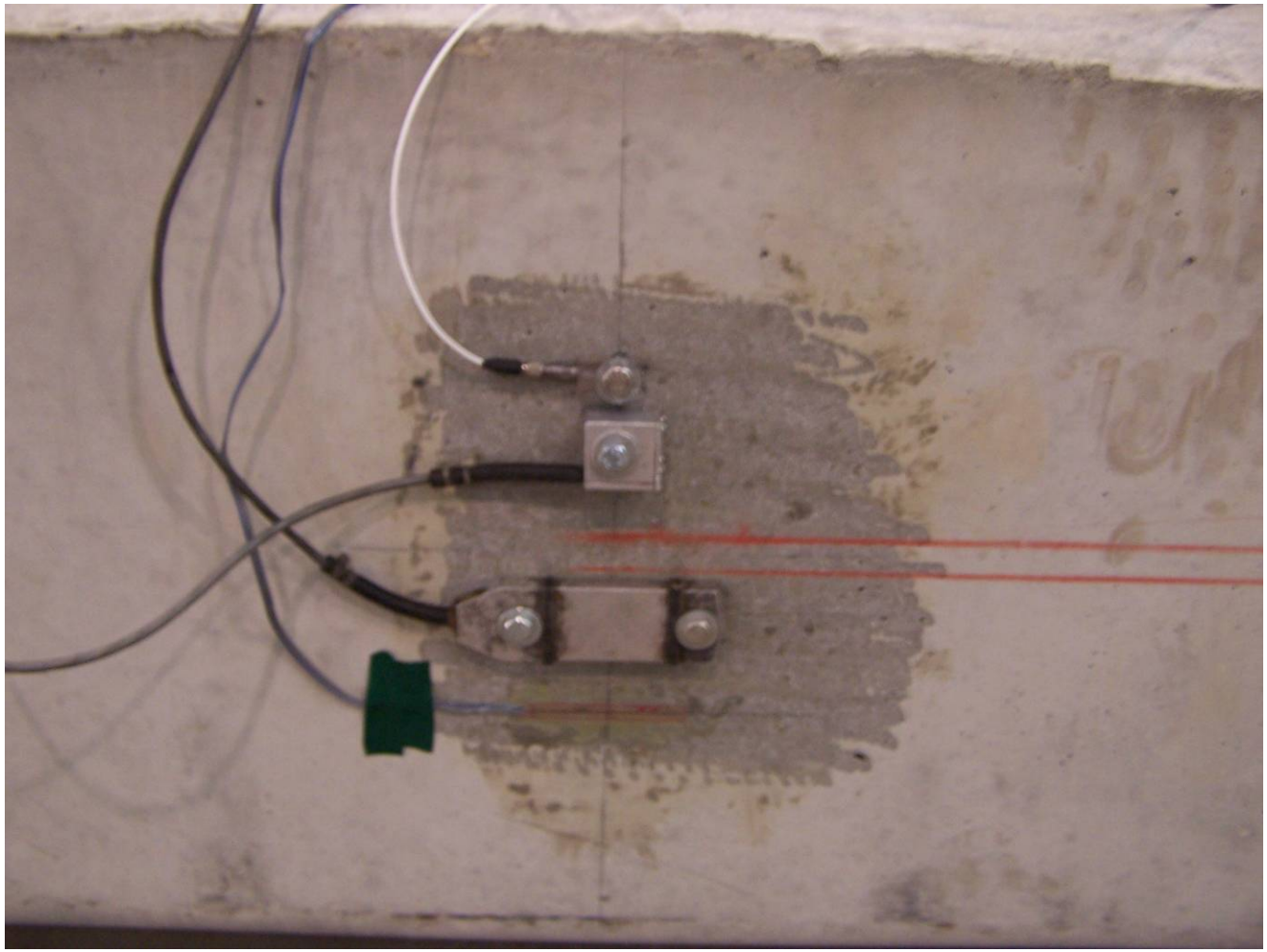

Figure 3-7. Instrumentation at 18 in from pile tip: PDI (strain and accelerometers) and Tracer DAQ (strain and accelerometers).

3.3 Top and Bottom Pile Response for Low and High Hammer Impact Energies

The embedded 18-in × 18-in × 30-ft pile was struck by a 1000-lb hammer (steel casing filled with concrete) at various drop heights (Figure 3-8). The hammer was suspended as a pendulum by a 20-ft square channel connected to a roller bearing at top of a 30-ft steel gantry of a large forklift. The hammer strike distances (Figure 3-8) were controlled at approximately two different lengths: 1) 4 to 6 ft and 2) 14 to 16 ft. The 4- to 6-ft chord length (Figure 3-8) corresponds to a vertical drop height of approximately 1 ft, whereas the 14- to 16-ft chord corresponds to a vertical hammer drop of 6 ft (i.e., potential energy). Since the mobilized skin friction and damping of each may be different (pile movements of 0.006 in vs. 0.25 in), it was decided to analyze each separately.

Figure 3-8. Setting up for dynamic impact of 18-in × 18-in × 30-ft embedded pile.

Both the EDC and PDA had their own data collection system which was set to record five thousand samples per second. In the case of the UF gages (Figure 3-9) a Tracer DAQ data acquisition system capable of reading twenty thousand samples per second was used. For all systems, the triggering for data recovery was done manually. The process involved raising the hammer to the appropriate stand off distance, and holding it with either a wood support or a cable until the data acquisition system was setup. Next, the wood support or cable was released, then the data acquisition system was triggered and the pile was struck by the hammer. For all tests, a 3/4-in thick plywood plate was used as the pile cushion.

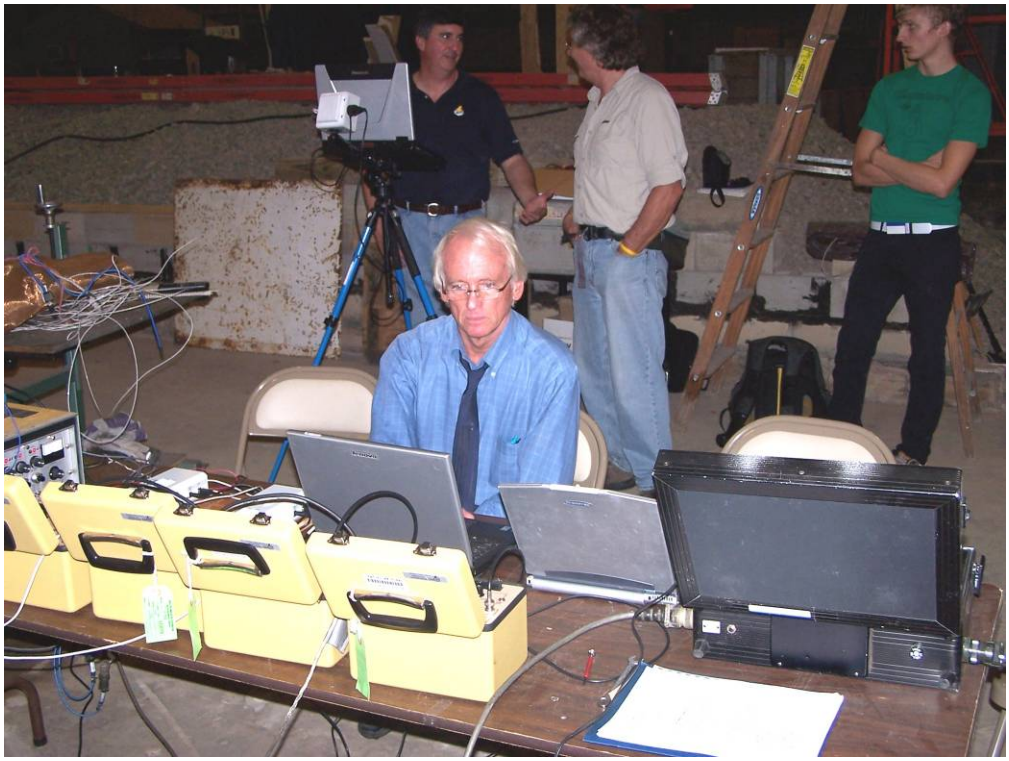

Figure 3-9. Tracer DAQ, EDC and PDA Data Acquisition Systems.

3.3.1 Pile Response for Low Impact Hammer Energies

Approximately ten low impact hammer energy (4- to 6-ft chord length, 1-ft vertical drop) blows were performed on the 18-in × 18-in × 30-ft pile with the top and bottom pile

instrumentation. Shown in Figures 3-10 and 3-11 are the maximum recorded accelerations at the top and bottom of the pile from internal and externally mounted gages. Evident the comparison between the gages at both ends of the pile are quite good with the EDC showing slightly higher peaks. The latter may be due to their location, i.e., centroid vs. boundary location for the Tracer DAQ and PDA. Also note the increase in particle acceleration of the tip vs. the top of the pile (i.e., 1200 vs. 2000 gs). This was from the reflection of a compression wave to a tension wave (i.e., little tip resistance), which results in almost a doubling of particle motion at the tip. After integrating the acceleration to obtain velocity and then again, the displacements shown in Figures 3-12 and 3-13 are obtained for the top and bottom of the pile. The comparison of measured response is quite good for all the instruments compared to the accuracy of the devices (i.e., 0.05 in of movement). Interestingly, the pile is undergoing permanent deformation (0.0025-ft top and 0.0020-ft bottom), and the response is oscillating about the permanent values.

Shown in Figures 3-14 and 3-15 are measured strains at the top and bottom of the pile for blow 22 which is another 6-ft hammer drop. The displayed values are the raw data as outputted by the acquisition systems (i.e., Tracer DAQ, EDC and PDA). Due to the length of the cables and electric equipment in the UF's Coastal facility, the Tracer DAQ data exhibited some noise (approximately 4-8 microstrains). EDC and Tracer DAQ strains at the top of the pile are quite close. An examination of the PDA data at the top revealed that the top right gage was faulty and the reported results (left gage) are slightly lower than EDC and Tracer DAQ, and may have been exposed to bending strains.

The strains at the bottom of the pile (Figure 3-15) are all quite similar and are very small, due to small tip resistance, R ($R= \varepsilon_{tip} E A_{cross} = F_d + F_{up}$).

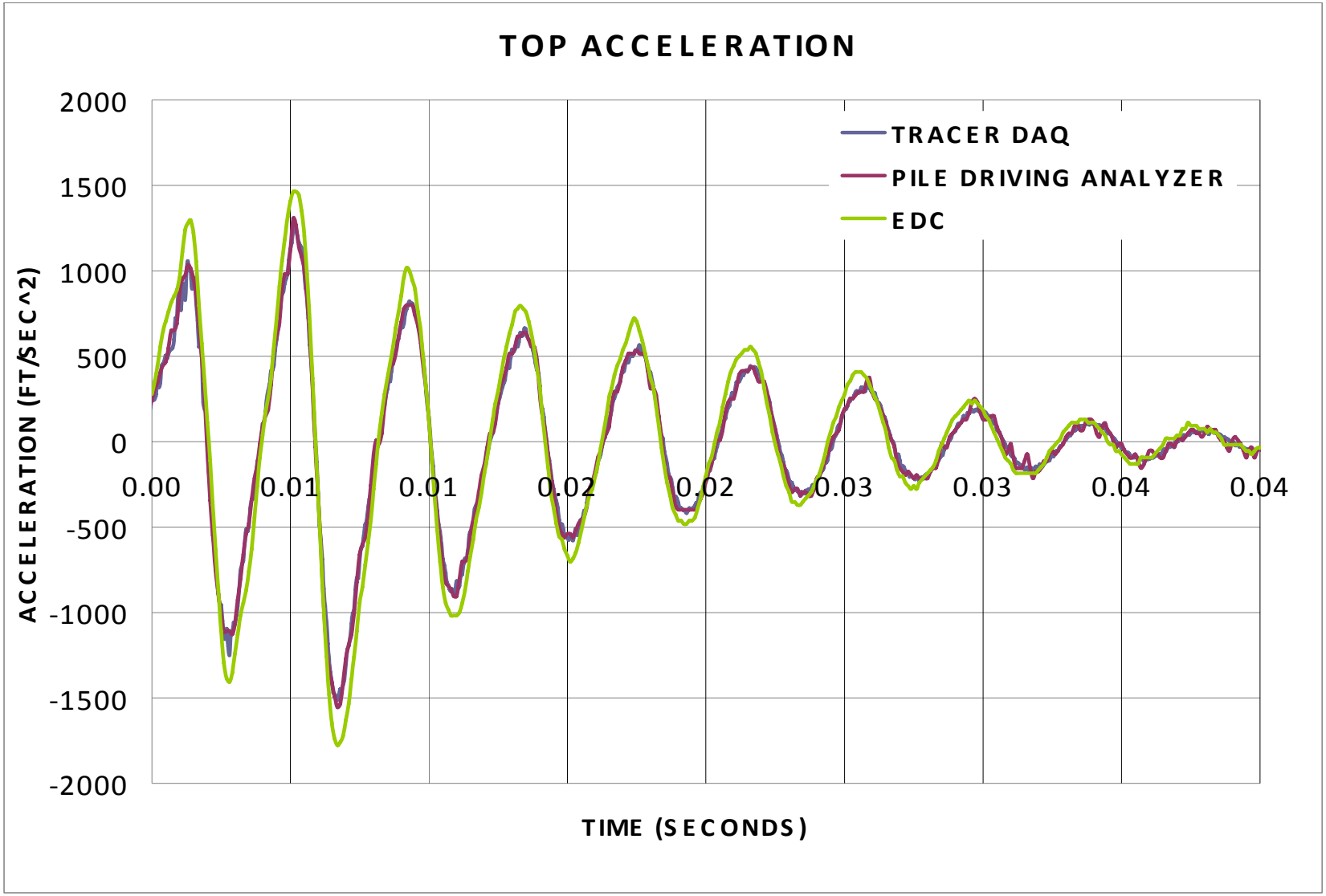

Figure 3-10. Comparison of measured top acceleration for blow 23 (1-ft drop).

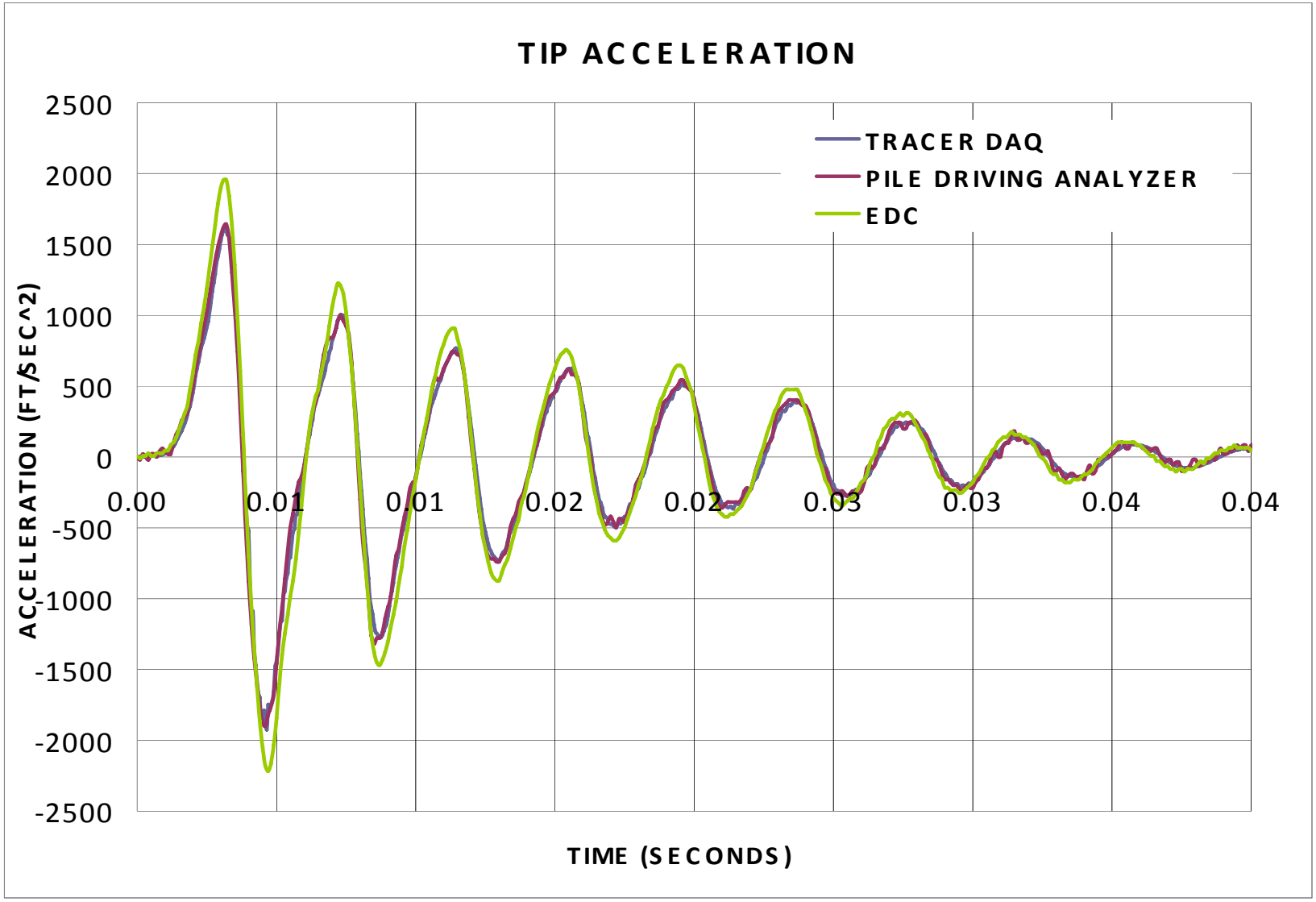

Figure 3-11. Comparison of measured tip acceleration for blow 23 (1-ft drop).

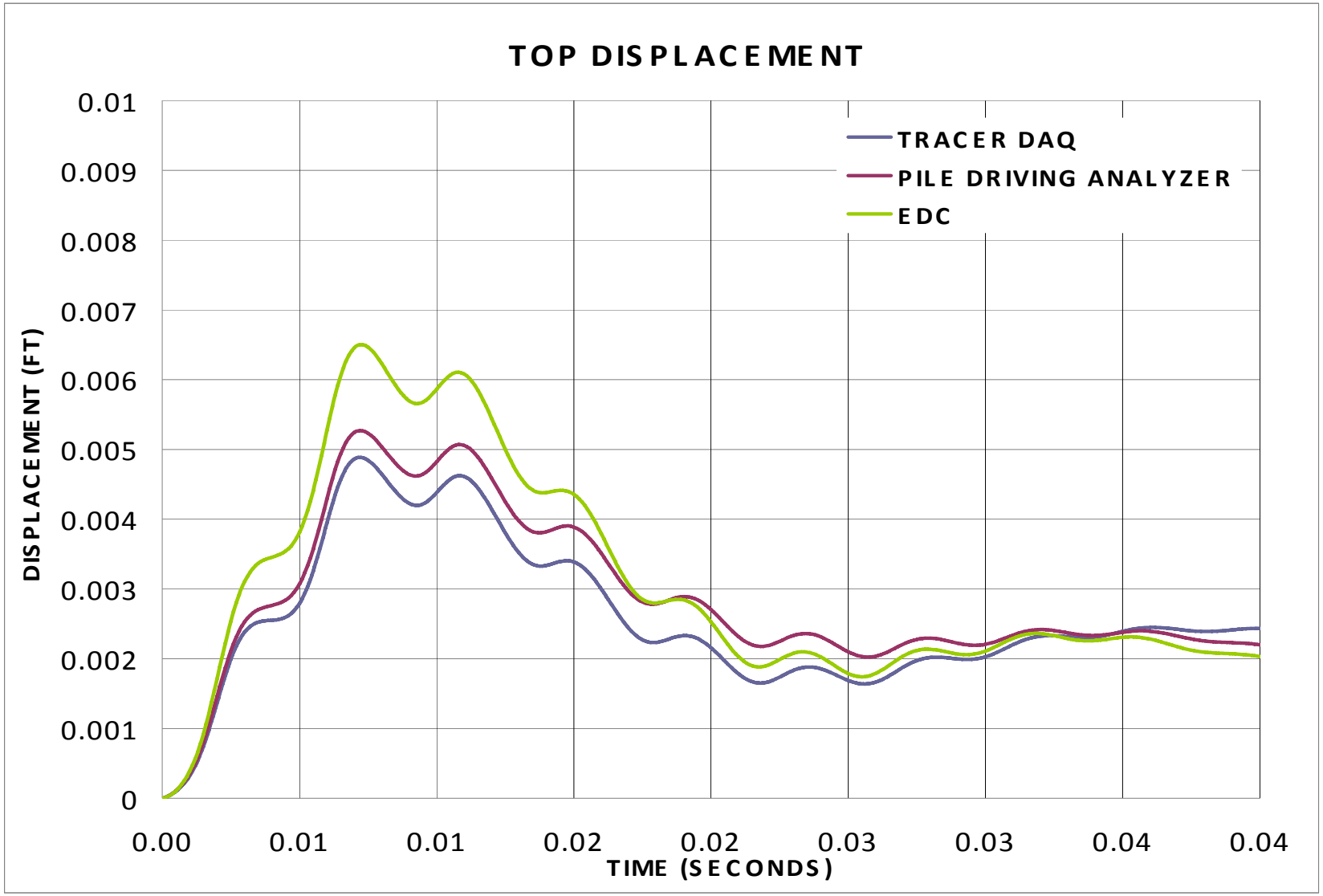

Figure 3-12. Comparison of measured top displacements for blow 23 (1-ft drop).

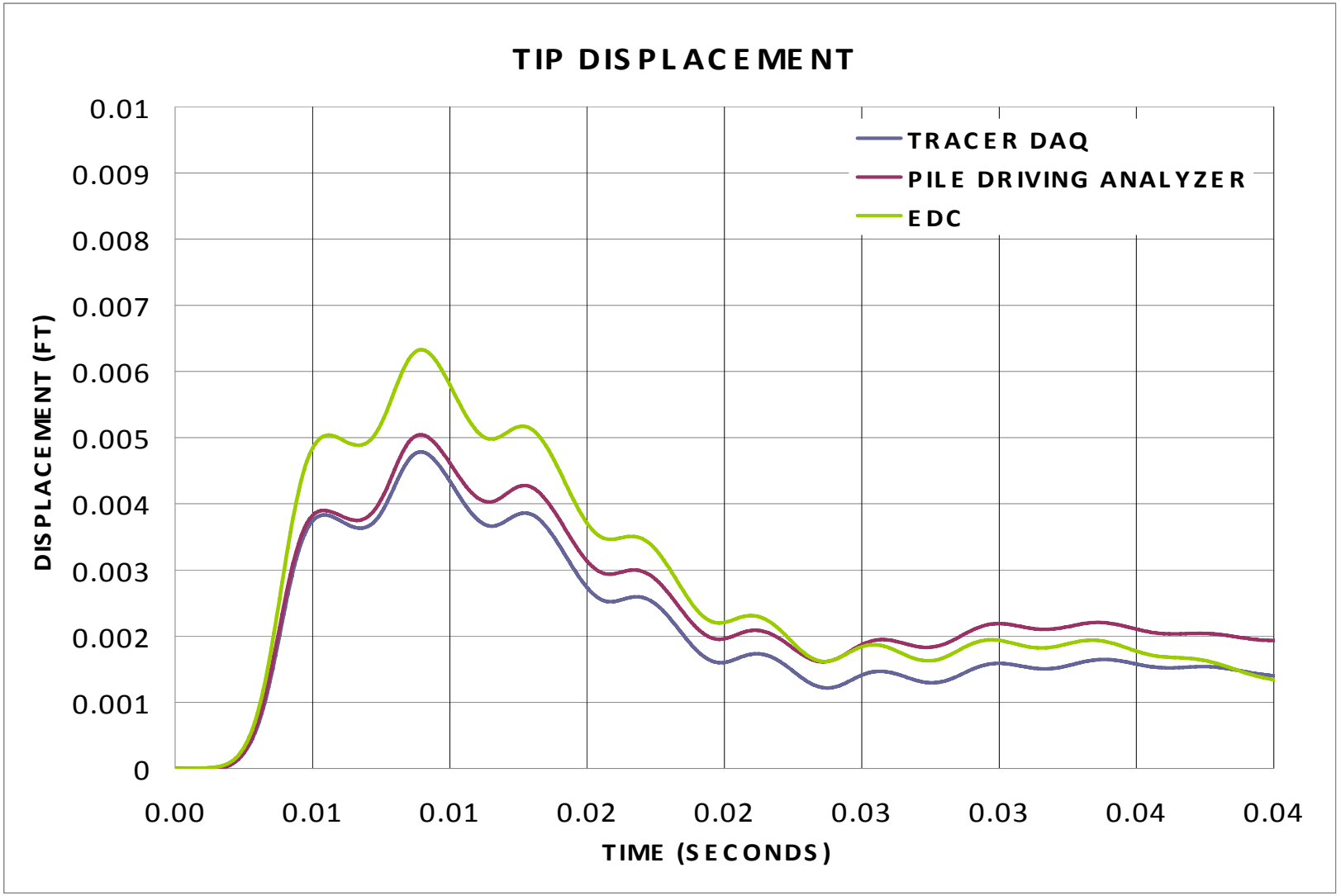

Figure 3-13. Comparison of measured tip displacements for blow 23 (1-ft drop).

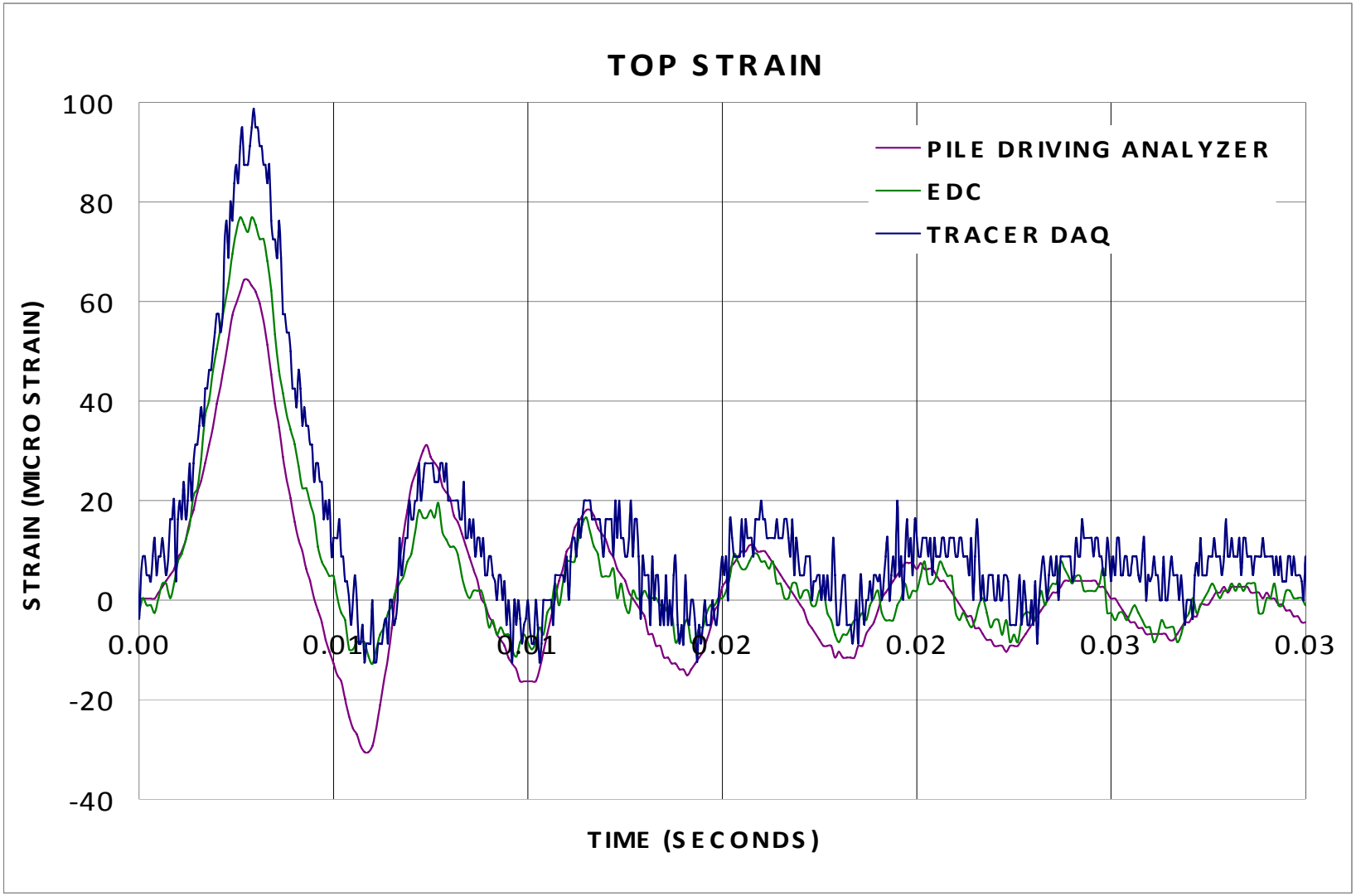

Figure 3-14. Comparison of measured top strains for blow 22 (1-ft drop).

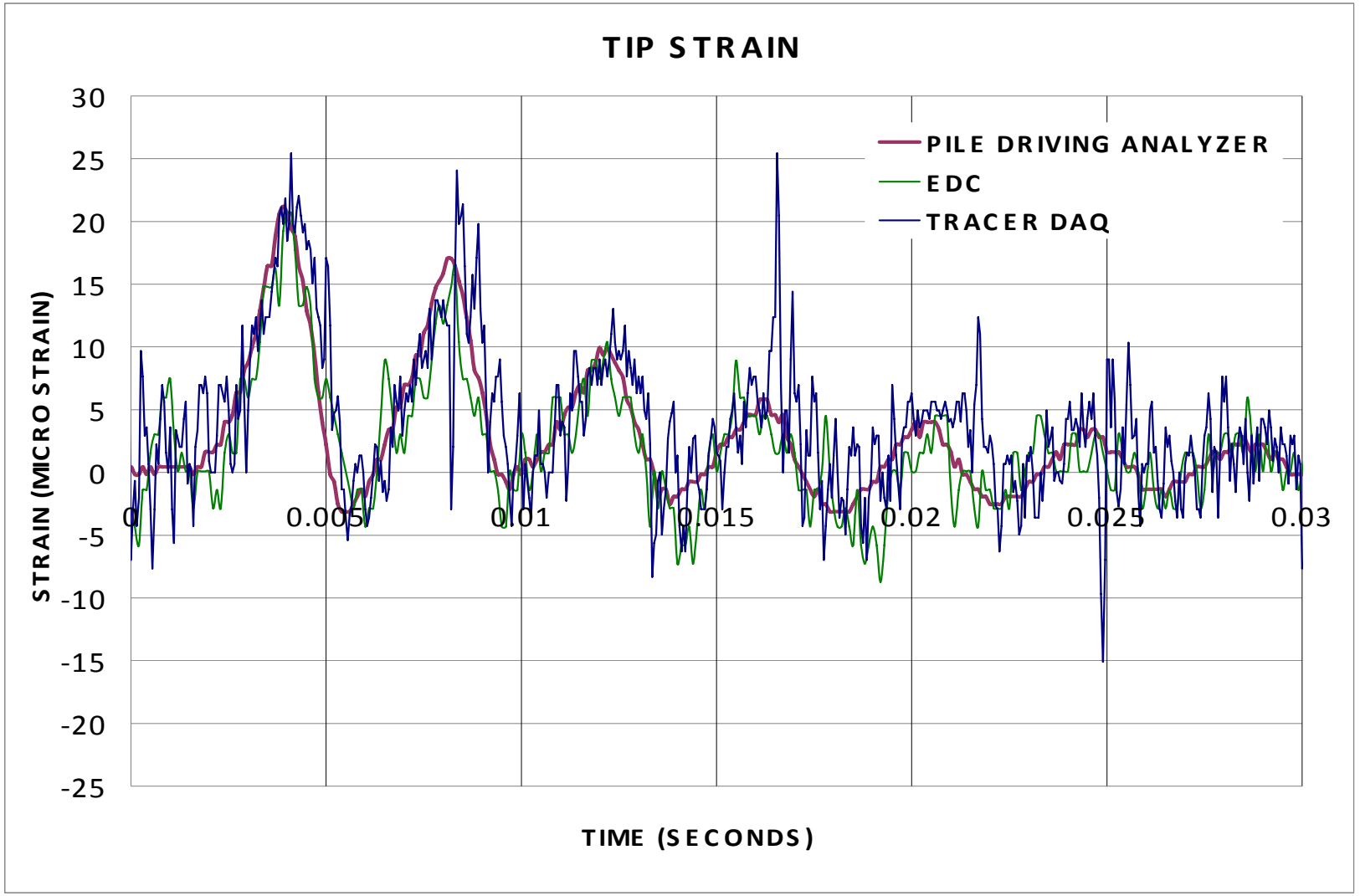

Figure 3-15. Comparison of measured tip strains for blow 22 (1-ft drop).

Using the velocities and strains at the top and bottom of the pile the forces from each may be found based on the pile impedance (Z), Young's Modulus, unit weight and cross-sectional area. Shown in Figures 3-16 and 3-17 are estimated forces from both the Tracer DAQ and EDC for blow 21. The difference in peak force from the Tracer DAQ and the EDC (i.e., 140 vs. 125 kips) is well within the accuracy of the gages. The data from the PDA is not shown due to the earlier identified one faculty top gage and only single top strain gage data was recorded (i.e., bending). Next, the wave down forces at both the top and bottom of the pile were found at both the top and bottom of the pile,

$$F_{down} = (P + ZV) / 2 \qquad \text{(Eq. 3-1)}$$

where P is the total force measured from the strain gage (ε E A) and V is the velocity computed from the acceleration at top and bottom of the pile and Z is the pile impedance. Figures 3-18 and 3-19 are the computed wave down forces at the top (Figure 3-18) and the bottom (Figure 3-19) of the pile from the Tracer DAQ and EDC data. Evident from a comparison of each instrument set, the correlation is quite good with maximum difference of 20 kips, well within the accuracy of each set of instrumentation. Also note, from the top and bottom forces, there was a loss in magnitude due to skin friction and damping. The latter is the focus of the Chapter 4, the assessment of damping and skin friction from the dynamic signals.

3.3.2 Pile Response for High Impact Hammer Energies

Approximately ten high impact hammer energy (14- to16-ft chord length, 6-ft vertical drop) blows were performed on the 18-in $\times$ 18-in $\times$ 30-ft pile with the top and bottom pile instrumentation. Typical compression stresses varied from 1.2 to 1.4 ksi with pile permanent displacements from 0.25 to 0.3 in per blow (i.e., blow rate of 40 to 48).

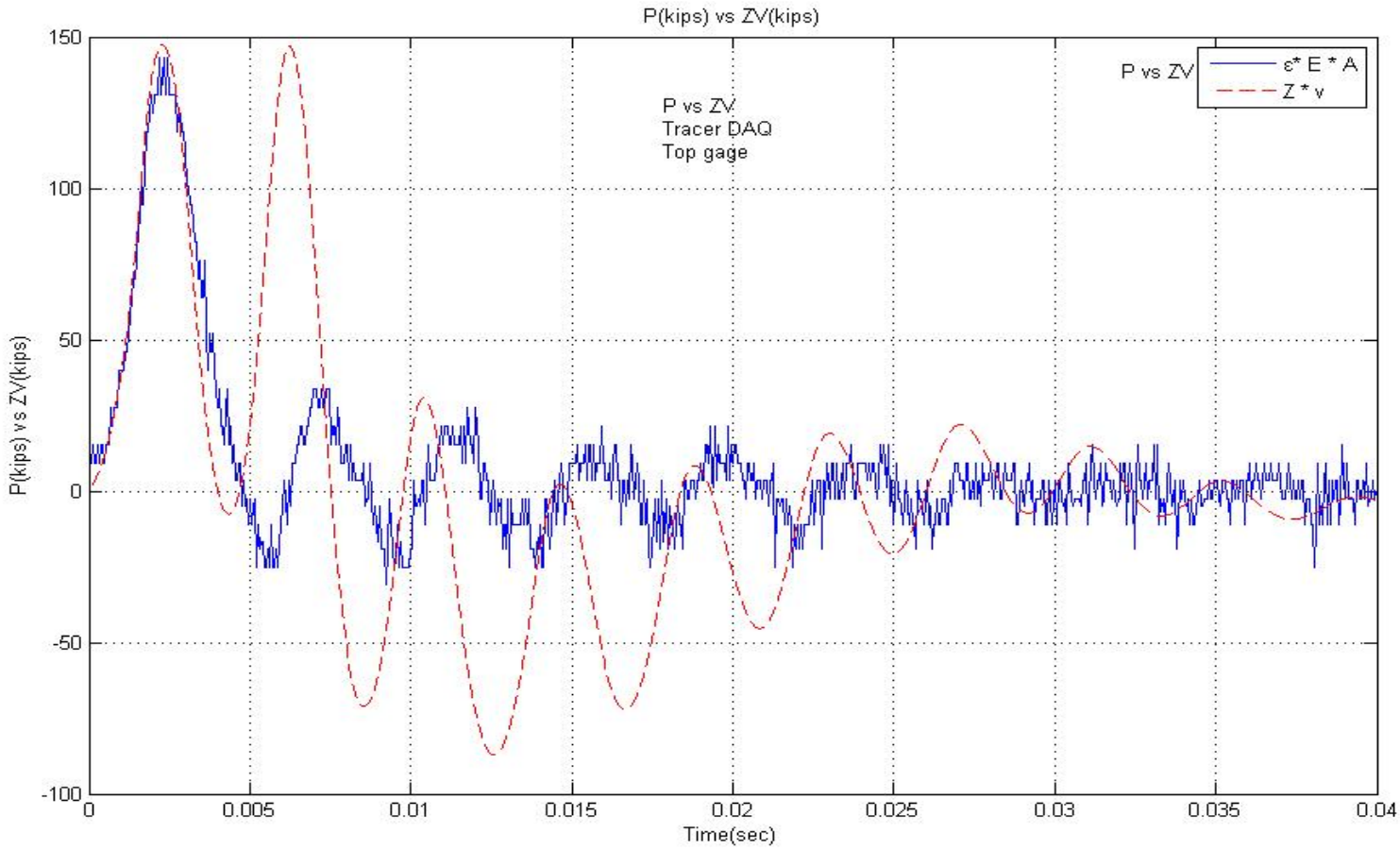

Figure 3-16. Force measured from Tracer DAQ strain and acceleration sensors at pile top.

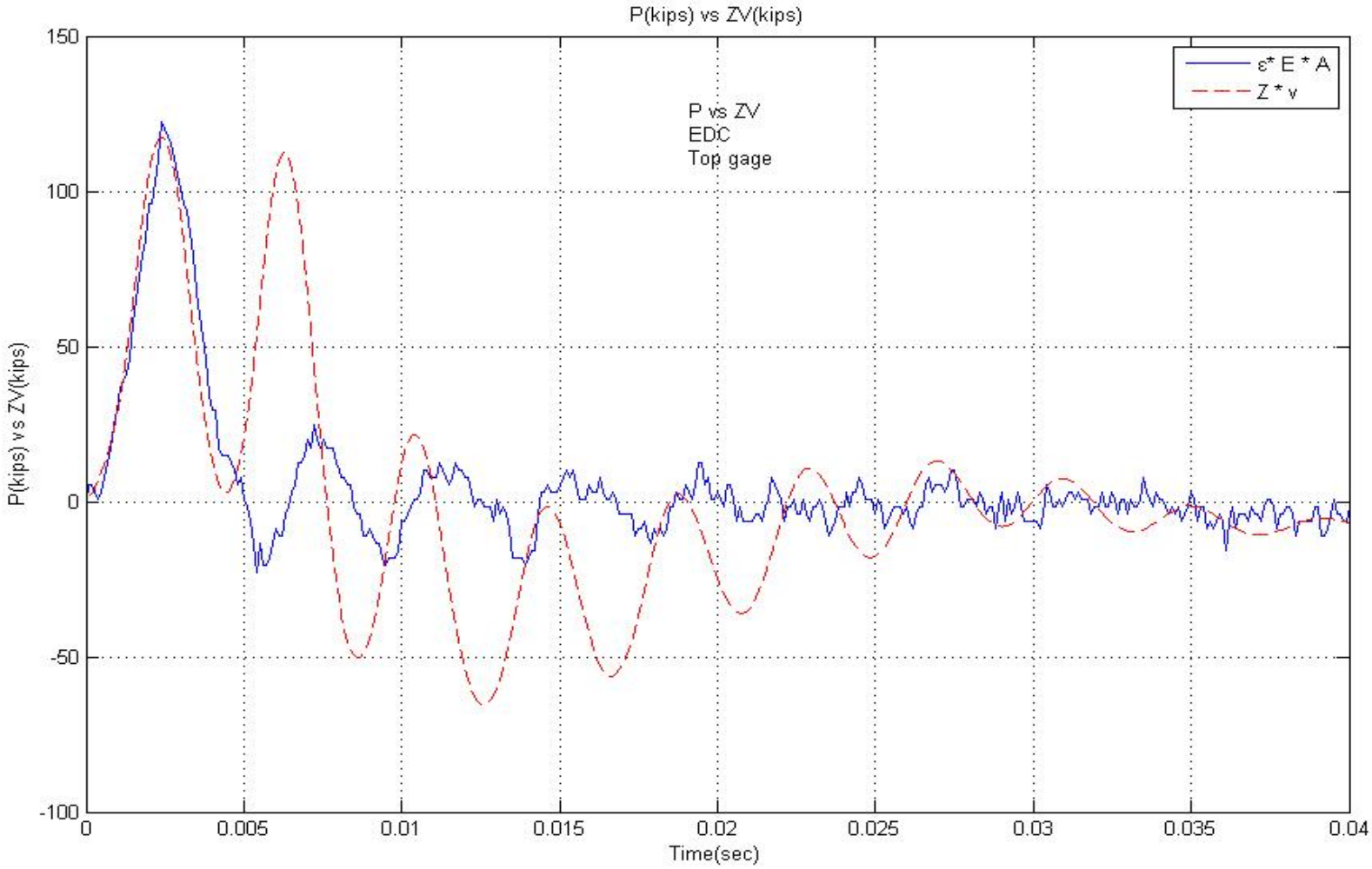

Figure 3-17. Force measured from EDC strain and acceleration sensors at pile top.

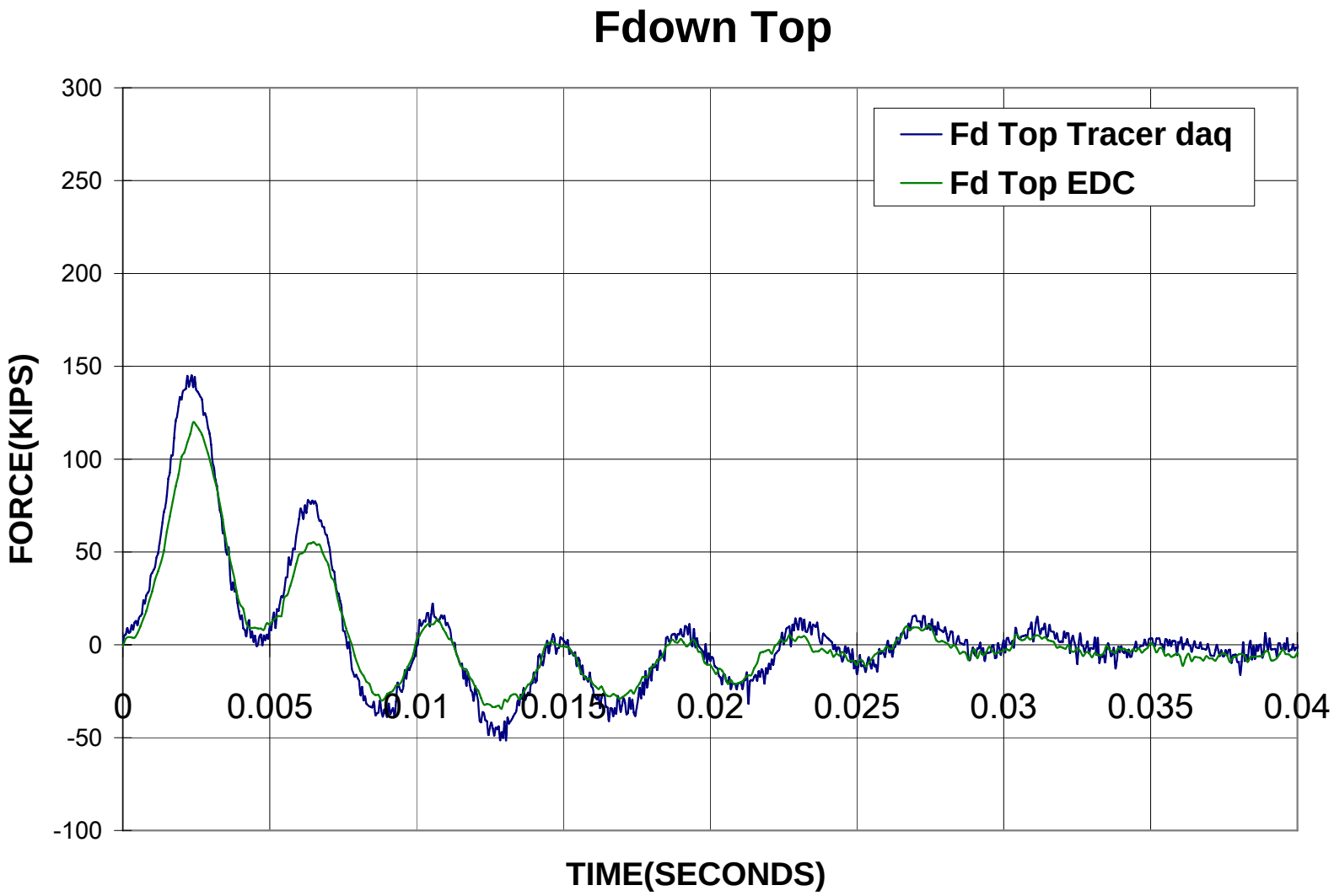

Figure 3-18. F_{down} measurements at top of pile for blow 21.

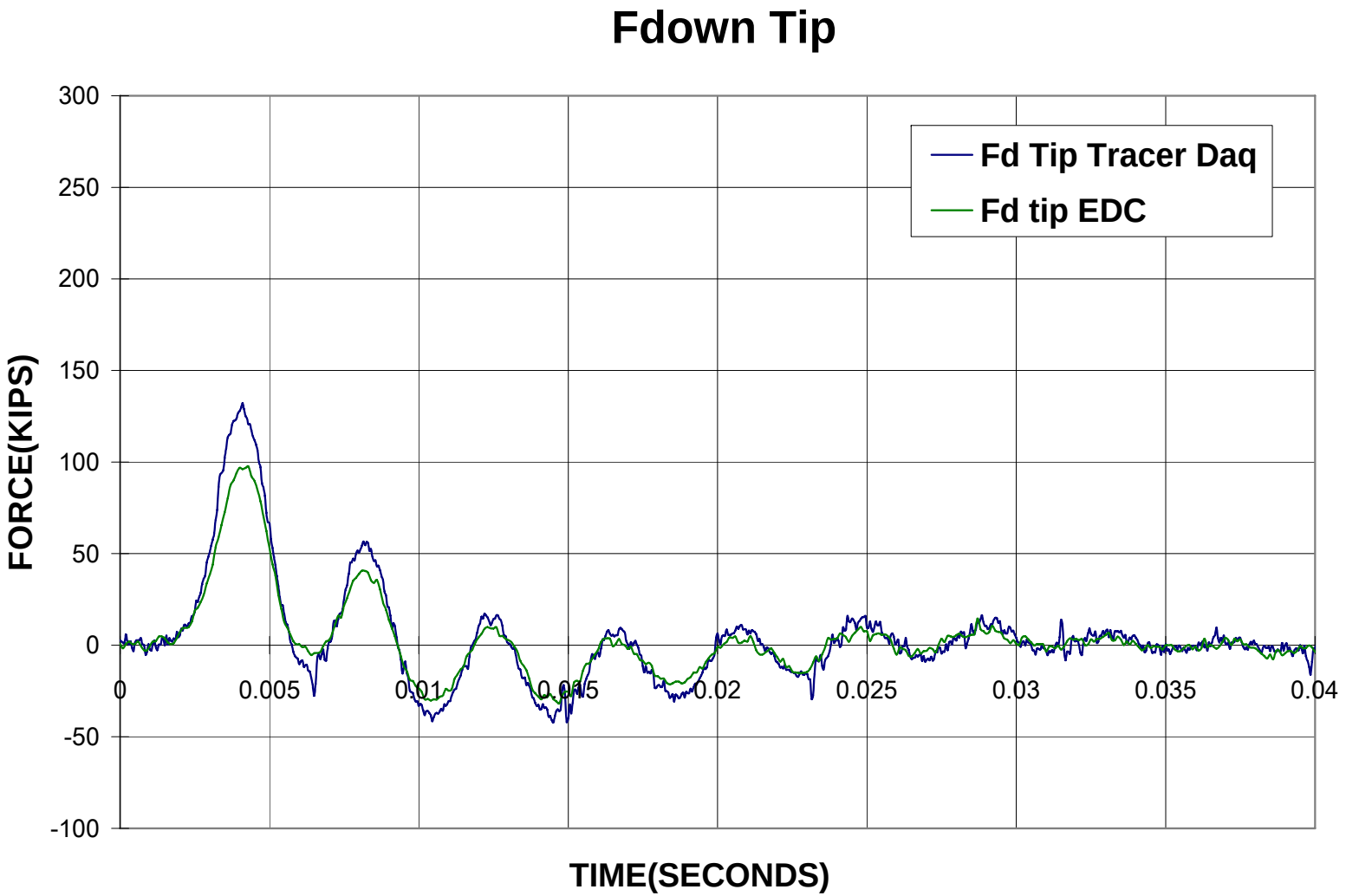

Figure 3-19. F_{down} measurements at bottom of pile for blow 21.

Shown in Figures 3-20 and 3-21 are the recorded accelerations at the top and bottom of the pile from internal and externally mounted gages. Evidently, the comparison between the gages at both ends of the pile is quite good with the EDC showing slightly higher peaks than the externally mounted gages. The latter may be due to their location, i.e., centroid vs. boundary location for the Tracer DAQ and PDA. Given in Figures 3-22 and 3-23 is integration of the acceleration twice to give displacements at the top and bottom of the pile. The data reveals the top and bottom of the pile had a maximum downward movement of 0.025 ft to 0.30 ft and a permanent deformation of 0.02 ft to 0.22 ft.

Integrating the accelerations (Figures 3-20 and 3-21) gives the velocities multiplied by the impedance (Z) giving force, and substituted into Eq. 3-1 along with the force from the strain gages (i.e., $P= \varepsilon E A_{cross}$), gives the wave down force. Shown in Figures 3-24 and 3-25 are the measured wave down forces at the top and the bottom of the pile determined for the EDC, PDA, and Tracer DAQ instrumentation. The comparison is excellent. Similar to the low impact blows (Figures 3-18 and 3-19), the high impact downward traveling wave looses approximately 25 to 35 kips of dynamic force between the top and bottom of the pile. Of interest is the separation into damping and static skin components which is discussed in Chapter 4.

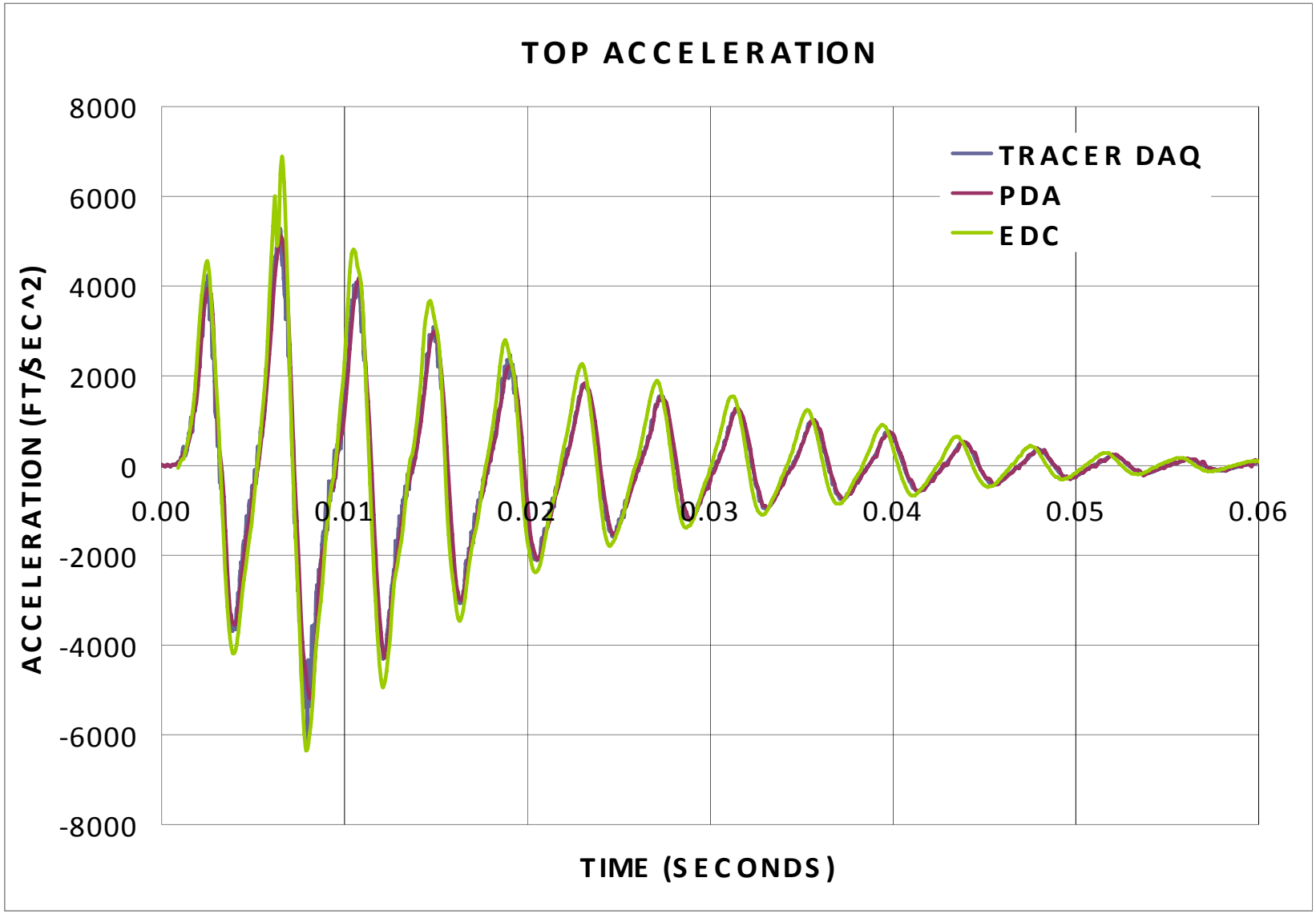

Figure 3-20. Comparison of measured top acceleration for blow 5 (6-ft drop).

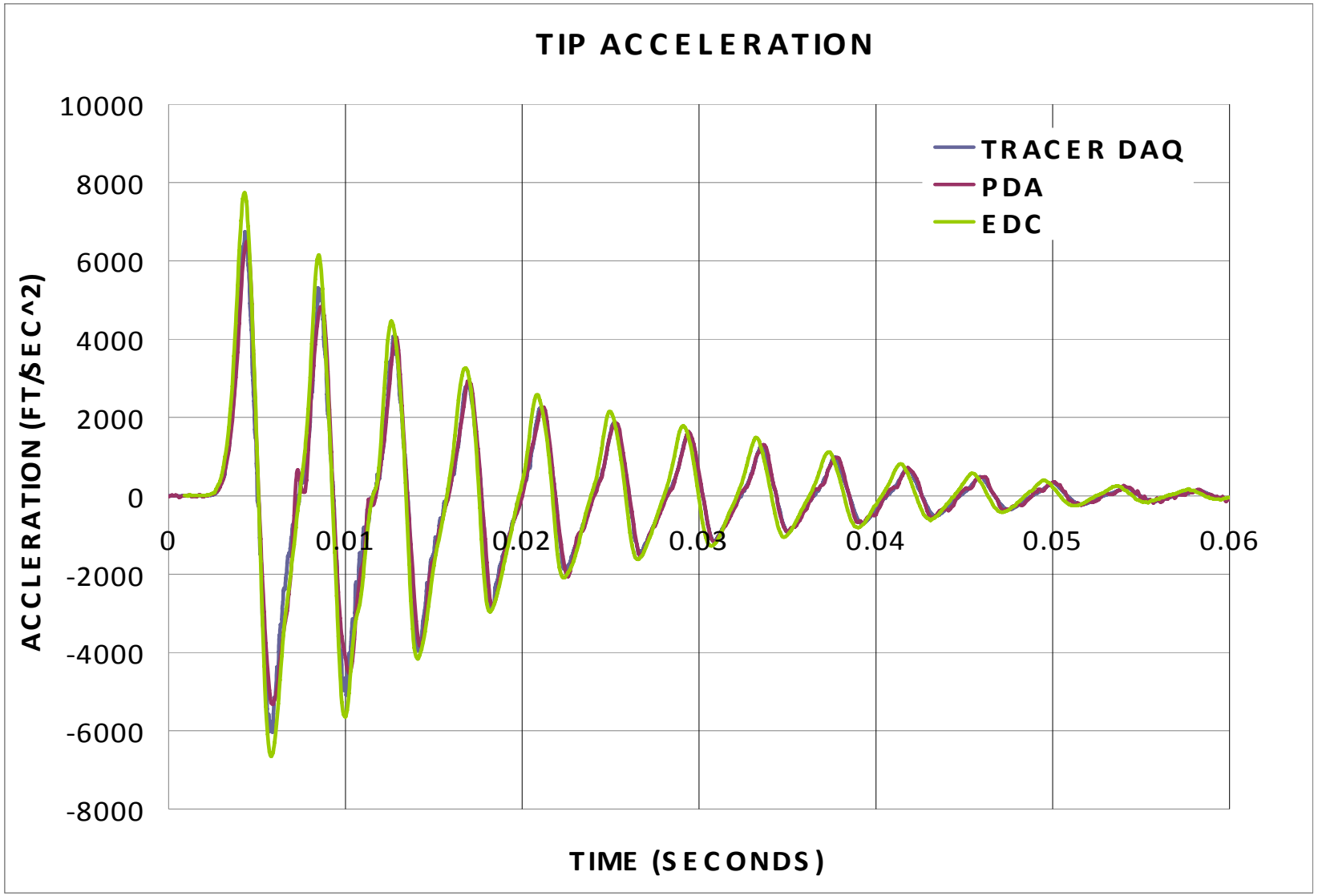

Figure 3-21. Comparison of measured tip acceleration for blow 5 (6-ft drop).

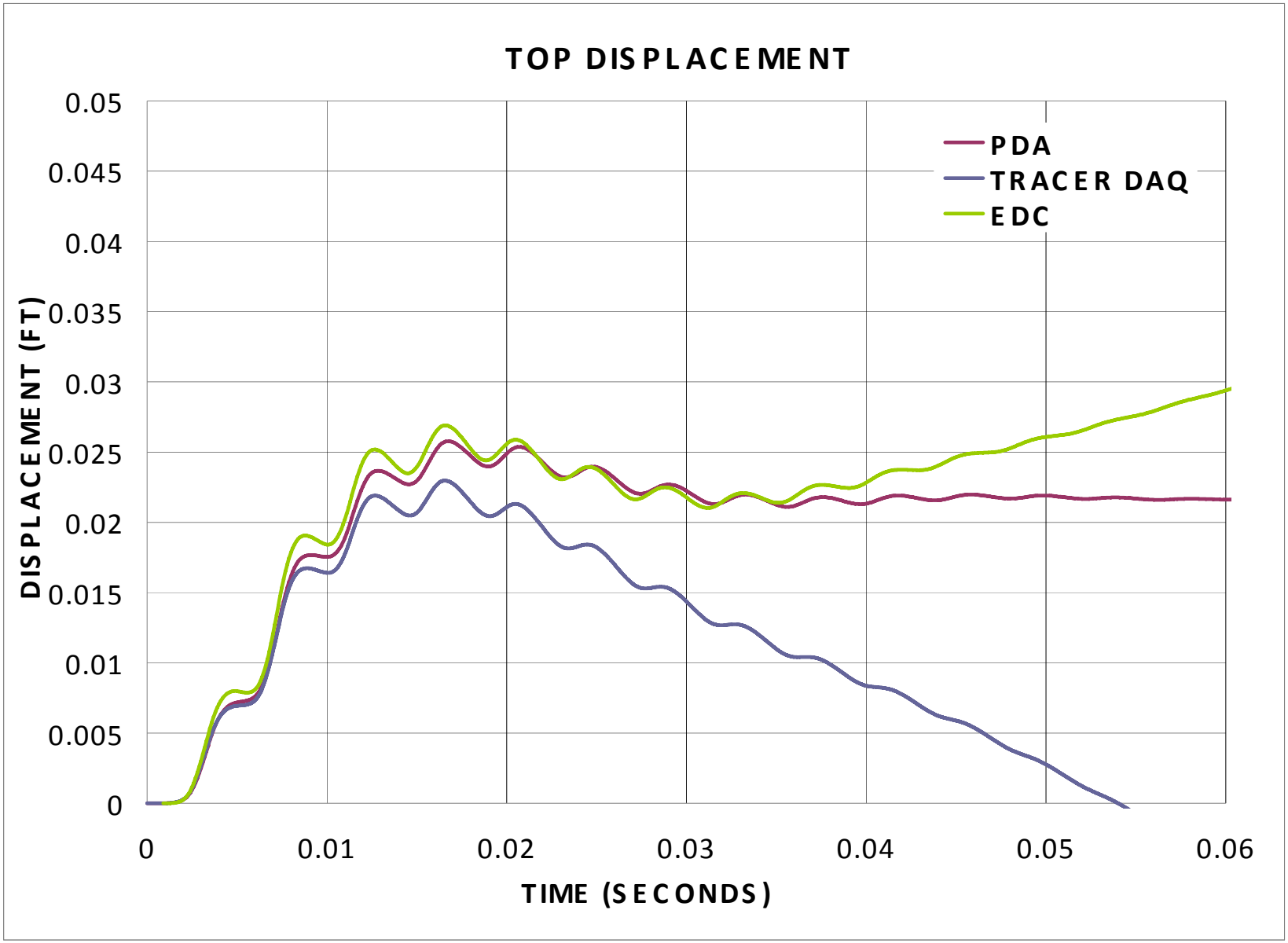

Figure 3-22. Comparison of measured top displacement for blow 5 (6-ft drop).

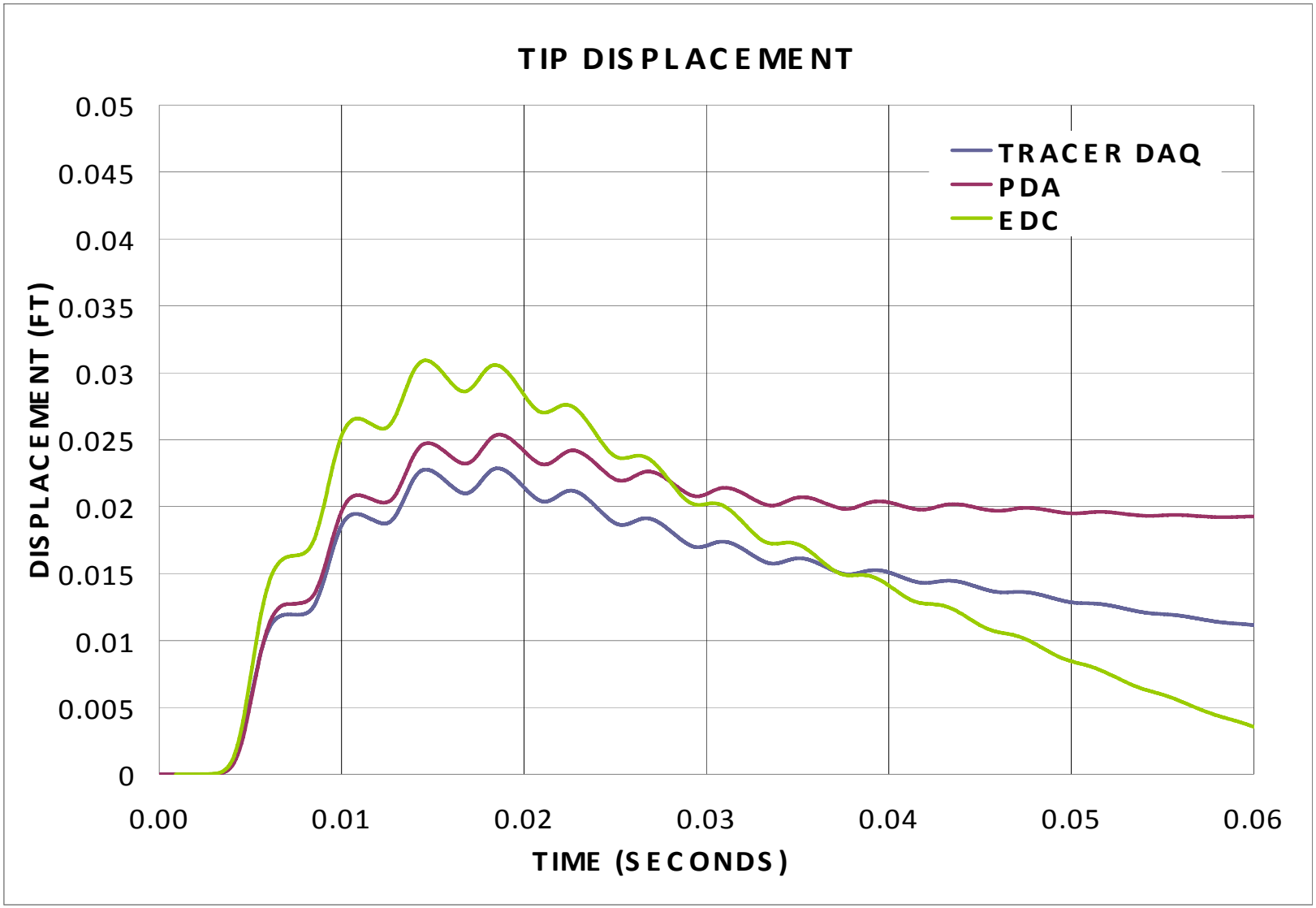

Figure 3-23. Comparison of measured tip displacement for blow 5 (6-ft drop).

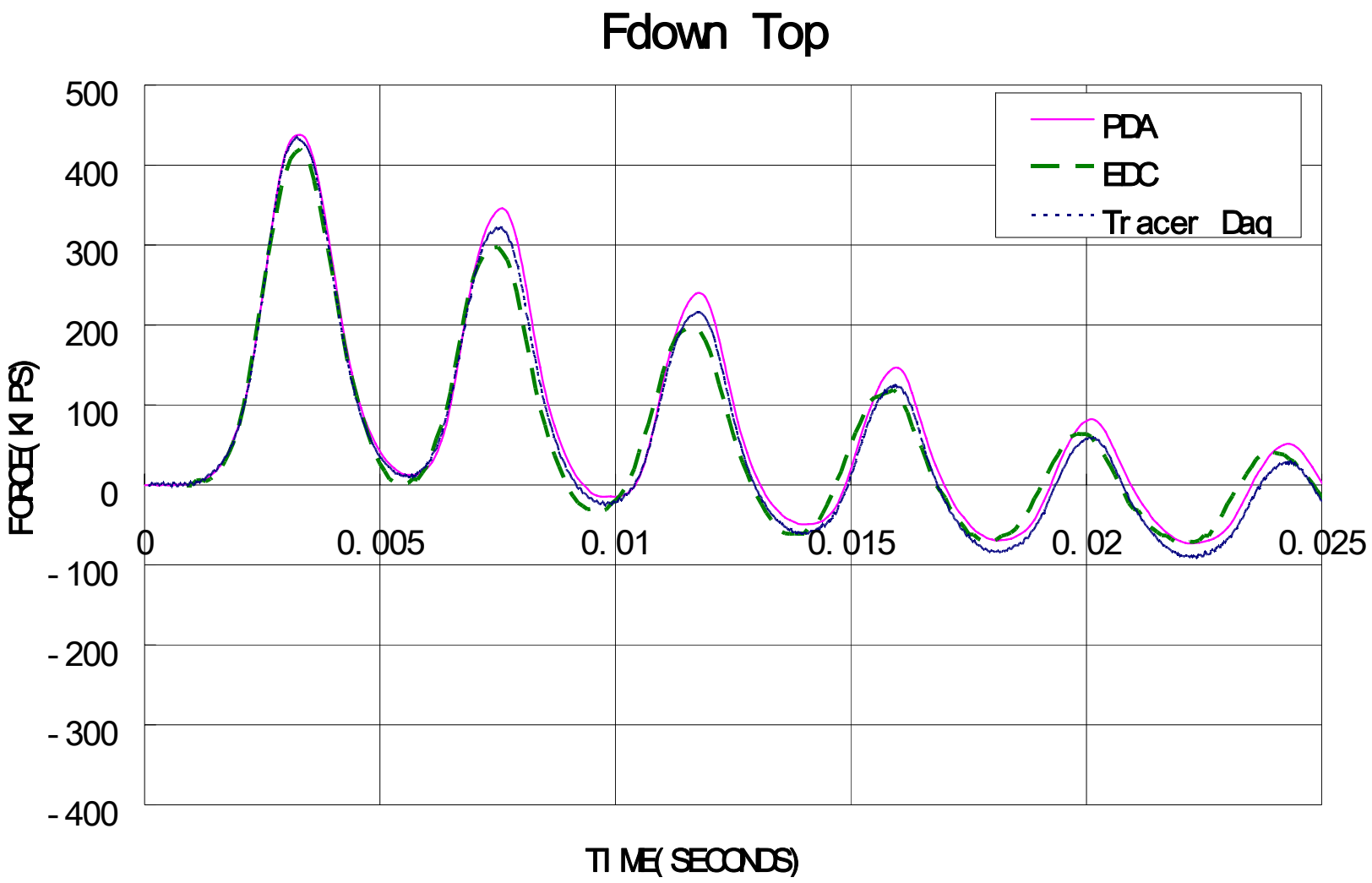

Figure 3-24. Comparison of F_{down} measurements at top of pile for blow 5 (6-ft drop).

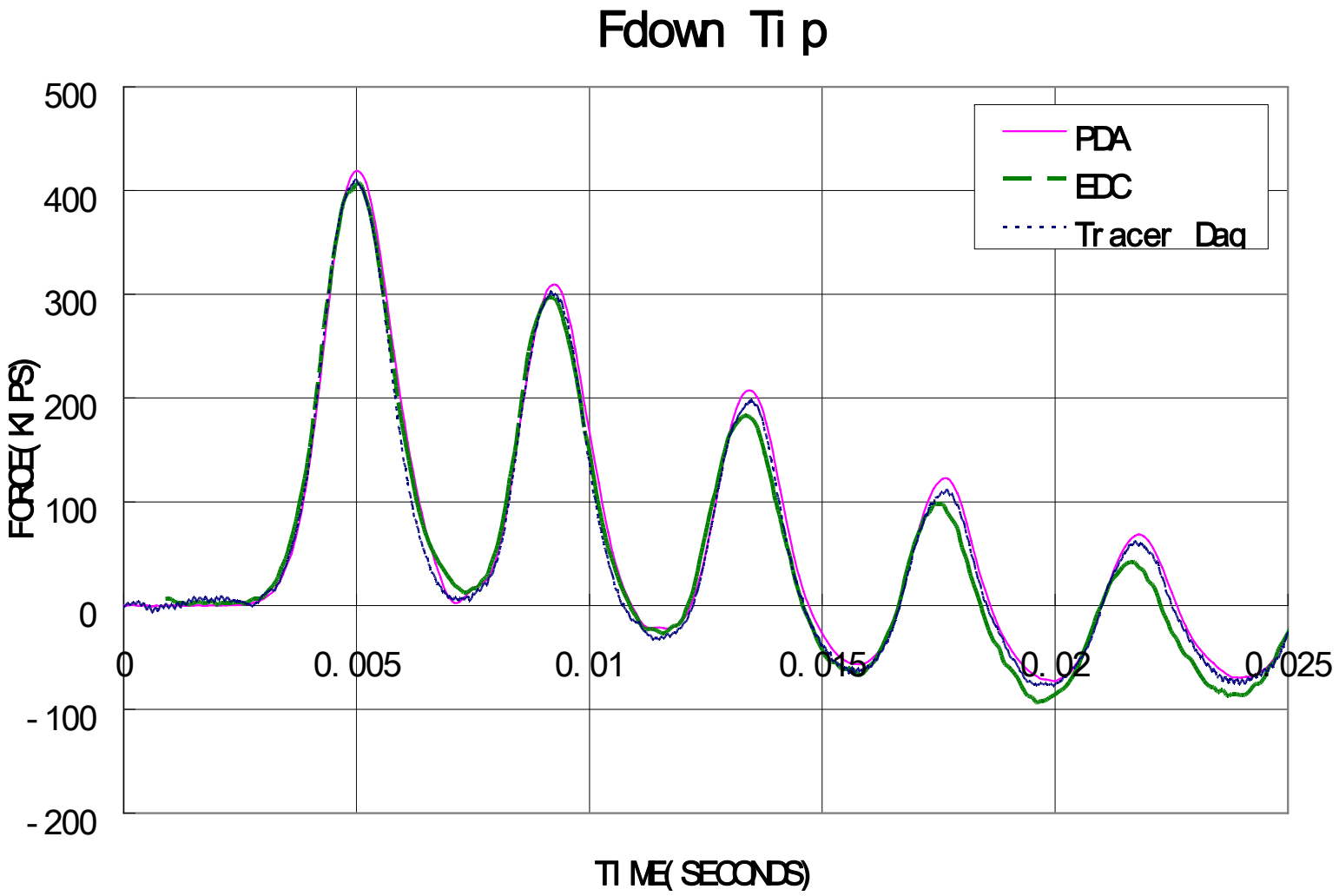

Figure 3-25. Comparison of F_{down} measurements at tip of pile for blow 5 (6-ft drop).

CHAPTER 4
ONE-DIMENSIONAL WAVE PROPAGATION WITH SIDE FRICTION AND DAMPING

4.1 Theory

As discussed in Section 2.3, classical one-dimensional wave propagation was developed for a rod/pile in air. For the case of a pile driven into soil, both skin friction and damping develops as shown in Figure 4-1. Generally, skin friction (F_S, force) is characterized as unit skin friction (fs, stress), times the surface area it acts over. The unit skin friction (fs) is usually characterized as a function of the pile displacement [u(x,t)], e.g., T-Z curve in FB-MultiPier, FB-DEEP, etc. A secant stiffness (K) is defined as the unit skin friction per unit of displacement [u(x,t)]. Using the secant stiffness (K), the skin friction (F_S) force acting on segment dx (Figure 4-1) may be found. Next, assuming a general damping form, i.e., viscous with coefficient (Cr), the damping force (F_d) is obtained from particle velocity times density and surface area (Figure 4-1). Summing the forces on the segment, results in

$$\downarrow \sum F_v = 0 = F_B - F_T - F_I - F_S - F_d$$

$$\left(\sigma + \frac{\partial \sigma}{\partial x} dx\right) A - \sigma A - \rho A\, dx \frac{\partial^2 u}{\partial t^2} - K' P\, dx\, u(x,t) - C_r P\, dx \rho_s \frac{\partial u}{\partial t} = 0 \qquad \text{(Eq. 4-1)}$$

Next, cancelling plus and minus terms, and then dividing by dx and A results in

$$\frac{\partial \sigma}{\partial x} - \rho \frac{\partial^2 u}{\partial t^2} - \frac{K' P}{A} u(x,t) - \frac{C_r P \rho_s}{A} \frac{\partial u}{\partial t} = 0 \qquad \text{(Eq. 4-2)}$$

relating stress to strain and subsequently to particle displacement,

$$\sigma = E\,\varepsilon = E\frac{\partial u}{\partial x} \qquad Then \quad \frac{\partial \sigma}{\partial x} = E\frac{\partial^2 u}{\partial x^2}$$

$$Also \quad \frac{Perimeter}{cross-sectional\ \ Area} = \frac{P}{A} = \frac{4}{B}$$

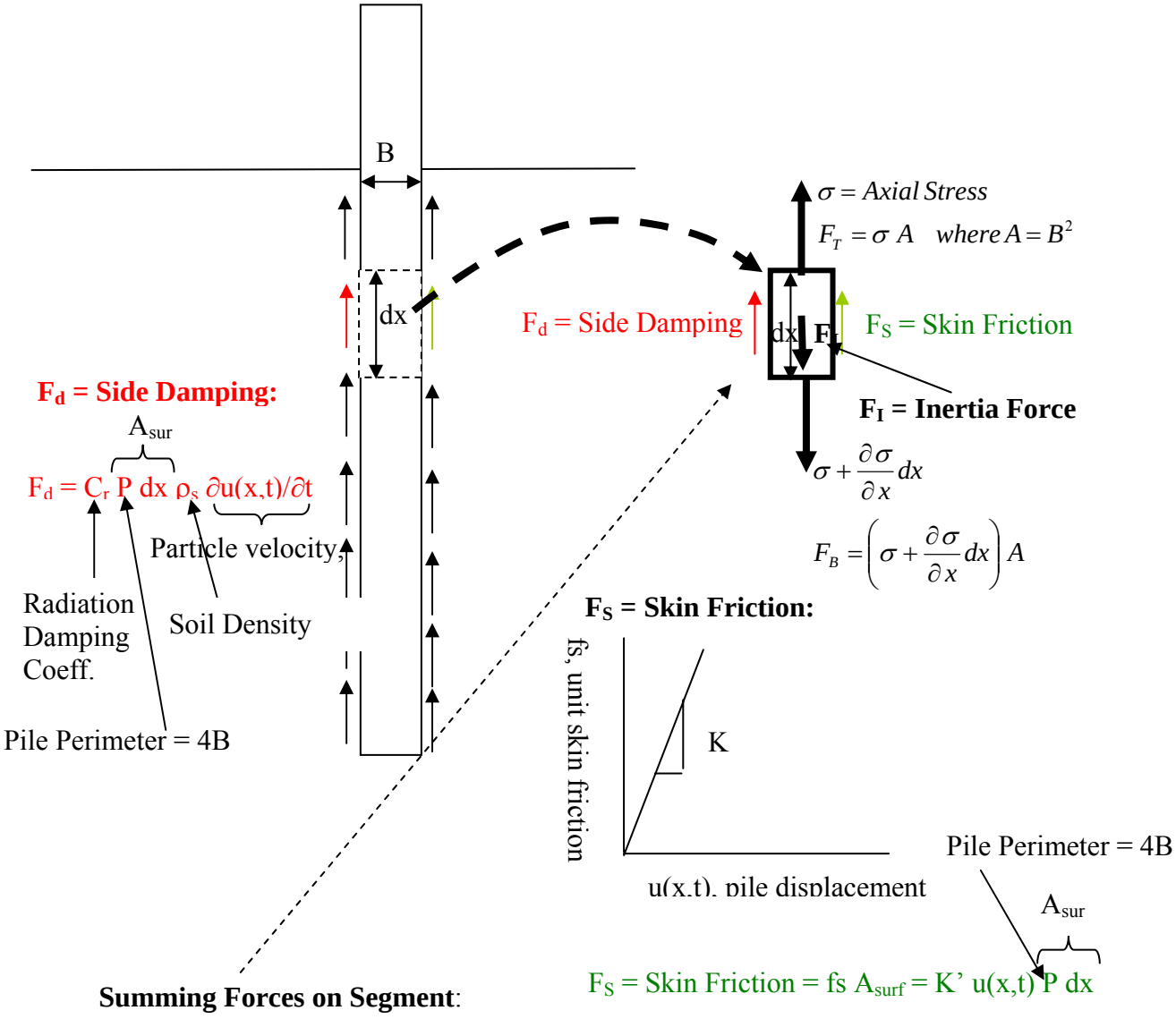

Figure 4-1. Forces acting on pile segment during driving.

Substituting $\partial\sigma/\partial x$ and P/A into Eq. 4-2 and dividing by ρ (mass density of pile), results in:

$$\frac{E}{\rho}\frac{\partial^2 u}{\partial x^2} - \frac{\partial^2 u}{\partial t^2} - \frac{4K'}{\rho B}u(x,t) - \frac{4C_r\ \rho_s}{B\rho}\frac{\partial u}{\partial t} = 0$$

$$Let:\quad a^2 = \frac{E}{\rho} \quad b = \frac{4K'}{\rho B} \quad c = \frac{4C_r\ \rho_s}{B\rho}$$

Then the final Equation is

$$a^2\frac{\partial^2 u}{\partial x^2} = \frac{\partial^2 u}{\partial t^2} + c\frac{\partial u}{\partial t} + b\,u(x,t) \qquad \text{(Eq. 4-3)}$$

Equation 4-3 originally appeared in the literature as the telegraph equation which identifies line voltage as function of losses (e.g., capacitance, etc.). However, Eq.4-3 has been found in many other disciplines from waves in water to fiber optics and is known generally as the dispersive wave propagation equation (NDT – SASW analysis).

If the damping (c) and static skin resistance (b) are set to zero, then the classical one-dimensional wave equation with the following solution is obtained,

$$u(x,t) = f(x + \mathbf{a}\,t) + g(x - \mathbf{a}\,t) \qquad \text{(Eq. 4-4)}$$

where f is a traveling wave going down the pile and g is a traveling wave going up the pile with velocity ($\mathbf{a} = \sqrt{E/\rho}$; E, Young's Modulus and ρ, density of pile). Generally, due to a hammer strike, the response is composed of a multitude of different frequency, ω waves defined with the following characteristics:

- Wave length (distance between 2 sequential crests), $\lambda = 2\pi / m$ (where m =1, 2…..)
- Wave number, $k = 2\pi / \lambda$
- Frequency, $\omega = 2\pi\,\mathbf{a} / \lambda$

And, Eq. 4-4 may be expressed as

$$u(x,t,) = \Sigma_m A_m \exp [i (kx \pm \omega t)] \qquad \text{(Eq. 4-5)}$$

where $\omega/k = \mathbf{a}$ = wave propagation velocity (Eq. 4-5b)

and A_m is amplitude of wave number k. Instead of expressing the wave in terms of exp function, cosine function could be used by employing Euler's formula, e.g.,

$$\cos(x) = \text{Re} \{ \exp (i x) \} \qquad \text{(Eq. 4-6)}$$

where Re = real, and i = sqrt(-1), or

$$u(x,t) = \text{Re} \Sigma_m \{A_m \exp [i (kx \pm \omega t)] \} = \Sigma_m A_m \cos (kx \pm \omega t) \qquad \text{(Eq. 4-7)}$$

The interesting case is if the damping c and soil-pile static skin friction b are no longer zero in Eq. 4-3. Then the solution of Eq. 4-3 becomes:

$$u(x,t) = \sum_m \exp\left(-\frac{c\,t}{2}\right) A_m \exp\left\{ i\,k \left[x \pm \frac{t}{2k}\left(4\,a^2\,k^2 + 4\,b - c^2\right)^{\frac{1}{2}} \right] \right\} \qquad \text{(Eq. 4-8)}$$

Note if b and c are again zero, then Eq. 4-8 gives Eq. 4-7 as expected. Of great interest is the term within the exp{ } in Eq. 4-8, as well as the exp(-ct/2) term. Within the exp { } term, the expression,

$$(4\,a^2\,k^2 + 4\,b - c^2)^{1/2} / 2k \qquad \text{(Eq. 4-9)}$$

represents the wave travel speed for each individual wave number k or frequency ω [i.e., v(ω)]. Evident from Eq. 4-9, the shape of the traveling wave form changes as it propagates down the pile unless the soil damping and static skin friction is such that $4\,b = c^2$, then each wave number has a wave speed equal to **a** as given in Eq. 4-5b. The former is referred to as dispersion and occurs in many instance of wave propagation. For instance, when white light passes through a glass prism, spatial separation of the light into

components of different wavelengths (i.e., colors) occurs. Obviously, there are generally two unknowns (b, c) in Eq. 4-9, which makes the use of Eq. 4-9 by itself questionable for one wave number (k); however there are probably 5 to 10 predominate frequencies (ω) at top and bottom of pile to assist with the analysis.

The other term in Eq. 4-8 of great interest is exp(-c t /2) which is a function of soil damping (c). It suggests that with increasing time (i.e., wave propagating down the pile), the product of amplitude (A_m, constant) of each wave form/number times exp(-c t /2) is diminishing. Moreover, for the case of no dispersion of the propagating wave (i.e., $4b = c^2$), the ratio of top to bottom response is directly proportional to damping. Note the latter is the present approach used in Smart Structures Software to assess damping, i.e., dynamic tip to skin response. Since the skin friction, secant stiffness (K in Figure 4-1) is expected to be dependent on magnitude of particle motion, the analyses and solutions are divided into small impact (i.e., 1-ft hammer drops) and large (i.e., 6-ft hammer drops) impact energies. Of interest are the damping (c) and skin friction (fs) for both small and large impacts.

4.2 SASW Analysis

To investigate Eq. 4-7, the use of standard Spectral Analysis of Surface Waves (i.e., SASW) was employed. Specifically, the wave down forces at the top and bottom of the pile for small impact energy (Figures 3-18 and 3-19) were transformed to the frequency domain using a Fast Fourier Transform algorithm. For instance, shown in Figure 4-2 is amplitude vs. frequency of the measured downward traveling wave at top of the pile for blow 21 (low impact). Evident from the magnitudes of the amplitudes of the various wave

frequencies, the primary excitation occurs at approximately 245 Hz. If the velocity of 245 Hz wave was 12,500 ft/sec (i.e., v (ω=245Hz) = 12,500 ft/sec), then the wavelength of the primary excitation (λ in ft) would be

$$\lambda(\omega = 245) = \frac{v(\omega = 245)}{\omega} = \frac{12{,}500 \frac{ft}{\sec}}{245 \frac{cycles}{\sec}} \approx 51\, ft \qquad \text{(Eq. 4-10)}$$

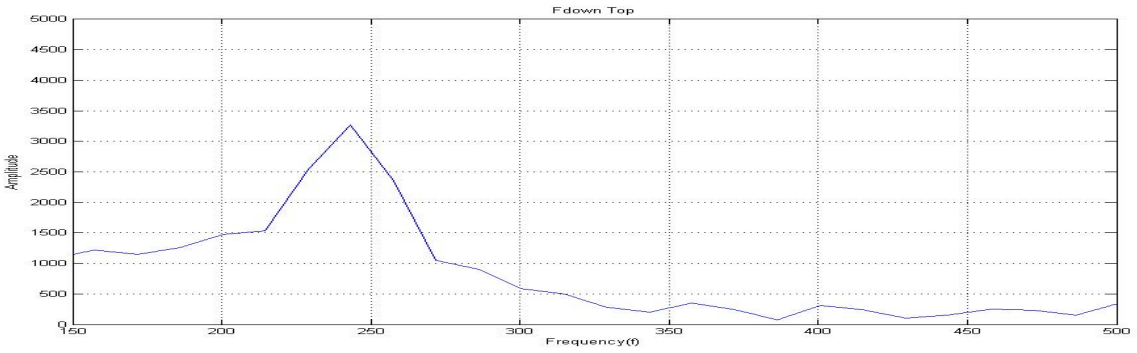

Figure 4-2. Amplitude of various frequency waves in F_{down} at pile top from Figure 3-18.

Since the distance between the gages and the bottom of the pile is 27 ft (Figure 3-5), then the distance from the gages to the bottom of the pile and back again to the gages is 54 ft which is approximately equal to the wavelength (51 ft, Eq. 4-10) of the primary excitation. The latter suggests that the energy being imparted to the pile is being used to primarily excite or resonate the motion of the whole pile.

Shown in Figure 4-3 are the amplitudes of the different frequency waves traveling downward at the top of the pile for blow 5 of the high energy impact (Figure 3-24). Note the order of magnitude increase in the force amplitude (i.e., Figure 4-2 vs. Figure 4-3) with most of the energy again located in the 245 to 250 Hz range or wavelength equal to twice the pile length.

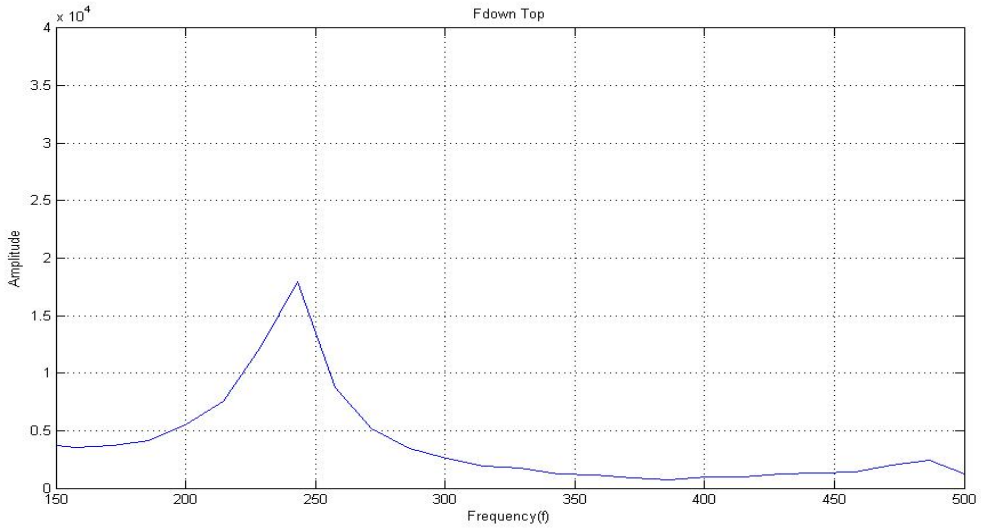

Figure 4-3. Amplitude of various frequency waves in F_{down} at pile top from Figure 3-24.

Next the phase difference ($\phi(\omega)$) between the top and bottom signal were calculated (Figure 4-4) for each frequency and a travel time ($t(\omega)$) between sensor sets was obtained for each frequency,

$$t(\omega) = \frac{\phi(\omega)}{2\pi\omega} \qquad \text{(Eq. 4-11)}$$

where the phase difference $\phi(\omega)$ for each frequency is in radians and the frequency ω is in cycles per second. Knowing the distance between the sensors (Δd) and wave travel time ($t(\omega)$), the wave velocity $v(\omega)$ (i.e., Eq. 4-9) may be found as

$$v(\omega) = \frac{\Delta d}{t(\omega)} \qquad \text{(Eq. 4-12)}$$

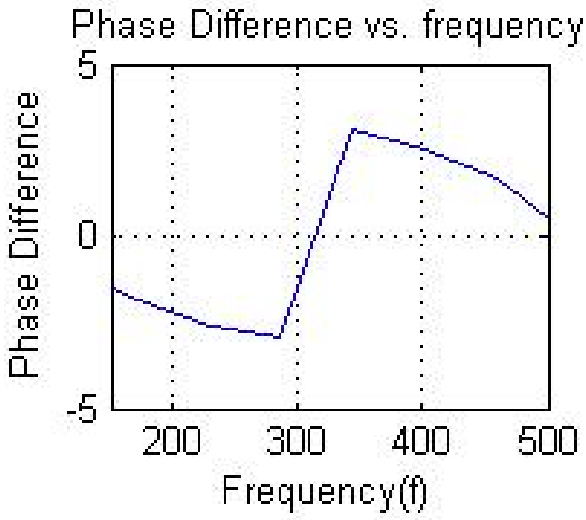

Figure 4-4. Phase difference vs. frequency for low impact blow 21.

Shown in Figure 4-5 are wave velocities for the low impact energy blow 21 from the original data given in Figures 3-18 and 3-19. Figure 4-6 gives the wave velocities in the case of high energy impact blow 8. Both Figures 4-5 and 4-6 suggest that there may be small differences between velocities for different frequencies, i.e., dispersion (Eq. 4-9).

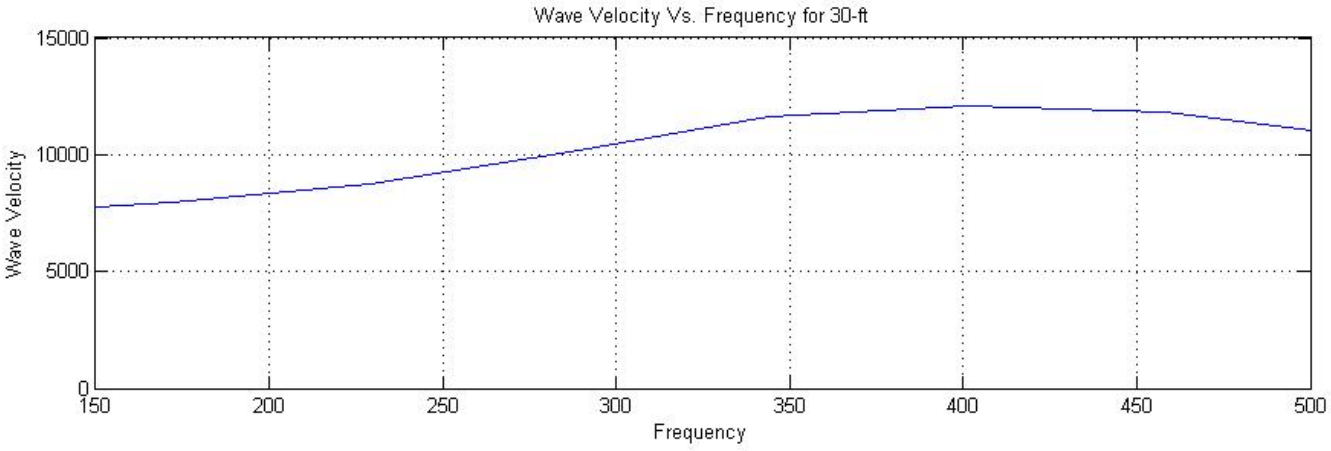

Figure 4-5. Wave velocities as function of frequency for low impact blow 21.

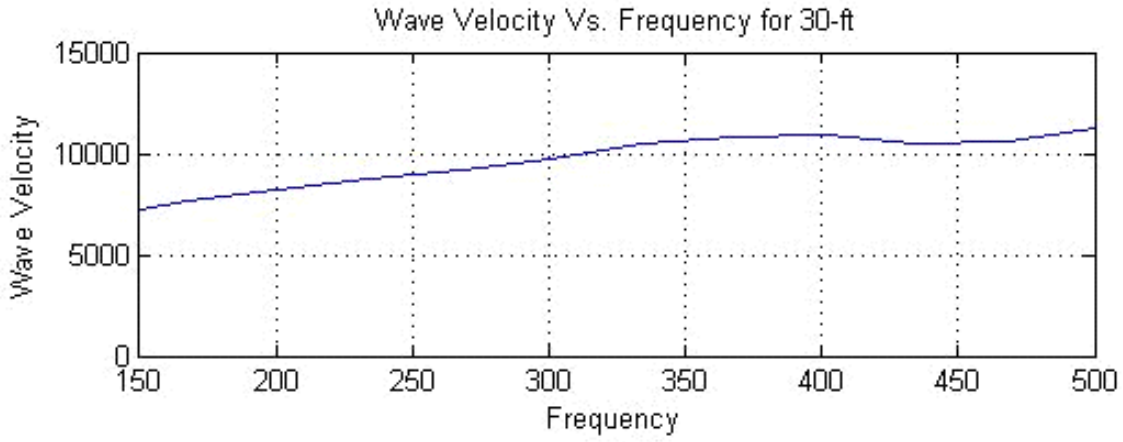

Figure 4-6. Wave velocities as function of frequency for high impact blow 8.

However, careful inspection of the figures reveals that velocities are relatively constant for frequencies above 300 Hz. In addition, it is generally recognized in the literature that SASW processing of wave velocities for lower frequencies which have wavelengths (i.e., Eq. 4-9) larger than spacing between the sensors may not be accurate and should be validated by other methods.

Consequently, it was tentatively decided to assume that there was no dispersion (discussed in next section on wavelets) in the pile (i.e., $c^2 = 4b$, Eqs. 4-8 and 4-9) then the damping could directly be obtained from the change in amplitude of the waves between the top and bottom set of gages (Eq. 4-8) or

$$c = \frac{2}{\Delta t} Ln\left(\frac{A_{m\ top}}{A_{m\ bottom}}\right) \qquad \text{(Eq. 4-13)}$$

where Δt is the time it takes a wave to go from top to bottom set of gages. The low energy impact damping c as a function of frequency for blow 21 is given in Figure 4-7. Evident from the figure, the damping varies somewhat by frequency, but generally has an average of approximately 162.

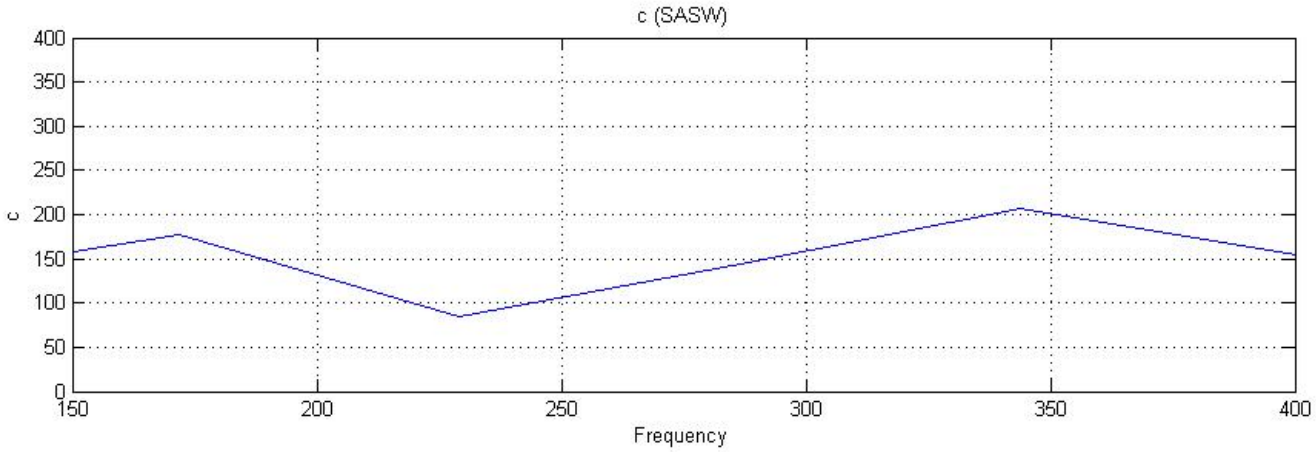

Figure 4-7. Damping (c) vs. frequency for low energy impact blow 21.

In the case of high energy impact (e.g., blow 5, EDC, Figures 3-24 and 3-25), the computed damping is shown in Figure 4-8 as a function of frequency. Evident the damping is lower for most of the frequencies for higher impact energies (i.e., Figure 4-7 vs. Figure 4-8). It is believed that the lower damping value (c) is due to the larger relative movement of the pile to the soil for the high energy impact blows.

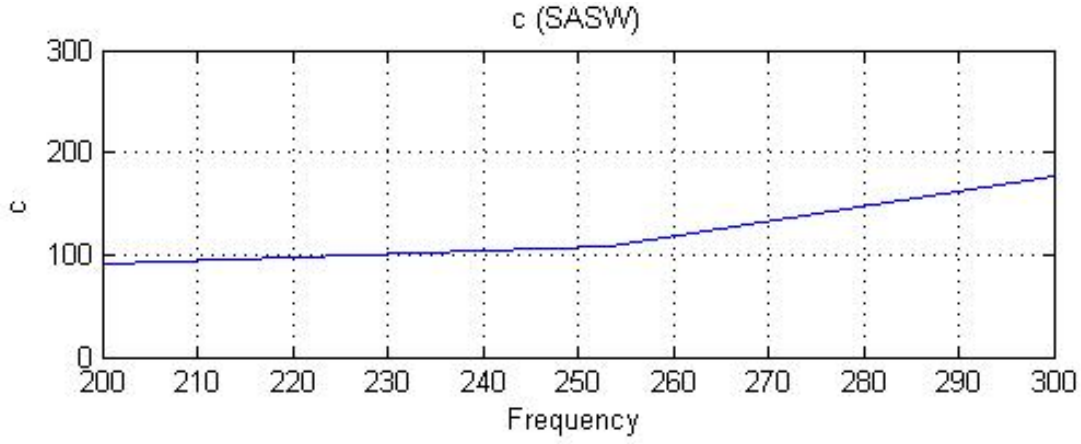

Figure 4-8. Damping (c) vs. frequency for high energy impact blow 21.

4.3 Wavelet Analysis

Due to the accuracy concerns of the wave velocity estimates from SASW with gage separation distances smaller than the primary wavelengths, it was decided to employ wavelet analysis or more specifically continuous wavelet transform (CWT). Wavelet analysis involves dividing the continuous time signal into components or windows (time). Within each window a mother wavelet is used to match the signal components, i.e., frequency and amplitude. These scaled and translated copies are generally referred to as "daughter wavelets". Each scale component can then be studied with a resolution that matches its scale. Wavelet transforms have advantages over traditional Fourier transforms for representing functions that have discontinuities and sharp peaks and for accurately deconstructing and reconstructing finite, non-periodic and non-stationary signals. Also, it is generally recognized that Continuous Wavelet Transform (CWT) is very efficient in determining the damping ratio of oscillating signals (e.g., identification of damping in dynamical systems) and is very resistant to the noise in the signal. The mother wavelet used in this analysis is the Morlet wave, shown in Figure 4-9. Note the CWT may be done on any set of sensors, i.e., top or bottom.

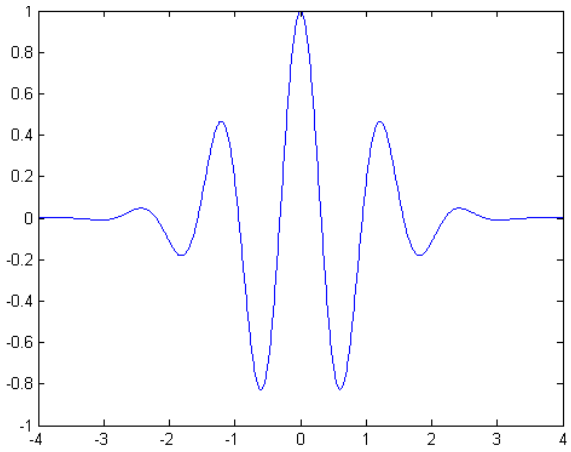

Figure 4-9. Morlet wave used in CWT analysis.

For this work, the F_{down} signal was analyzed using both the top and bottom set of sensors for both the low and high hammer impact energies. Shown in Figure 4-10 is a typical Wavelet Analysis of F_{down} signal (Figure 3-18) from the EDC instruments at the top of the pile. Shown on the X axis is time given in sec. and the Y axis is the wave frequency. The color red represents the peak positive amplitude of a given wave frequency and the blue color is the negative value. If a particular frequency, e.g., 250 Hz, was to be selected, then both the amplitude and the arrival time of that specific harmonic may be readily be extracted. For instance shown in Figure 4-11 is the amplitude vs. time for the 250 Hz wave. If the various frequencies contained in F_{down} were exhibiting dispersion (i.e., Eq 4-9: $c^2 \neq 4b$), then each specific peak amplitude (Eq. red) in Figure 4-10 would be inclined (i.e., not vertical). Specifically, if low frequencies had slower velocities than the higher frequencies, the red lines would be sloping upward to the left.

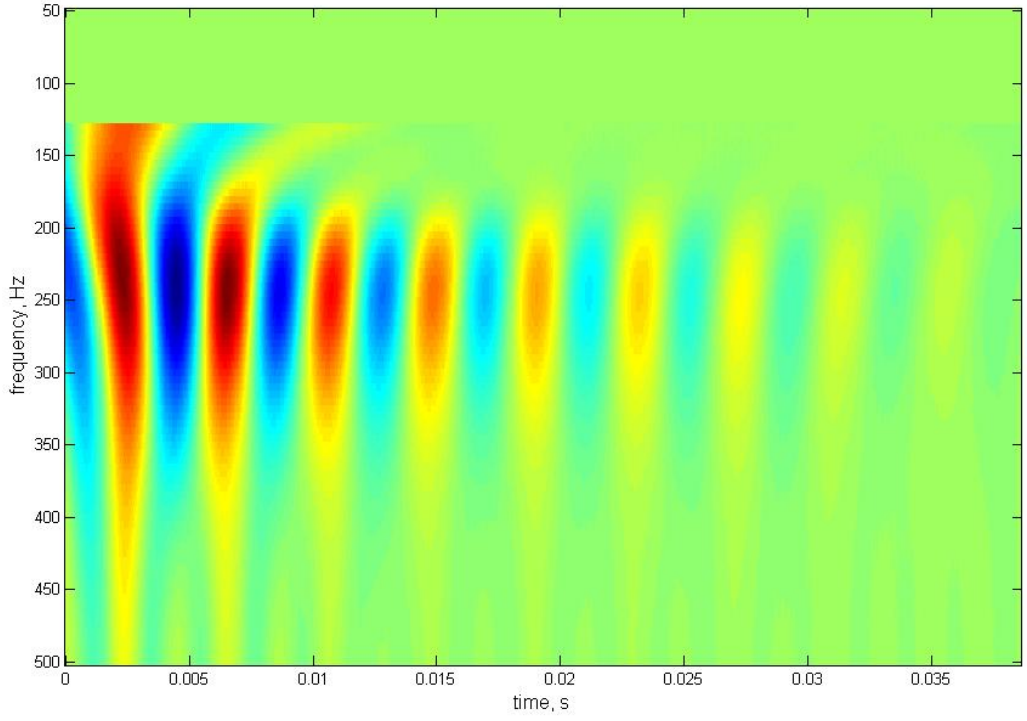

Figure 4-10. Wavelet analysis of F_{down} from top EDC signal for blow 21.

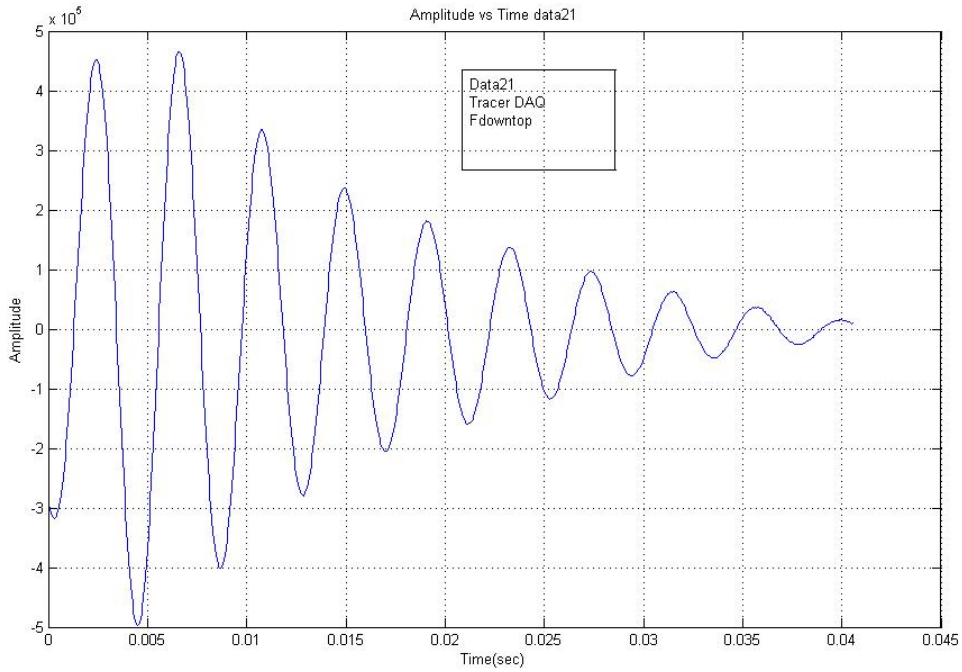

Figure 4-11. Amplitude vs. time for 250 Hz wave from low energy impact blow 21.

Evident from Figure 4-10, F_{down} for blow 21 analyzed has little if any dispersion. Based on Figure 4-11 and distance of 54 ft (down and back), the wave speed for this frequency wave (250 Hz) and all others is approximately 12,200 ft/sec. In addition using any peak amplitudes (successive or multiples thereof) in Eq. 4-13 gives the damping, c value.

Shown in Figure 4-12 is the Wavelet Analysis of F_{down} signal (Figure 3-24) from the EDC instruments at the top of the pile from high energy impact blow 5. Evident from the peak amplitude times, little if any dispersion is occurring (i.e., Eq. 4-9: $c^2 = 4b$). Given in Figures 4-13 and 4-14 are the extracted 250 Hz wave amplitude vs. time from Figure 4-12 and a similar wavelet analysis on the bottom F_{down} EDC signal (Fig 3-25). Using Eq. 4-9, the damping (c) may be computed from Figures 4-13 and 4-14 as well as other frequencies and blows.

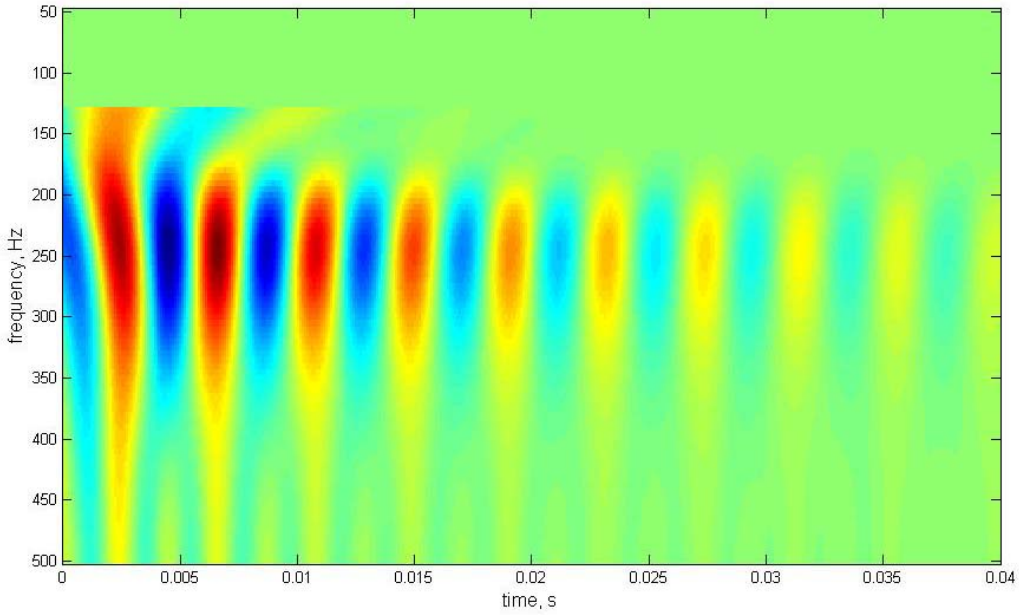

Figure 4-12. Analysis of F_{down} from top EDC signal for high energy impact blow 5.

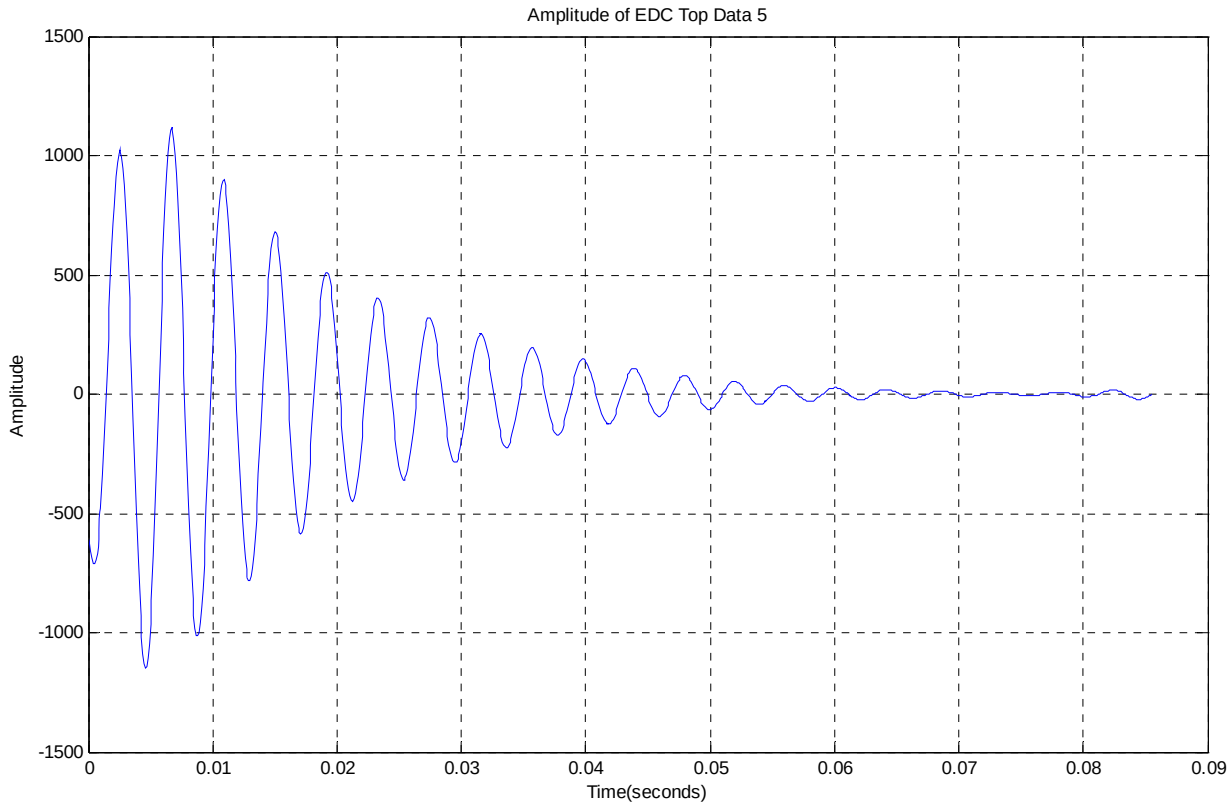

Figure 4-13. Amplitude vs. time for high energy impact EDC top signal, blow 5.

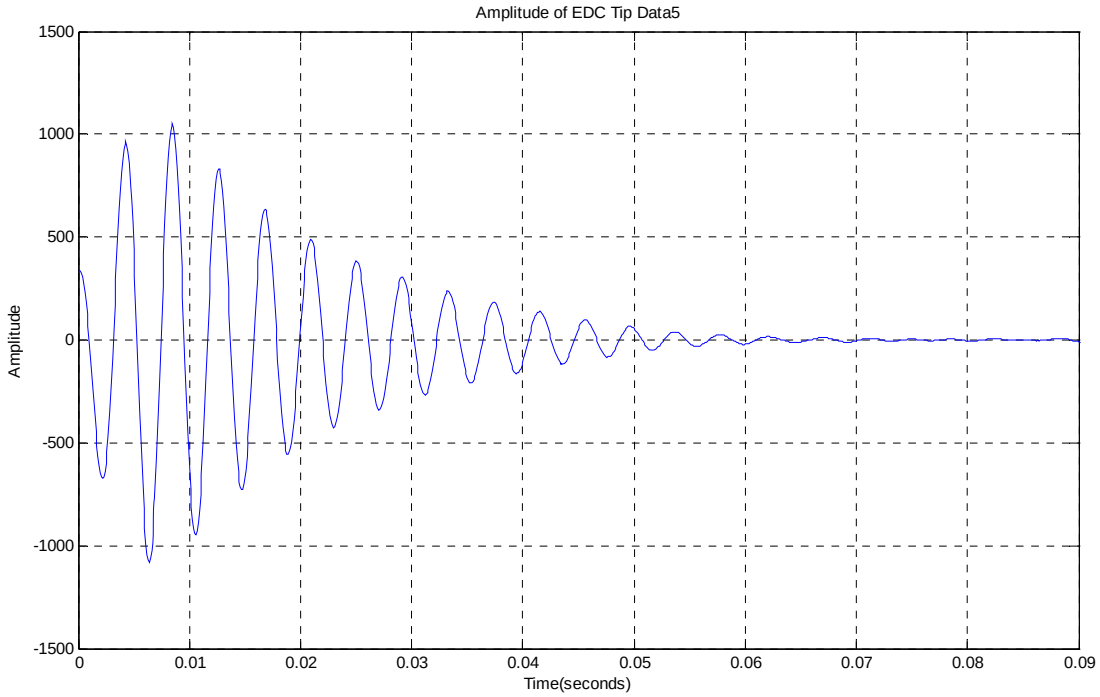

Figure 4-14. Amplitude vs. time for high energy impact EDC tip signal, blow 5.

Presented in Table 4-1 are the computed damping (c) using different low energy hammer impact blows (1-ft hammer drop) for F_{down} from both the CWT analysis and SASW. Table 4-2 gives the computed damping (c) for the high energy hammer impact blows (6-ft hammer drop). A comparison of damping from the low and high energy hammer impacts, reveal that the low energy hammer impact damping is greater (160 to 175 1/sec vs. 105 to 120 1/sec).

Table 4-1. Damping (c) and Soil Friction/Unit of Displacement (K) for Low Energy Impact

No.			c (1/sec) (Wavelet)	b (1/sec^2) (Wavelet)	K (lb/ft^3)	c (1/sec) (SASW)
Data19	**Tracer DAQ**	Top Gage	174.8812	7645.9	13356.51	165
		Tip Gage	173.7201	7544.7	13179.74	
	EDC	Top Gage	168.0065	7056.546	12327.04	
		Tip Gage	176.7464	7809.822	13642.94	

Data20	**Tracer DAQ**	Top Gage	168.4964	7097.759	12399.04	162
		Tip Gage	162.8506	6630.079	11582.05	
	EDC	Top Gage	165.852	6876.721	12012.91	
		Tip Gage	170.963	7307.087	12764.71	
Data21	**Tracer DAQ**	Top Gage	163.1956	6658.201	11631.17	162
		Tip Gage	164.9013	6798.11	11875.58	
	EDC	Top Gage	164.4394	6760.079	11809.14	
		Tip Gage	166.9228	6965.805	12168.53	
Data22	**Tracer DAQ**	Top Gage	161.2872	6503.39	11360.74	160
		Tip Gage	164.7021	6781.7	11846.91	
	EDC	Top Gage	176.2147	7762.905	13560.98	
		Tip Gage	176.2995	7770.378	13574.03	

Table 4-2. Damping (c) and Soil Friction/Unit of Displacement (K) for High Energy Impact

No.			**c (1/sec) (wavelet)**	**b ($1/sec^2$) (wavelet)**	**K (lb/ft^3)**	**c (1/sec) (SASW)**
Data8	**PDA**	Top Gage	111.8049	3125.084	5459.192	125
		Tip Gage	106.4661	2833.758	4950.275	
	EDC	Top Gage	112.4888	3163.433	5526.183	120
		Tip Gage	115.0635	3309.902	5782.05	
	Tracer Daq	Top Gage	106.0762	2813.04	4914.084	125
		Tip Gage	130.0373	4227.425	7384.865	
Data7	**PDA**	Top Gage	111.0059	3080.577	5381.444	125
		Tip Gage	115.3109	3324.151	5806.941	
	EDC	Top Gage	116.1198	3370.952	5888.697	120
		Tip Gage	120.1887	3611.331	6308.614	
	Tracer Daq	Top Gage	122.7518	3767.001	6580.553	120
		Tip Gage	207.1121	10723.86	18733.44	

Data5	**PDA**	Top Gage	113.3547	3212.322	5611.587	122
		Tip Gage	116.6410	3401.281	5941.678	
	EDC	Top Gage	120.5824	3635.029	6350.011	120
		Tip Gage	120.2440	3614.655	6314.42	
	Tracer Daq	Top Gage	115.3575	3326.838	5811.635	125
		Tip Gage	127.4408	4060.289	7092.897	

Having computed the c and knowing that there is no dispersion for this pile, then b may be found (Eq. 4-9) as $c^2 / 4$ and it is also given in Tables 4-1 and 4-2. Based on the pile geometry (B) and density (ρ), the unit skin friction/unit of displacement, i.e., K (slope of T-z curve), may be found (Eq. 4-3) and is given in Tables 4-1 and 4-2.

4.4 Analytical Estimates of Static Pile Friction and Damping

The K value, i.e., slope of T-Z curve varies from 11,300 lb/ft^3 - 13,600 lb/ft^3 (Table 4-1) for the low energy hammer impacts down to 4,900 lb/ft^3 - 7,300 (Table 4-2) for the high energy hammer impacts. Note, the K values represent the secant slope of T-Z curve, which for a typical bilinear T-Z curve results in smaller values for larger displacements (Figure 4-15).

The static skin friction force (Fs – Figure 4-1) on the pile may be computed from pile movement for a specific blow times K for unit skin friction (fs) times the surface area (4 B $\times$ L) of pile within the soil mass (4 $\times$ 1.5 ft $\times$ 20 ft = 120 ft^2). For instance, using the measured movements of 0.006 ft for the low energy impact (Figures 3-12 and 3-13) and K value from Table 4-1 of 13,600 lb/ft^3 with a surface area of 120 ft^2, a skin friction of 8,640 lbs should have been developed for blow 21. In the case of the high energy impact, Table

4-2 with K value of 5,500 lb/ft^3 and displacement u (Figures 3-22 and 3-23) of 0.025 ft, a unit skin friction (fs) of 138 psf (0.95 psi) develops which multiplied by surface area (120 ft^2) results in static pile skin friction of 16,500 lbs. Generally from Table 4-2, the static side resistance (R^{side}_{Static}) varies between 15,000 to 20,000 lbs.

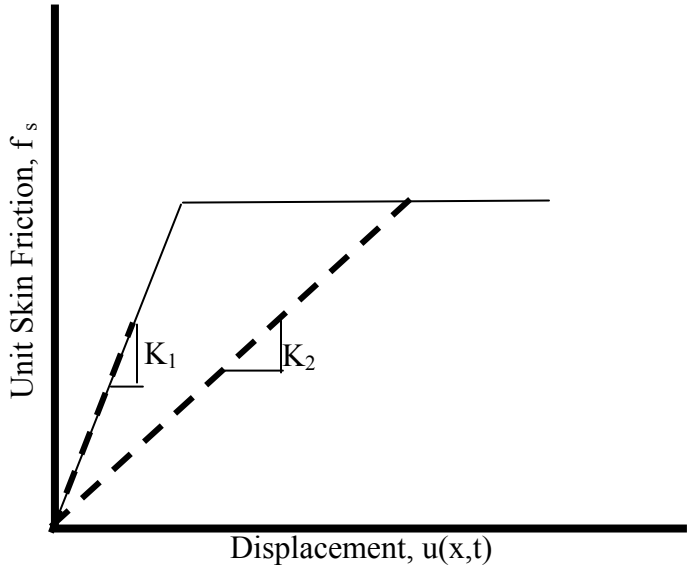

Figure 4-15. Static T-Z curve with secant slope (K).

Also of interest is a comparison of the estimated properties (i.e., static skin friction and side damping) with current practice. Typical unit skin friction in sand varies from 0 psi (ground surface) to a value of 12 psi (1700psf) with movements of 0.2 in which results in a range of K (lb/ft^3) values from 0 to 100,000 lb/ft^3. In the case of side damping, Zhang et al. (2001) have a range of Case skin damping factors (J_{cs}) from 0.05 to 0.65 for Florida Silty-Sand. To convert c to J_{cs},

$$J_{cs} = c\ B\ \rho\ A_{surf} / 4\ Z \qquad \text{(Eq. 4-14)}$$

where B is pile width, ρ is pile density, A_{surf} is surface area of embedded pile, and Z is pile impedance. Using the range of c from Tables 4-1 and 4-2 from 105 to 178 and pile

impedance (Z) of 130,000 lb-sec/ft gives range of J_{cs} from 0.17 to 0.3 well within reported values.

Besides Case side damping, J_{cs}, the computed c damping, Table 4-2 may be converted to Smith side damping factor, j_{ss}, or

$$j_{ss}\ (\text{sec/ft}) = J_{vs} / R^{side}_{static} \qquad \text{(Eq. 4-15)}$$

where viscous side damping (J_{vs}) may be found from Table 4-2 c values using Eq. 4-3, as,

$$J_{vs}\ (\text{lb-sec/ft}) = c\ B\ \rho\ A_{surf} / 4 \qquad \text{(Eq. 4-16)}$$

Using typical c values from Table 4-2, J_{vs} will range from 22,000 lb-sec/ft to 26,000 lb-sec/ft for the whole length of the pile. If the typical J_{vs} were to be substituted into Eq. 4-15, along with static side resistance, R^{side}_{static} of 15,000 to 20,000 lbs, Smith side damping would range from 1.3 to 1.7 sec/ft. For the case of blow 8, j_{ss} was 1.6 sec/ft for the whole side of the pile. If the length of the pile was divided into five equal segments (CAPWAP analysis), j_{ssi} for each segment would be 1.6/5 = 0.32 sec/ft.

4.5 Comparison of Analytical Forces with CAPWAP and Static Load Test

The total pile-soil structure interaction force (i.e., static and damping) removed in a blow is the summation of side and tip resistance,

$$R_T = R_T^{Side} + R_T^{Toe} \qquad \text{(Eq. 4-17)}$$

Each side and toe total forces may be split in terms of static and damping forces,

$$R_T^{Side} = R_{Static}^{Side} + R_{Damping}^{Side}$$

and

$$R_T^{Toe} = R_{Static}^{Toe} + R_{Damping}^{Toe} \qquad \text{(Eq. 4-18)}$$

For any blow, the value of R_T may be computed as F_{down} $(P_1 + ZV_1)/2$ at time t_1 (peak force) plus the value of F_{up} $(P_2 - ZV_2)/2$ at time t_2 given as $t_1 + 2L/c$. For a typical high energy impact (e.g., blow 5), F^{top}_{down} (Figure 3-24) was 435 kips, and F_{up} at time t_2 (t_1 + 2L/c**)** was -265 kips or the total force, R_T (Eq. 4-17) was 170 kips [430 +(-265)]. For other high energy blows, the value of R_T varied from 170kips to 180 kips. The distribution of total side and tip forces are readily obtained using the tip gages multiple ways. For instance, R_T^{Side} is equal to the difference in $(F^{top}_{down} - F^{tip}_{down}) \times 2$ (i.e., two directions: up and down) where F^{tip}_{down} occurs at t_1+ L/c. For instance for blow 5 (Figure 3-25), a value of 395 kips was recorded, giving R_T^{Side} [(430 -395) × 2] as 70 kips. For blows 5 through 8, the value of R_T^{Side} varied from 70 to 90 kips. Another way to determine R_T^{Side} is to first find R_T^{Toe} and subtract from total R_T (Eq. 4-17). Shown in Figure 4-16 is the measured R_T^{Toe} for blow 5. Note, R_T^{Toe} is simply the measured strain gage force measured at the toe

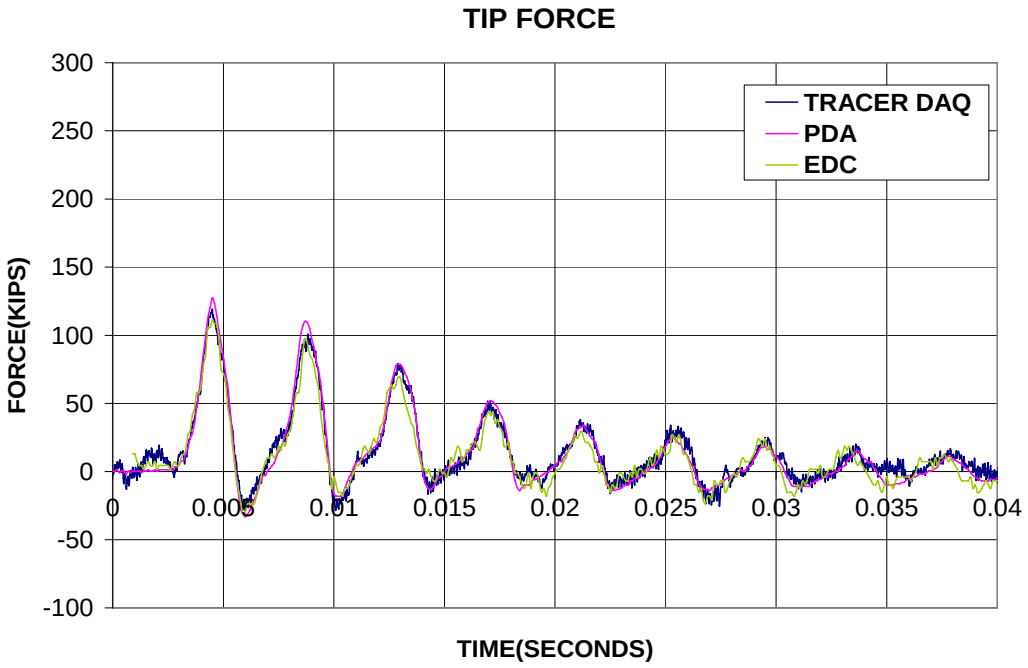

Figure 4-16. Measured total toe resistance (R_T^{Toe}) for blow 5

which for blow 5 is 120 kips. For other blows, R_T^{Toe} varied from 80 to 120 kips which when substituted into Eq. 4-17 gave a range of R_T^{side} in the range of 80 to 100 kips. For blow 8 (CAPWAP analysis), R_T was 175 kips and the bottom gage gave R_T^{Toe} as 95 kips and R_T^{side} was computed as 80 kips (or 40kips down and 40 kips up).

Knowing the distribution of total forces, R_T^{side} and R_T^{Toe}, the static forces may be assessed if the Smith damping is known. For instance, from Eq. 4-18 for total side resistance,

$$R_T^{Side} = R_{Static}^{Side} + R_{Damping}^{Side}$$

or, in terms of segments (i.e., break pile into equal length pieces) and Smith damping is given as,

$$R_T^{Side} = R_{Static}^{Side} + \Sigma\ j_{ss,i}\ V_{si}\ R_{Static}^{Side} \qquad \text{(Eq. 4-19)}$$

where $j_{ss,i}$ represents Smith damping for the slice and V_{si} is the average particle velocity in the slice. V_{si} for a segment may be obtained from $F_{down,average}/Z$ or 420 kips / 130 kip-sec/ft $\approx$ 3 ft/sec. In the case of five equal segments (e.g., uniform pile laid horizontally), with the earlier analytical value of j_{ssi} of 0.3 sec/ft and R_{Static}^{Side} of 15 kips /2 = 7.5 kips for a side, substitution into Eq. 4-19 gives, R_T^{Side} = 7.5kips +0.3 sec/ft x 3ft/sec x 5 segments x 7.5 kips = 41 kips. The latter represents the side force going down and if multiplied by two gives a total (up and down) of 82 kips. The latter compares favorably with the measured value of R_T^{side} for blow 8 (80 kips), suggesting that the static side resistance of 15kps to 20 kips given earlier is very reasonable.

Also of interest is static total resistance which may be calculated from the sum of the static side and static tip or computed directly through the use of Case Equation using a lumped Case damping parameter, J_{cL} as,

$$R_{Static}^{Total} = (1 - J_{cL}) (P_1 + ZV_1)/2 + (1 + J_{cL}) (P_1 - ZV_1)/2 \qquad \text{(Eq 4-20)}$$

The FDOT Phase I study of PDA vs. EDC uses Eq. 4-20 with J_{cL} found in Figure 4-17 with the peak force ratio ($F_{down,tip}/F_{down,top}$). For blow 8, $F_{down,tip}/F_{down,top}$ is approximately 0.8 and from Figure 4-17, J_{cL} is approximately 0.2.

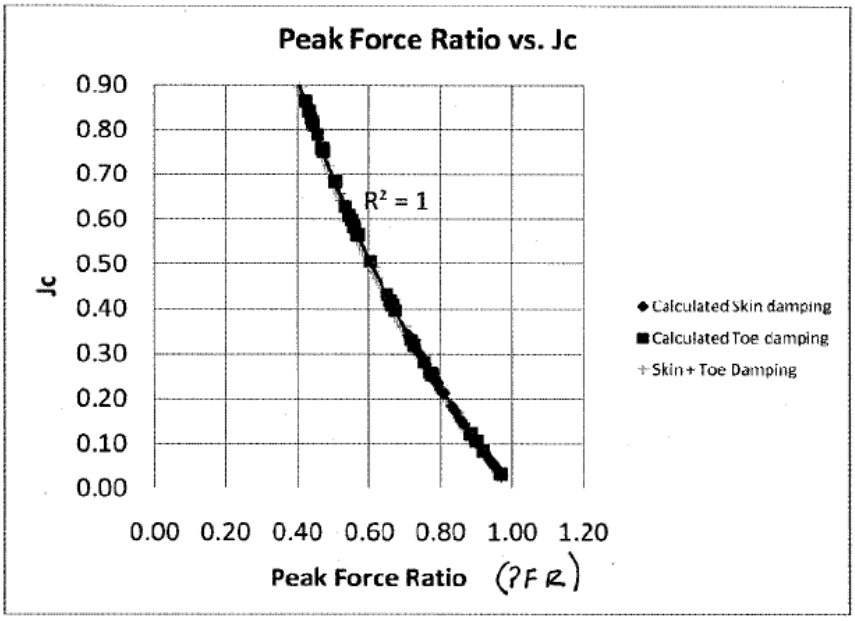

Figure 4-17. Estimated J_{cL} from peak force ratio

For blows 5 to 8, R_{Static}^{Total} from Eq. 4-20 varies from 45kips to 56 kips which gives a static tip resistance, R_{Static}^{Toe} of 25 kips to 31 kips (i.e. R_{Static}^{Total} - R_{Static}^{Side}).

Of interest are the force (R_T^{Side}, $R_{Damping}^{Side}$, R_{Static}^{Side}, R_T^{Toe}, R_{Static}^{Toe} and R_{Static}^{Total}) comparisons between CAPWAP, the analytical, and EDC. Shown in Figure 4-18 are the CAPWAP results for blow 8. First, CAPWAP predicts a total static resistance, R_{Static}^{Total}, of 52 kips which agrees quite well with EDC J_{cL} approach (i.e., 45 to 56 kips). Next, CAPWAP estimates a uniform Smith damping per slice (5 slices embedded in soil) as 0.332 sec/ft (Figure 4-18) which again agrees quite well with the analytical solution of 0.32 sec/ft. However, CAPWAP predicts the static side resistance, R_{Static}^{Side} as 38 kips and

edcpile; Pile: 043009 Test: 30-Apr-2009 10:03:
Blow: 8 CAPWAP(R) 2006
Florida Department of Transportation

CAPWAP SUMMARY RESULTS

Total CAPWAP Capacity: 52.0; along Shaft 38.0; at Toe 14.0 kips

Soil Sgmnt No.	Dist. Below Gages ft	Depth Below Grade ft	Ru kips	Force in Pile kips	Sum of Ru kips	Unit Resist. (Depth) kips/ft	Unit Resist. (Area) ksf	Smith Damping Factor s/ft
				52.0				
1	10.1	3.1	0.0	52.0	0.0	0.00	0.00	0.000
2	13.5	6.5	0.8	51.2	0.8	0.24	0.04	0.332
3	16.9	9.9	5.3	45.9	6.1	1.57	0.26	0.332
4	20.3	13.3	8.0	37.9	14.1	2.37	0.40	0.332
5	23.6	16.6	10.6	27.3	24.7	3.14	0.52	0.332
6	27.0	20.0	13.3	14.0	38.0	3.94	0.66	0.332
Avg. Shaft			6.3			1.90	0.32	0.332
Toe			14.0				6.22	0.183

Figure 4-18. CAPWAP analysis of blow 8.

R_{Static}^{Toe} as 14 kips or twice the analytical side resistance and ½ EDC static tip using J_{cL}. Interestingly, CAPWAP's estimate of R_T^{Side} from Eq. 4-19 [38kip +0.332 (0.8kip x 4ft/sec +5.3x4.6+8x5.6+10.6x6.5+13.3x6.9)]] was 116 kips and R_T^{Toe} [$(1 + j_{s,toe} V) R_{Static}^{Toe}$ = (1. + 0.183 sec/ft × 13.8 ft/sec) × 14 kips] was 50 kips or the total R_T force (Eq. 4-17) was 166 kips which agrees within 5% of the measured value of 175 kips. The latter suggest that the CAPWAP is having a difficult time in separating the R_T^{Side} from R_T^{Toe}. It should be noted that the EDC system measures R_T^{Side} from R_T^{Toe} directly, i.e., they are **not estimated**. The findings are in agreement with FDOT EDC Phase I study which revealed tip stress ratio (EDC/PDA) of 0.8 and a COV of 0.4.

After completion of the dynamic testing a static load test was performed on the pile, Figure 4-19. A 30-kip forklift bolted to the floor with a 10-kip concrete dead weight placed in front were used as resistance for the test. Shown in Figure 4-20 is the measured applied load vs. top pile displacement. Also shown in the figure is measured tip resistance for the applied top load and displacements. Approximately 20 kips were applied and a

Figure 4-19. Static load test on instrumented pile.

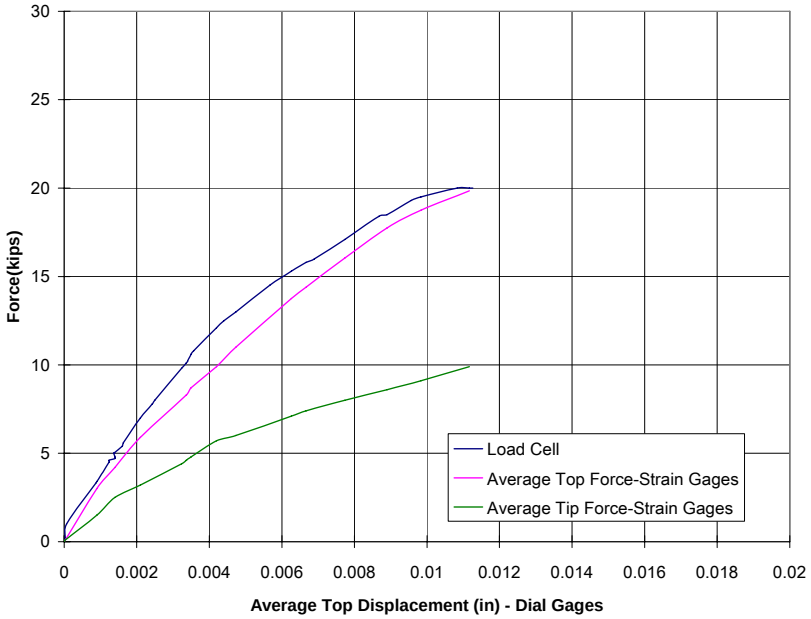

Figure 4-20. Static load test results for instrumented pile.

measured top movement of 0.015 in occurred when the forklift began to slide and the test was stopped. For the peak load of 20 kips, 10 kips of skin and 10 kips of tip resistance were mobilized (i.e., 50/50). It is expected that both the side resistance and tip resistance should increase more under larger applied loads, but the skin friction should peak prior to full tip mobilization.

CHAPTER 5
SUMMARY AND CONCLUSIONS

A major task of this research was to ensure under laboratory conditions that internally cast gages would give the same results as existing externally mounted accelerometers and strain gages. Moreover, the validation (e.g., response EDC system for pile top and tip) should occur under free, fixed, and intermediate end restraint conditions which cover the full range of field conditions. In the case of no soil (i.e., laboratory), the gages should show zero velocities and doubling of compression stress at the bottom of the pile under fixed condition, and a doubling of the velocity and zero stress in the case of a free condition. Of great interest is the case of soil along the length of the pile (i.e., field conditions). The gages should show a reduction in peak stress and velocity as the compression stress wave travels down the pile from soil resistance (static and dynamic); and at the end of the pile the compression wave should reflect with conditions in between the fixed and free condition in the laboratory.

Validation of wave propagation (incidence and reflection) is critical in separating skin and tip resistance from the applied dynamic force. Specifically, using the wave down and wave up results with one-dimensional wave theory with the inclusion of side damping and skin friction, allows for a direct "real-time" assessment of static side friction independently of static end bearing or static total pile capacity. The latter is a significant improvement of past total static pile capacity (i.e., PDA - lumped Case damping, J_{cL}) or total static pile capacity (i.e., J_{cL}) minus static tip resistance (unloading point method for tip – SmartPile Review Software).

The verification of wave propagation monitoring (i.e., internal and external) began with a 15-ft instrumented pile shown in Figure 5-1. The pile which was donated had EDC embedded sensors at the top and bottom of the pile. Sets of externally mounted gages (PDA and Tracer DAQ acceleration and strain gages) were placed at the top and bottom of the pile. The pile was supported horizontally (i.e., no body weight influences) and the pile was struck repeatedly with a 1000-lb hammer, Figure 5-1.

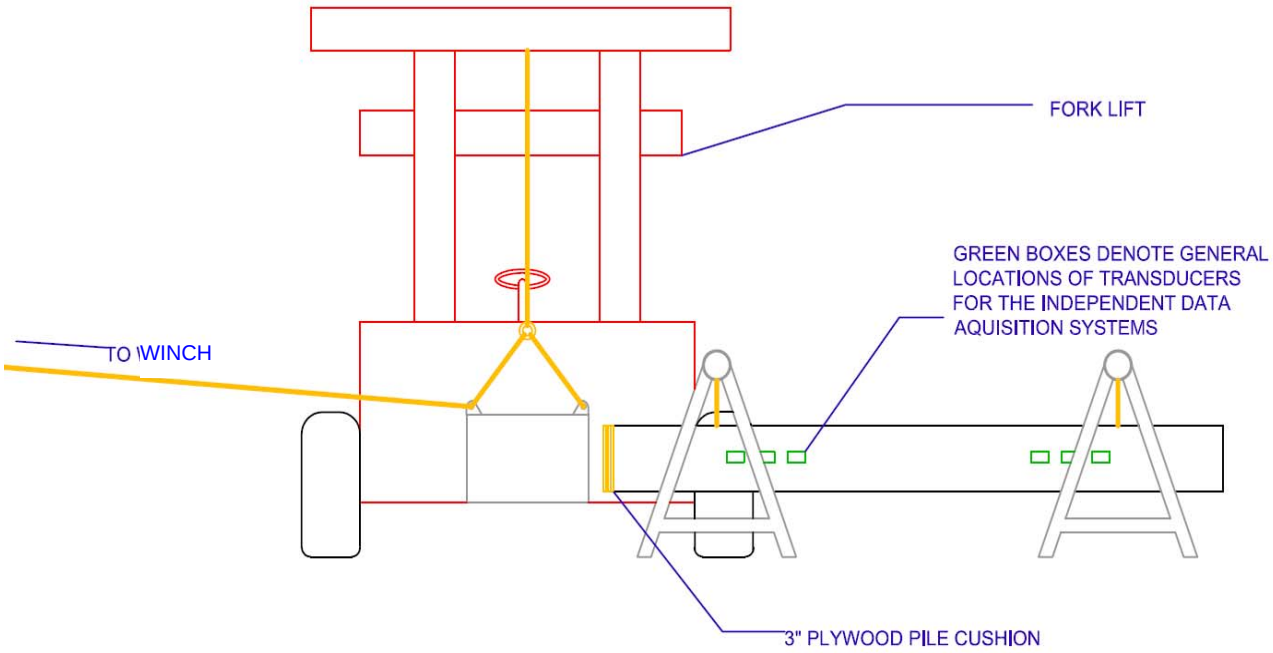

Figure 5-1. A 1000-lb hammer striking the 15-ft EDC instrumented pile (3-ft to 5-ft drop heights).

Analysis of all the data, revealed that the wave up forces that were reflected off the free end of the pile (Figure 5-1) did match each other in magnitude (wave propagation theory, Figures 5-2 and 5-3) and that the internal and external gages gave very similar readings and differences were either associated with boundary effects or accuracy of the gages.

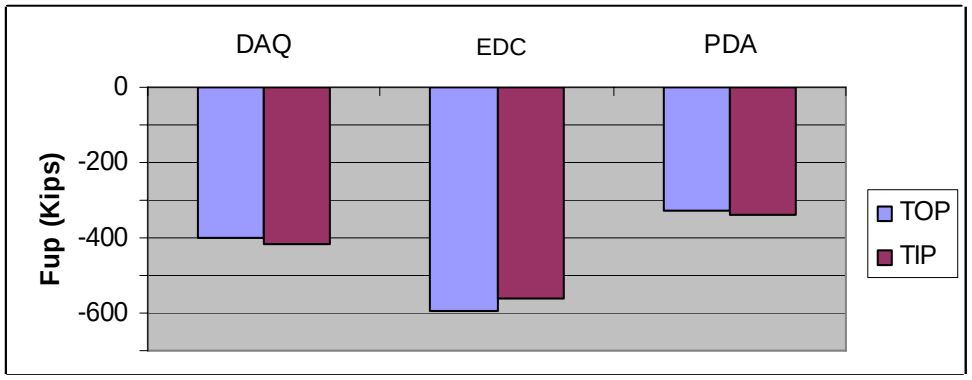

Figure 5-2. Comparison of peak F_{up} between tip and top of pile.

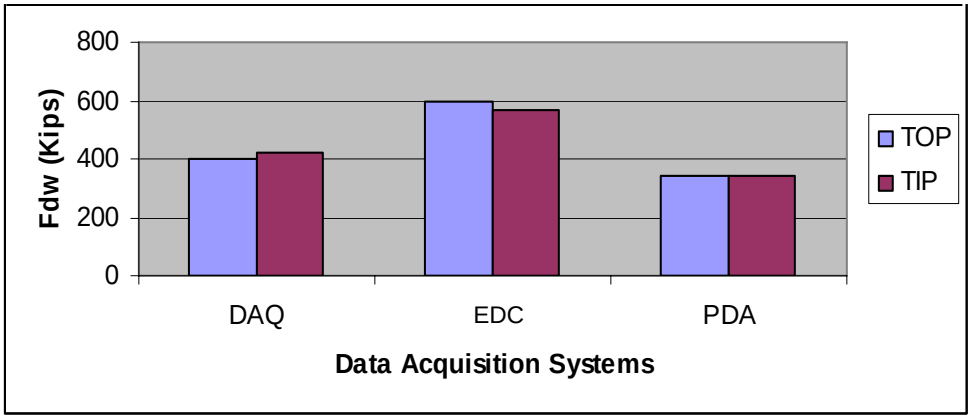

Figure 5-3. Comparison of peak F_{dw} between tip and top of pile.

Subsequently, a new 18-in × 18-in × 30-ft prestressed concrete pile was cast with EDC instrumentation at the top and bottom of the pile (Figure 5-4). PDA instruments as well as other commercially available strain and acceleration gages (Tracer DAQ) were attached to the top and the bottom of the pile. The pile was subsequently embedded in a compacted sand embankment (Figures 5-5 and 5-6) and struck with the 1000-lb hammer. The hammer strikes involved both small (i.e., 1-ft vertical) and large (i.e., 6-ft vertical) drop heights. Multiple blows were performed at each height to ensure repeatability.

Figure 5-4. 18-in×18-in×30-ft internally and externally instrumented pile at top and bottom.

Figure 5-5. 18-in × 18-in × 30-ft embedded horizontally in 15-ft high by 45-ft long sand embankment.

Figure 5-6. Top of 18-in × 18-in × 30-ft exposed 10-ft out of sand embankment.

Again, the wave down forces (Figure 5-7 and 5-8) from the internal and external gages showed excellent correlation. In addition, the magnitude reduction and shape from top to bottom were as expected.

Having verified internal vs. internal wave response, one-dimensional wave analysis was extended to include damping and skin friction (c and b, Eq. 5-1) which could be obtained from the new top and tip EDC instrumentation. The solution of Eq. 5-1, in terms of particle displacements (Eq. 5-2) revealed that the wave propagation could exhibit dispersion. That is, the individual wave frequencies making up hammer force blow could possibly travel at different velocities down the wave, Eq. 5-3.

$$a^2 \frac{\partial^2 u}{\partial x^2} = \frac{\partial^2 u}{\partial t^2} + c \frac{\partial u}{\partial t} + b\, u(x,t) \qquad \text{(Eq. 5-1)}$$

$$u(x,t) = \sum_m \exp\left(-\frac{c\,t}{2}\right) A_m \exp\left\{i\,k\left[x \pm \frac{t}{2k}\left(4\,a^2\,k^2 + 4\,b - c^2\right)^{\frac{1}{2}}\right]\right\} \qquad \text{(Eq. 5-2)}$$

$$V(k, \omega) = (4\,a^2\,k^2 + 4\,b - c^2)^{1/2} / 2k \qquad \text{(Eq. 5-3)}$$

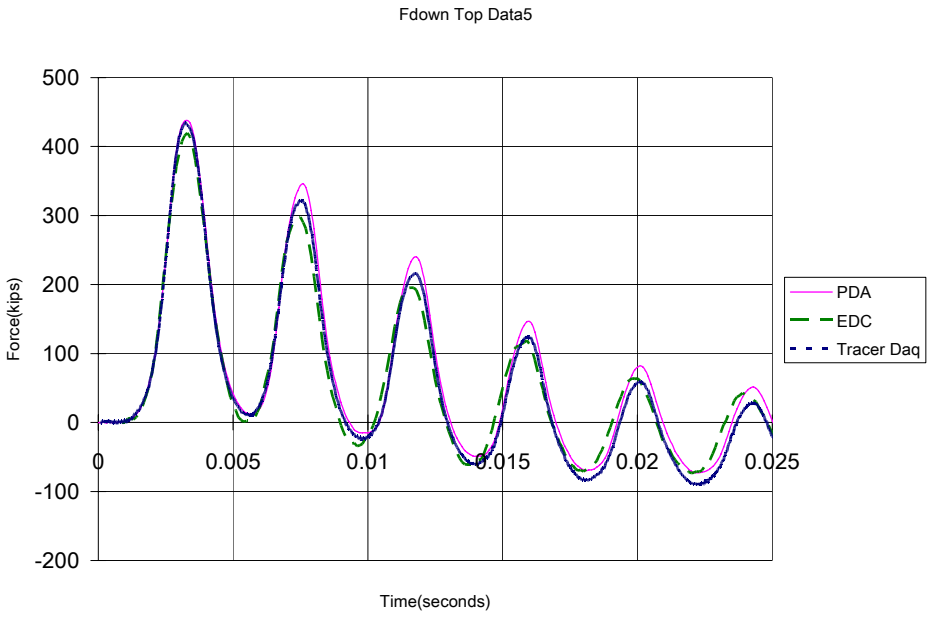

Figure 5-7. Comparison of F_{down} measurements at top of pile for blow 5 (6-ft drop).

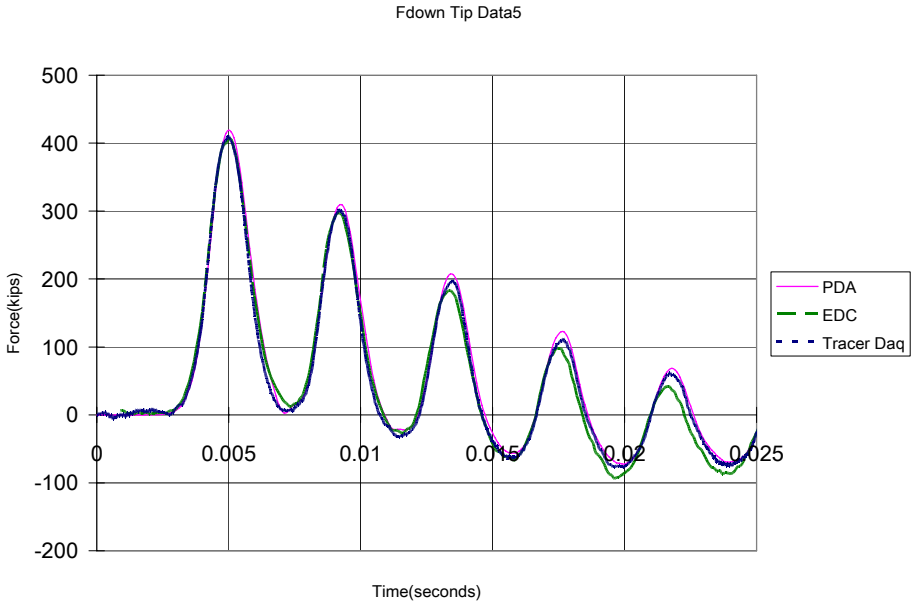

Figure 5-8. Comparison of F_{down} measurements at tip of pile for blow 5 (6-ft drop).

Next, using Spectral Analysis of Surface Waves (SASW) solution strategy, as well as Wavelet Theory, the solutions to Eqs. 5-2 and 5-3 were obtained from the top and bottom gage response. For instance, shown in Figure 5-9 are individual wave frequency responses for one of the high energy impact hammer force blows of the embedded pile. Evident from Figure 5-9, the peak arrival times of the individual harmonics are quite similar suggesting no dispersion (i.e., Eq. 5-3: $4b - c^2 = 0$). Consequently, the damping (c, Eq. 5-2) may be directly assessed from change in particle motion over time (Figure 5-10). In addition, the SASW analysis revealed that the most of the hammer energy goes into exciting the first primary pile mode of the pile which has a wavelength equal to twice the pile length. Also, pile response which exhibits no dispersion satisfies Smith damping. That is, by satisfying $4b - c^2 = 0$ for all frequencies, the static skin friction (function of b) is proportional to damping (c).

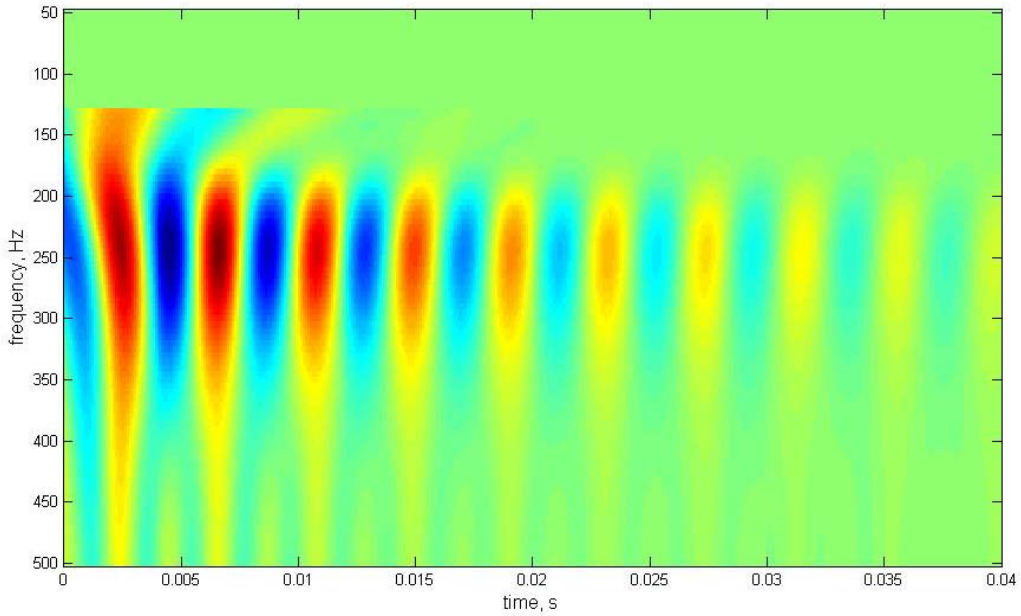

Figure 5-9. Analysis of the EDC signal for high energy impact blow 5.

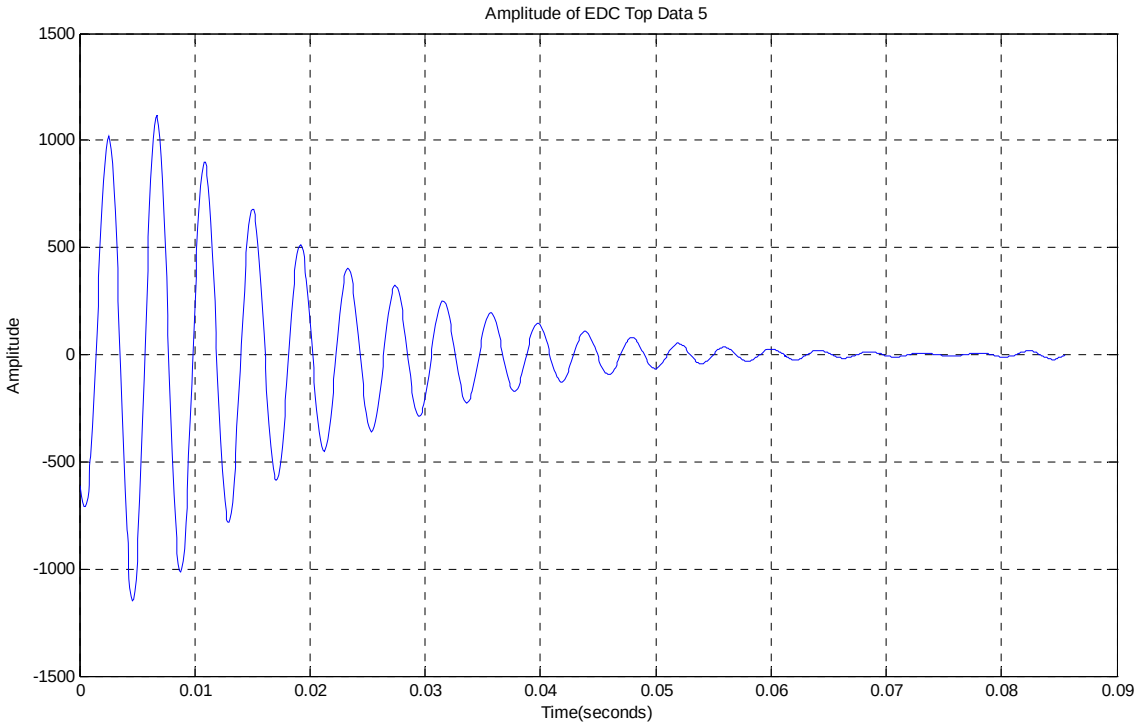

Figure 5-10. Amplitude vs. time for high energy impact EDC top signal, blow 5.

Knowing damping (c) the secant slope of the T-Z curve (i.e., static skin friction), K was found (Eq. 4-3). The K (lb/ft^3) for low and high energy impacts were assessed along the static skin friction for the 20-ft embedded pile.

A comparison of the analytical solution with existing software (i.e., CAPWAP) revealed very similar damping (i.e., Smith, Case, etc.) was developed for the side of the pile (i.e., J_{cs} and j_{ss}). Also, the total static pile capacity, R_{Static}^{Total} of 45 to 56 kips estimated from the Case Equation with the lumped Case damping parameter(J_{cL}) using the peak force ratio (Zang et al. 2001) agreed with CAPWAP. However, the distribution of forces within the pile (i.e., (R_T^{Side}, $R_{Damping}^{Side}$, R_{Static}^{Side}, R_T^{Toe}, and R_{Static}^{Toe}) did not agree between CAPWAP and analytical or EDC. The latter suggest that the CAPWAP is having a difficult time in separating the R_T^{Side} from R_T^{Toe}. It should be noted that the EDC system

measures R_T^{Side} from R_T^{Toe} directly, **not estimated**. The latter findings are in agreement with FDOT EDC Phase I study which revealed tip stress ratio (EDC/PDA) of 0.8 and a COV of 0.4.

In summary, the research showed that the embedded EDC instrumentation gives quite comparable results with externally mounted gages. Moreover, the use of top and bottom sets of instruments allows direct assessment of damping and static skin friction for both the side and the tip of the pile. In addition, the assessment may be real time (i.e., Lab View, MatLab, etc.) and it will require no interpretation or multiple assessments to check match quality. However, it is also strongly recommended that the work be continued under field scenarios, in order to add to our understanding of wave propagation, specifically in the study of wave dispersion (i.e., $4b = c^2$), layering, etc.

REFERENCES

Zhang, L., McVay, M., and Ng, C. (2001). "A Possible Physical Meaning of Case Damping in Pile Dynamics." *Canadian Geotechnical Journal*, Vol. 38, pp. 83-94.